Sushi domain-containing protein 4 controls synaptic plasticity and motor learning

I. González-Calvo[1,2,8,†], K. Iyer[1,†], M. Carquin[1], A. Khayachi[1], F.A. Giuliani[2], S.M. Sigoillot[1], J. Vincent[3], M. Séveno[4], M. Veleanu[1], S. Tahraoui[1], M. Albert[1], O. Vigy[5], C. Bosso-Lefèvre[1], Y. Nadjar[6], A. Dumoulin[6], A. Triller[6], J.-L. Bessereau[7], L. Rondi-Reig[3], P. Isope[2], F. Selimi[1]*

Affiliations:

[1] Center for Interdisciplinary Research in Biology (CIRB), Collège de France, CNRS, INSERM, PSL Research University, Paris, France.

[2] Institut de Neurosciences Cellulaires et Intégratives (INCI), CNRS, Université de Strasbourg, Strasbourg, France.

[3] Institut Biology Paris Seine (IBPS), Neuroscience Paris Seine (NPS), CeZaMe, CNRS, Sorbonne University, INSERM, Paris, France.

[4] BioCampus Montpellier, CNRS, INSERM, Université de Montpellier, Montpellier, France.

[5] Institut de Génomique Fonctionnelle, CNRS, INSERM, Université de Montpellier, Montpellier, France.

[6] École Normale Supérieure, Institut de Biologie de l'ENS, INSERM, CNRS, PSL Research University, Paris, France.

[7] Université de Lyon, Université Claude Bernard Lyon 1, CNRS UMR 5310, INSERM U 1217, Institut Neuromyogène, 69008, Lyon, France.

[8] Present address: Univ. Bordeaux, CNRS, Interdisciplinary Institute for Neuroscience, IINS, UMR 5297, F-33000 Bordeaux, France

† Equal contribution.

* Correspondence to: fekrije.selimi@college-de-france.fr

Summary

Fine control of protein stoichiometry at synapses underlies brain function and plasticity. How proteostasis is controlled independently for each type of synaptic protein in a synapse-specific and activity-dependent manner remains unclear. Here we show that *Susd4*, a gene coding for a complement-related transmembrane protein, is expressed by many neuronal populations starting at the time of synapse formation. Constitutive loss-of-function of *Susd4* in the mouse impairs motor coordination adaptation and learning, prevents long-term depression at cerebellar synapses, and leads to misregulation of activity-dependent AMPA receptor subunit GluA2 degradation. We identified several proteins with known roles in the regulation of AMPA receptor turnover, in particular ubiquitin ligases of the NEDD4 subfamily, as SUSD4 binding partners. Our findings shed light on the potential role of *SUSD4* mutations in neurodevelopmental diseases.

Introduction

Proteostasis is at the core of many cellular processes and its dynamics needs to be finely regulated for each protein in each organelle. In neurons, additional challenges are imposed by their spatial complexity. In particular, during long-term synaptic plasticity, the proposed substrate for learning and memory (Collingridge et al., 2010; Nicoll, 2017), the number of neurotransmitter receptors needs to be regulated independently in a synapse-specific and activity-dependent manner. At excitatory synapses, the modification of AMPA receptor numbers is a highly dynamic process, involving regulation of receptor diffusion (Choquet and Triller, 2013; Penn et al., 2017), their insertion in the plasma membrane, anchoring at the postsynaptic density and endocytosis (Anggono and Huganir, 2012). After activity-dependent endocytosis, AMPA receptors are either recycled to the plasma membrane or targeted to the endolysosomal compartment for degradation (Ehlers, 2000; Lee et al., 2004; Park et al., 2004). The decision between these two fates, recycling or degradation, regulates the direction of synaptic plasticity. Recycling promotes long-term potentiation (LTP) and relies on many molecules, such as GRASP1, GRIP1, PICK1 and NSF (Anggono and Huganir, 2012). Targeting to the endolysosomal compartment and degradation promote long-term depression (LTD; Fernandez-Monreal et al., 2012; Kim et al., 2017; Matsuda et al., 2013), but the regulation of the targeting and degradation process remains poorly understood.

The Complement Control Protein domain (CCP), an evolutionarily conserved module also known as Sushi domain, was first characterized in proteins with role in immunity, in particular in the complement system. In the past few years, proteins with CCP domains have been increasingly recognized for their role at neuronal synapses. Acetylcholine receptor clustering is regulated by CCP domain-containing proteins in *Caenorhabditis elegans* (Gendrel et al., 2009) and in *Drosophila melanogaster* (Nakayama et al., 2016). In humans, mutations in the CCP domain-containing secreted protein SRPX2 are associated with epilepsy and speech dysfunction, and SRPX2 knockdown leads to decreased synapse number and vocalization in mice (Sia et al., 2013). Recently SRPX2 has been involved in the regulation of synapse elimination in the visual and somatosensory systems (Cong et al., 2020). Despite the increase in the diversity of CCP domain-containing proteins in evolution (11 CCP domain-containing in *C. elegans* and 56 in humans; smart.embl.de), the function of many CCP domain-containing proteins remains unknown.

The mammalian *SUSD4* gene codes for a transmembrane protein with four extracellular CCP domains (**Figure 1A**) and is highly expressed in the central nervous system (Holmquist et al., 2013). The *SUSD4* gene is located in a genomic region deleted in patients with the 1q41q42 syndrome that includes developmental delays and intellectual deficiency (ID; Rosenfeld et al., 2011). *SUSD4* is also amongst the 124 genes enriched in *de novo* missense mutations in a large cohort of individuals with Autism Spectrum Disorders (ASDs) or IDs (Coe et al., 2019). A copy number variation and several *de novo* mutations with a high CADD score, which indicates the deleteriousness of the mutations, have been described in the *SUSD4* gene in patients with ASDs ((Cuscó et al., 2009); denovo-db, Seattle, WA (denovo-db.gs.washington.edu) 10, 2019). The SUSD4 protein has been described to regulate complement system activation in erythrocytes by

binding the C1Q globular domain (Holmquist et al., 2013). Interestingly, this domain is found in major synaptic regulators such as C1QA (Stevens et al., 2007), CBLNs (Matsuda et al., 2010; Uemura et al., 2010) and C1Q-like proteins (Bolliger et al., 2011; Kakegawa et al., 2015; Sigoillot et al., 2015). Altogether these studies point to a potential role of SUSD4 in synapse formation and/or function and in the etiology of neurodevelopmental disorders.

Proper development and function of the cerebellar circuitry is central for motor coordination and adaptation, and a range of cognitive tasks (Badura et al., 2018; Hirai et al., 2005; Ichise et al., 2000; Lefort et al., 2019; Rochefort et al., 2011; Tsai et al., 2012). Cerebellar dysfunction is associated with several neurodevelopmental disorders including ASDs (Stoodley, 2016; Stoodley et al., 2018; Wang et al., 2014). In this circuit, cerebellar Purkinje cells (PCs) receive more than a hundred thousand parallel fiber (PF) synapses whose formation, maintenance and plasticity are essential for cerebellar-dependent learning (Gutierrez-Castellanos et al., 2017; Hirai et al., 2005; Ito, 2006; Kashiwabuchi et al., 1995). Postsynaptic LTD was first described at synapses between PFs and cerebellar PCs (Gao et al., 2012; Hirano, 2018; Ito, 2001; Ito and Kano, 1982), where it can be induced by conjunctive stimulation of PFs with the other excitatory input received by PCs, the climbing fiber (CF; Coesmans et al., 2004; Ito, 2001; Suvrathan et al., 2016). The function of members of the C1Q family, such as CBLN1 and C1QL1, is essential for excitatory synapse formation and LTD in cerebellar PCs (Hirai et al., 2005; Kakegawa et al., 2015; Matsuda et al., 2010; Sigoillot et al., 2015; Uemura et al., 2010), suggesting that proteins such as SUSD4, that interact with the C1Q globular domain, could regulate these processes.

Gene expression studies from our laboratory revealed that *Susd4* is highly expressed in the olivocerebellar system of the mouse. In order to uncover the potential link between SUSD4 and neurodevelopmental disorders, we sought to identify the role of SUSD4 in brain development and function, by analyzing the phenotype of a *Susd4* constitutive loss-of-function mouse model. Here we show that knockout of the *Susd4* gene leads to deficits in motor coordination adaptation and learning, misregulation of synaptic plasticity in cerebellar PCs, as well as an impairment in the degradation of GluA2 AMPA receptor subunits after chemical induction of LTD. Proteomic analysis of SUSD4 binding complexes affinity-purified from synaptosome preparations identified proteins that are involved in the regulation of several parameters controlling AMPA receptor turnover. We showed that SUSD4 directly interacts with E3 ubiquitin ligases of the NEDD4 family, which are known to regulate ubiquitination and degradation of their substrates. Our results also show that SUSD4 and GluA2 can interact in transfected HEK293 cells and partially colocalize in cultured Purkinje cells. Altogether, these findings suggest a function of SUSD4 in the regulation of GluA2 trafficking and degradation allowing proper synaptic plasticity and learning.

Results

Susd4 is broadly expressed in neurons during postnatal development

Given the potential synaptic role for SUSD4, its pattern of expression should correlate with the timing of synapse formation and/or maturation during postnatal development. *In situ* hybridization experiments using mouse brain sections showed high expression of *Susd4* mRNA in neurons in many regions of the central nervous system, including the cerebral cortex, the hippocampus, the cerebellum and the brainstem (**Figure 1B** and **Figure 1-figure supplement 1**). *Susd4* expression was already detected as early as postnatal day 0 (P0) in some regions, but

129 increased with brain maturation (**Figure 1-figure supplement 1**). In the cerebellum, a structure
130 where the developmental sequence leading to circuit formation and maturation is well described
131 (Sotelo, 2004), quantitative RT-PCR showed that *Susd4* mRNA levels start increasing at P7 and
132 by P21 reach about 15 times the levels detected at birth (**Figure 1B**). At P7, a major increase in
133 synaptogenesis is observed in the cerebellum. At this stage, hundreds of thousands of PF
134 excitatory synapses form on the distal dendritic spines of each PC, and a single CF arising from
135 an inferior olivary neuron translocates and forms about 300 excitatory synapses on proximal PC
136 dendrites (Leto et al., 2016). In the brainstem, where cell bodies of inferior olivary neurons are
137 located, the increase in *Susd4* mRNA expression occurs earlier, already by P3, and reaches a
138 peak by P14 (**Figure 1B**). Similarly to the cerebellum, this pattern of *Susd4* expression parallels
139 the rate of synaptogenesis that increases during the first postnatal week in the inferior olive
140 (Gotow and Sotelo, 1987). To identify the subcellular localization of the SUSD4 protein and
141 because of the lack of suitable antibodies for immunolabeling, viral particles enabling CRE-
142 dependent coexpression of HA-tagged SUSD4 and GFP in neurons were injected in the
143 cerebellum of adult mice expressing the CRE recombinase specifically in cerebellar PCs.
144 Immunofluorescent labeling against the HA tag demonstrated the localization of HA-SUSD4 in
145 dendrites and in some of the numerous dendritic spines present on the surface of distal dendrites
146 (**Figure 1C**). These spines are the postsynaptic compartments of PF synapses in PCs.
147 Immunofluorescence analysis of transduced cultured PCs showed that HA-tagged SUSD4 could
148 be immunolabeled in non-permeabilizing conditions and located at the surface of dendrites and
149 spines (**Figure 1D**). Double labeling with the postsynaptic marker GluD2 (GRID2) further
150 showed partial colocalization at the surface of some, but not all, spines. Therefore, the timing of
151 *Susd4* mRNA expression during postnatal development and the subcellular localization of the
152 SUSD4 protein in cerebellar PCs are in agreement with a potential role for SUSD4 in excitatory
153 synapse formation and/or function.

154

155 ***Susd4* loss-of-function leads to deficits in motor coordination and learning**

156 To determine the synaptic function of SUSD4, we analyzed the phenotype of *Susd4*$^{-/-}$
157 constitutive knockout (KO) mice with a deletion of exon 1 (**Figure 1E, 1G** and **Figure 1-figure**
158 **supplement 2**). RT-PCR using primers encompassing the last exons and the 3'UTR show the
159 complete absence of *Susd4* mRNA in the brain of these *Susd4* KO mice (**Figure 1-figure**
160 **supplement 2**). No obvious alterations of mouse development and behavior were detected in
161 those mutants, an observation that was confirmed by assessment of their physical characteristics
162 (weight, piloerection), basic behavioral abilities such as sensorimotor reflexes (whisker
163 responses, eye blinking) and motor responses (open field locomotion; cf. **Table S1**). We further
164 assessed the behavior of *Susd4* KO mice for motor coordination and motor learning (Kayakabe et
165 al., 2014; Lalonde and Strazielle, 2001; Rondi-Reig et al., 1997). Using a footprint test, a slightly
166 larger print separation of the front and hind paws in the *Susd4* KO mice was detected but no
167 differences in the stride length and stance width were found (**Figure 1-figure supplement 3**). In
168 the accelerated rotarod assay, a classical test of motor adaptation and learning (Buitrago et al.,
169 2004), the mice were tested three times per day at one hour interval during five consecutive days.
170 The *Susd4* KO mice performed as well as the *Susd4*$^{+/+}$ (WT) littermate controls on the first trial
171 (**Figure 1F, day 1, trial 1**). This indicates that there is no deficit in their balance function,
172 despite the slight change in fine motor coordination found in the footprint test. However, while
173 the control mice improved their performance as early as the third trial on the first day, and

174 further improved with several days of training, no learning could be observed for the *Susd4* KO
175 mice either during the first day, or in the following days (**Figure 1F**). These results show that
176 *Susd4* loss-of-function leads to impaired motor coordination and learning in adult mice.

177

178 ***Susd4* loss-of-function prevents long-term depression (LTD) at cerebellar parallel**
179 **fiber/Purkinje cell synapses**

180 Because of the high expression of *Susd4* in cerebellar Purkinje cells (**Figure 1G** and **Figure 1-**
181 **figure supplement 1**), we focused on this neuronal type to identify the morphological and
182 functional consequences of *Susd4* loss-of-function. No deficits in the global cytoarchitecture of
183 the cerebellum and morphology of PCs were found in *Susd4* KO mice (**Figure 1-figure**
184 **supplement 4**). Using high density microelectrode array, we assessed the spontaneous activity of
185 PCs in acute cerebellar slices from *Susd4* KO mice, and compared to *Susd4* WT mice (**Figure 1-**
186 **figure supplement 5**). No differences were detected in either the mean spiking frequency, the
187 coefficient of variation of interspike intervals (CV) and the intrinsic variability of spike trains
188 (CV2, Holt and Douglas, 1996) indicating that the firing properties of PCs are not affected by
189 *Susd4* loss-of-function.

190 Co-immunolabeling of PF presynaptic boutons using an anti-VGLUT1 antibody and PCs using
191 an anti-calbindin antibody in cerebellar sections from juvenile WT mice revealed an extremely
192 dense staining in the molecular layer corresponding to the highly numerous PFs contacting PC
193 distal dendritic spines (**Figure 2A**). The labeling pattern appeared to be similar in *Susd4* KO.
194 High-resolution microscopy and quantitative analysis confirmed that there are no significant
195 changes in the mean density and volume of VGLUT1 clusters following *Susd4* loss-of-function
196 (**Figure 2A**). Electric stimulation of increasing intensity in the molecular layer allows the
197 progressive recruitment of PFs (Konnerth et al., 1990), and can be used to assess the number of
198 synapses and basic PF/PC transmission using whole-cell patch-clamp recordings of PCs on acute
199 cerebellar slices (**Figure 2B**). No difference was observed in the amplitude and the kinetics of
200 the responses to PF stimulation in PCs from *Susd4* KO and control littermate mice (**Figure 2C**
201 and **Figure 2-figure supplement 1**). Furthermore, the probability of vesicular release in the
202 presynaptic PF boutons, as assessed by measurements of paired pulse facilitation (Atluri and
203 Regehr, 1996; Konnerth et al., 1990; Valera et al., 2012), was not changed at PF/PC synapses
204 (**Figure 2C**). Finally, no differences in the frequency and amplitude of PF/PC evoked quantal
205 events were detected (**Figure 2-figure supplement 1**). Thus, in accordance with the
206 morphological analysis, *Susd4* invalidation has no major effect on the number and basal
207 transmission of PF/PC synapses in the mouse.

208 Long-term synaptic plasticity of PF/PC synapses is involved in proper motor coordination and
209 adaptation learning (Gutierrez-Castellanos et al., 2017; Hirano, 2018; Kakegawa et al., 2018).
210 We first assessed LTD in PF/PC synapses using conjunctive stimulation of PFs and CFs and
211 whole-cell patch-clamp recordings of PCs in acute cerebellar slices from juvenile mice. The LTD
212 induction protocol produced a 42% average decrease in the amplitude of PF excitatory
213 postsynaptic currents (EPSCs) in PCs from WT mice while the paired pulse facilitation ratio was
214 not changed during the course of our recordings (**Figure 2D** and **Figure 2-figure supplement**
215 **1**). In *Susd4* KO PCs, the same LTD induction protocol did not induce any significant change in
216 PF EPSCs during the 30 minutes recording period, showing that LTD induction and maintenance
217 are greatly impaired in the absence of SUSD4 (**Figure 2D**). We then assessed LTP induction

218 using high frequency stimulation of PF in the absence of inhibition blockade as in Binda et al.
219 (2016). In slices from *Susd4* WT mice, tetanic stimulation every 3 seconds during 5 minutes
220 induced only a transient increase in transmission of about 20% and the amplitude of the response
221 returned to baseline after only 15 minutes (**Figure 2E** and **Figure 2-figure supplement 1**). This
222 result suggests that under our experimental conditions and in this particular genetic background,
223 LTD might be favored in contrast to previously obtained results (Binda et al., 2016; Titley et al.,
224 2019). In the case of *Susd4* KO PCs, the same protocol induced LTP with a 27% increase in
225 transmission that was maintained after 35 minutes (**Figure 2E**). These results indicate that the
226 absence of *Susd4* expression promoted LTP induction at PF/PC synapses.

227 Lack of LTD of PF/PC synapses could arise from deficient CF/PC transmission. To test this
228 possibility, we first crossed the *Susd4* KO mice with the *Htr5b*-GFP BAC transgenic line
229 (http://gensat.org/MMRRC_report.jsp?founder_id=17735) expressing soluble GFP specifically
230 in inferior olivary neurons in the olivocerebellar system to visualize CFs. We found that CFs had
231 a normal morphology and translocated along the proximal dendrites of their PC target in *Susd4*
232 KO mice (**Figure 3-figure supplement 1**). We then assessed whether developmental elimination
233 of supernumerary CFs was affected by *Susd4* invalidation using whole-cell patch-clamp
234 recordings of PCs on cerebellar acute slices (Crepel et al., 1976; Hashimoto and Kano, 2003). No
235 difference was found in the percentage of remaining multiply-innervated PCs in the absence of
236 *Susd4* (**Figure 3-figure supplement 1**). We next used VGLUT2 immunostaining to label CF
237 presynaptic boutons and analyze their morphology using high resolution confocal microscopy
238 and quantitative image analysis. VGLUT2 immunostaining revealed the typical CF innervation
239 territory on PC proximal dendrites, extending up to about 80% of the molecular layer height both
240 in control *Susd4* WT and in *Susd4* KO mice (**Figure 3A**). Furthermore, the number and density
241 of VGLUT2 clusters were not significantly different between *Susd4* WT and *Susd4* KO mice. To
242 test whether the lack of CF-dependent PF LTD was due to deficient CF transmission, we used
243 whole-cell patch-clamp recordings of PCs in acute cerebellar slices. Contrary to what could have
244 been expected, the typical all-or-none CF evoked EPSC was detected in PCs from *Susd4* KO
245 mice with increased amplitude when compared to WT PCs (**Figure 3B**) while no differences in
246 CF-EPSC kinetics were found (**Figure 3-figure supplement 1**). Analysis of the complex spikes
247 in current-clamp mode during LTD induction did not reveal any change in the complex spike
248 waveform, with the same mean number of spikelets in response to the repeated CF stimulation in
249 *Susd4* WT and *Susd4* KO mice (**Figure 3-figure supplement 1**). Therefore, the lack of CF-
250 dependent PF/PC synapse LTD in *Susd4* KO mice is not due to impaired CF/PC synapse
251 formation or transmission. Measurements of evoked quantal events revealed an increase in the
252 amplitude of the quantal EPSCs at CF/PC synapses from juvenile mice (**Figures 3C** and **Figure**
253 **3-figure supplement 1**). Paired-pulse facilitation and depression at PF/PC and CF/PC synapses,
254 respectively, are similar between *Susd4* KO and control mice, both in basal conditions and
255 during plasticity recordings (**Figure 2C, Figure 3B, Figure 2-figure supplement 1**) suggesting
256 strongly that the changes in PF/PC synaptic plasticity and in CF/PC transmission in *Susd4* KO
257 PCs have a postsynaptic origin. Overall our results show that *Susd4* loss-of-function in mice
258 leads to a highly specific phenotype characterized by misregulation of postsynaptic plasticity in
259 the absence of defects in synaptogenesis and in basal transmission in cerebellar PCs.

260

261 ***Susd4* loss-of-function leads to deficient activity-dependent degradation of GluA2**

262 What are the mechanisms that allow regulation of long-term synaptic plasticity by SUSD4? The
263 lack of LTD at PF/PC synapses and our analysis of evoked quantal events suggested the
264 involvement of SUSD4 in the regulation of postsynaptic receptor numbers. GluA2 subunits are
265 present in most AMPA receptor channels in PC excitatory synapses (Masugi-Tokita et al., 2007;
266 Zhao et al., 1998). To assess whether *Susd4* loss-of-function leads to misregulation of the GluA2
267 subunits at PC excitatory synapses, we first performed co-immunolabeling experiments using an
268 anti-GluA2 antibody and an anti-VGLUT2 antibody on cerebellar sections followed by high-
269 resolution microscopy. Several GluA2 clusters of varying sizes were detected in close
270 association with each VGLUT2 presynaptic cluster corresponding to a single CF release site,
271 while very small and dense GluA2 clusters were found in the rest of the molecular layer which
272 mostly correspond to GluA2 clusters at the PF/PC synapses (**Figure 4A**). No obvious change in
273 GluA2 distribution in the molecular layer in *Susd4* KO mice was found when compared to
274 controls, in accordance with normal basal transmission in PF/PC synapses (**Figure 2C**).
275 Quantitative analysis of the GluA2 clusters associated with VGLUT2 labelled CF presynaptic
276 boutons did not reveal a significant change in the total mean intensity of GluA2 clusters per CF
277 presynaptic bouton (**Figure 4A**). However, the proportion of CF presynaptic boutons with no
278 GluA2 cluster was smaller in juvenile *Susd4* KO mice than in WT mice (**Figure 4A**). This
279 decrease partially explains the increase in the amplitude of quantal EPSCs and CF transmission
280 (**Figure 3C**).

281 In cerebellar PCs, regulation of the GluA2 subunits at synapses and of their trafficking is
282 essential for PF LTD (Chung et al., 2003; Xia et al., 2000). To test whether activity-dependent
283 surface localization of GluA2-containing AMPA receptors is affected by loss of *Susd4*, we set up
284 a biochemical assay in which we induced chemical LTD (cLTD) in acute cerebellar slices (Kim
285 et al., 2017) and performed surface biotinylation of GluA2 subunits followed by immunoblot
286 quantification. In control conditions, the mean baseline levels of surface GluA2 were not
287 significantly different between *Susd4* WT and *Susd4* KO mice (**Figure 4-figure supplement 1**).
288 As expected, after cLTD a 35% mean reduction of surface GluA2 receptors was measured in
289 slices from WT mice (**Figure 4B;** p=0.0212, two-tailed Student t test with a null hypothesis of
290 1). In acute slices from *Susd4* KO mice, a similar, but not statistically significant, mean reduction
291 of surface GluA2 receptors was detected after cLTD (28%; p=0.0538, two-tailed Student t test
292 with a null hypothesis of 1). Thus SUSD4 loss-of-function does not lead on average to a major
293 change in the activity-dependent regulation of the number of surface GluA2 subunits.
294 Another parameter that needs to be controlled for proper LTD in PCs is the total number of
295 AMPA receptors in the recycling pool and the targeting of AMPA receptors to late endosomes
296 and lysosomes (Kim et al., 2017). Lack of LTD and facilitation of LTP in *Susd4* KO mice
297 (**Figures 2D** and **2E**) suggest that GluA2 activity-dependent targeting to the endolysosomal
298 compartment and its degradation is affected by *Susd4* loss-of-function. Using our cLTD assay in
299 cerebellar slices, we measured the total GluA2 levels either in control conditions or in presence
300 of inhibitors of the proteasome (MG132) and of lysosomal degradation (leupeptin). The
301 comparison of the GluA2 levels in the presence of both inhibitors and in control conditions
302 allowed us to estimate the GluA2 degraded pool, regardless of the mechanism behind this
303 degradation. On average, total GluA2 levels were not significantly different between *Susd4* WT
304 and *Susd4* KO cerebellar slices in basal conditions (**Figure 4-figure supplement 1**), in
305 accordance with our morphological and electrophysiological analysis of PF/PC synapses
306 (**Figures 2A** and **2C**). In slices from WT mice, chemical induction of LTD induced a significant
307 reduction of 13% in total GluA2 protein levels (**Figure 4C**). This reduction was prevented by

308 incubation with the mixture of degradation inhibitors, MG132 and leupeptin, showing that it
309 corresponds to the pool of GluA2 degraded in an activity-dependent manner (**Figure 4C**). In
310 slices from *Susd4* KO mice, this activity-dependent degradation of GluA2 was completely
311 absent. Additionally, the chemical induction of LTD had no effect on the total protein levels of
312 GluD2, another synaptic receptor highly present at PF/PC postsynaptic densities, either in slices
313 from WT or from *Susd4* KO mice (**Figure 4-figure supplement 1**). Thus, SUSD4 specifically
314 controls the activity-dependent degradation of GluA2-containing AMPA receptors during LTD.

315 Finally, co-immunoprecipitation experiments were performed using extracts from heterologous
316 HEK293 cells transfected with SEP-tagged GluA2 and HA-tagged SUSD4 or the transmembrane
317 protein PVRL3α as a control. After affinity-purification of SEP-GluA2, HA-SUSD4 was
318 detected in affinity-purified extracts while PVRL3α was not, showing the specific interaction of
319 SEP-GluA2 and HA-SUSD4 in transfected HEK293 cells (**Figure 4-figure supplement 2**). In
320 order to assess the potential colocalization of SUSD4 and GluA2 in neurons, we used a Cre-
321 dependent AAV construct to express HA-tagged SUSD4 in cultured PCs (**Figure 4D**) and
322 performed immunolabeling of surface GluA2 subunits. Clusters of HA-tagged SUSD4 partially
323 colocalize with GluA2 clusters at the surface of some dendritic spines (yellow arrowheads,
324 **Figure 4D**). Partial colocalization of GluA2 and SUSD4 in neurons was also confirmed in
325 transfection experiments in hippocampal neurons (**Figure 4-figure supplement 2**). Thus,
326 SUSD4 could regulate activity-dependent degradation of GluA2-containing AMPA receptors
327 through a direct interaction.

328

329 **SUSD4 interacts with NEDD4 ubiquitin ligases**

330 To better understand how SUSD4 regulates the number of GluA2-containing AMPA receptors at
331 synapses, we searched for SUSD4 molecular partners by affinity-purification of cerebellar
332 synaptosome extracts using GFP-tagged SUSD4 as a bait (**Figure 5A**). Interacting partners were
333 identified by proteomic analysis using liquid chromatography with tandem mass spectrometry
334 (LC-MS/MS; Savas et al., 2014). 28 candidates were identified including proteins with known
335 function in the regulation of AMPA receptor turnover (**Figure 5E**). Several candidates were
336 functionally linked to ubiquitin ligase activity by gene ontology term analysis (**Figure 5A** and
337 **Table 1**). In particular, five members of the NEDD4 subfamily of HECT E3 ubiquitin ligases
338 were found as potential interacting partners, three of them (*Nedd4l*, *Wwp1* and *Itch*) exhibiting
339 the highest enrichment factors amongst the 28 candidates. Ubiquitination is a post-translational
340 modification essential for the regulation of protein turnover and trafficking in cells (Tai and
341 Schuman, 2008). A survey of the expression of HECT-ubiquitin ligases shows that different
342 members of the NEDD4 subfamily are broadly expressed in the mouse brain, however with only
343 partially overlapping patterns (**Figure 5-figure supplement 1**, http://mouse.brain-map.org, Allen
344 Brain Atlas). *Nedd4* and *Wwp1* are the most broadly expressed, including in neurons that also
345 express *Susd4*, such as hippocampal neurons, inferior olivary neurons in the brainstem and
346 cerebellar PCs. Immunoblot analysis of affinity-purified synaptosome extracts confirmed the
347 interaction of SUSD4 with NEDD4, ITCH and WWP1 (**Figure 5B**). Removal of the intracellular
348 domain of SUSD4 (SUSD4ΔC_T mutant) prevented this interaction demonstrating the specificity
349 of SUSD4 binding to NEDD4 ubiquitin ligases (**Figure 5B**).

350 The NEDD4 subfamily of HECT ubiquitin ligases is known to ubiquitinate and target for
351 degradation many key signaling molecules, including GluA1- and GluA2-containing AMPA

352 receptors (Schwarz et al., 2010; Widagdo et al., 2017). Ubiquitin ligases of the NEDD4 family
353 bind variants of PY motifs on target substrates and adaptors (Chen et al., 2017). However,
354 GluA1 and GluA2 subunits lack any obvious motif of this type. In contrast, two potential PY
355 binding sites are present in the intracellular domain of SUSD4 (**Figure 5C**). To test whether
356 SUSD4 and GluA2 interaction is affected by SUSD4 binding to NEDD4 ubiquitin ligases, co-
357 immunoprecipitation experiments were performed on extracts from heterologous HEK293 cells
358 transfected with SEP-tagged GluA2 and various HA-tagged SUSD4 constructs (**Figure 5C** and
359 **5D**). In addition to several deletion constructs of SUSD4, we generated single- and double-point
360 mutants of the two PY motifs in its intracellular tail (**Figure 5C**). Lack of the cytoplasmic
361 domain completely abrogated binding of NEDD4 to SUSD4, confirming the results obtained
362 using synaptosome extracts (**Figure 5D**). Deletion of the N-terminus domain of SUSD4 did not
363 affect NEDD4 binding. Furthermore, while the mutation of the PPxY site in the intracellular tail
364 (SUSD4-ΔPY mutant) abrogated binding of NEDD4 only partially, mutation of the LPxY site
365 (SUSD4-ΔLY mutant) or of both sites (SUSD4-ΔPY/LY mutant) completely prevented the
366 binding to NEDD4 ubiquitin ligases (**Figures 5C** and **5D**). These mutations did not change
367 significantly the level of HA-SUSD4 protein in transfected HEK293 cells suggesting that the
368 degradation of SUSD4 itself is not regulated by binding of NEDD4 ubiquitin ligases (**Figure 5-**
369 **figure supplement 2**). In accordance with our results obtained using SEP-GluA2 as a bait
370 (**Figure 4-figure supplement 2**), GluA2 was detected in extracts obtained by affinity-
371 purification of the HA-tagged full length SUSD4 (HA-SUSD4), while it was absent if HA-
372 SUSD4 was replaced by a control transmembrane protein, PVRL3α (**Figure 5D** and **Figure 5-**
373 **figure supplement 2**). Deletion of the extracellular domain (HA-SUSD4ΔN_T) or the cytoplasmic
374 domain (HA-SUSD4ΔC_T) did not reduce significantly the ability to interact with SEP-GluA2
375 when compared to HA-SUSD4 (**Figure 5D** and **Figure 5-figure supplement 2**). Strong co-
376 immunoprecipitation of GluA2 was detected in anti-HA affinity-purified extracts from cells
377 expressing the HA-tagged extracellular domain of SUSD4 alone (HA-SUSD4-N_T construct),
378 showing that this domain is sufficient for GluA2 interaction (**Figures 5D and Figure 5-figure**
379 **supplement 2**). Finally using the SUSD4-ΔLY mutant or SUSD4-ΔPY/LY mutant as a bait did
380 not significantly modify the levels of co-immunoprecipitated GluA2 compared to HA-SUSD4,
381 showing that binding of NEDD4 ubiquitin ligases does not affect SUSD4's ability to interact
382 with GluA2.
383

384 **Discussion**

385 Our study shows that the CCP domain-containing protein SUSD4 starts to be expressed in
386 various neurons of the mammalian central nervous system when synapses are formed and
387 mature. *Susd4* loss-of-function in mice leads to impaired motor coordination adaptation and
388 learning, misregulation of synaptic plasticity in cerebellar PCs and perturbed degradation of
389 GluA2-containing AMPA receptors after chemically induced LTD. SUSD4 and the GluA2
390 AMPA receptor subunit interact in transfected heterologous cells, and colocalize partially in
391 transduced cultured neurons. Finally, we show that SUSD4 directly binds to ubiquitin ligases of
392 the NEDD4 family, which have been previously shown to regulate GluA2 degradation.

393

394 **SUSD4 promotes long-term synaptic depression**

395 The choice between recycling of AMPA receptors to the membrane or targeting to the
396 endolysosomal compartment for degradation is key for the regulation of the number of AMPA
397 receptors at synapses, as well as for the direction and degree of activity-dependent synaptic
398 plasticity (Ehlers, 2000; Lee et al., 2002). Blocking trafficking of AMPA receptors through
399 recycling endosomes, for example using a RAB11 mutant, prevents long-term potentiation (LTP)
400 in neurons (Park et al., 2004). Conversely, blocking the sorting of AMPA receptors to the
401 endolysosomal compartment, for example using a RAB7 mutant, impairs long-term depression
402 (LTD) in hippocampal CA1 pyramidal neurons and cerebellar Purkinje cells (PCs) (Fernandez-
403 Monreal et al., 2012; Kim et al., 2017). Further support for the role of receptor degradation
404 comes from mathematical modeling showing that in cerebellar PCs LTD depends on the
405 regulation of the total pool of glutamate receptors (Kim et al., 2017). The GluA2 AMPA receptor
406 subunit, and its regulation, is of particular importance for LTD (Diering and Huganir, 2018).
407 Phosphorylation in its C-terminal tail and the binding of molecular partners such as PICK1 and
408 GRIP1/2 is known to regulate endocytosis and recycling (Bassani et al., 2012; Chiu et al., 2017;
409 Fiuza et al., 2017), and mutations in some of the phosphorylation sites leads to impaired LTD
410 (Chung et al., 2003). The molecular partners regulating the targeting for degradation of GluA2
411 subunits in an activity-dependent manner during LTD remain to be identified. Our study shows
412 that loss-of-function of *Susd4* leads both to loss of LTD and loss of activity-dependent
413 degradation of GluA2 subunits. Loss-of-function of *Susd4* does not affect degradation of another
414 postsynaptic receptor, GluD2, showing the specificity of SUSD4 action. Furthermore, loss-of-
415 function of *Susd4* facilitates LTP of PF/PC synapses. Overall our results suggest a role for
416 SUSD4 in the targeting of GluA2-containing AMPA receptors to the degradation compartment
417 during synaptic plasticity.

418

419 **SUSD4 interacts with regulators of AMPA receptor turnover**

420 The degradation of specific targets such as neurotransmitter receptors must be regulated in a
421 stimulus-dependent and synapse-specific manner in neurons, to ensure proper long-term synaptic
422 plasticity, learning and memory (Tai and Schuman, 2008). How is this level of specificity
423 achieved? Adaptor proteins, such as GRASP1, GRIP1, PICK1 and NSF, are known to promote
424 AMPA receptor recycling and LTP (Anggono and Huganir, 2012). Such adaptors for the
425 promotion of LTD remain to be found.

426 Our results show that SUSD4 directly binds to HECT E3 ubiquitin ligases of the NEDD4 family.
427 The family of HECT E3 ubiquitin ligases contains 28 enzymes including the NEDD4 subfamily
428 that is characterized by an N-terminal C2 domain, several WW domains and the catalytic HECT
429 domain (Weber et al., 2019). This subgroup of E3 ligases adds K63 ubiquitin chains to their
430 substrate, a modification that promotes sorting to the endolysosomal compartment for
431 degradation (Boase and Kumar, 2015). NEDD4 E3 ligases are highly expressed in neurons in the
432 mammalian brain and have many known substrates with various functions, including ion
433 channels and the GluA1 AMPA receptor subunit. Accordingly, knockout mice for the *Nedd4-1*
434 gene die during late gestation (Kawabe et al., 2010). The activity and substrate selectivity of
435 NEDD4 E3 ligases thus need to be finely tuned. Both GluA1 and GluA2 AMPA receptor
436 subunits are ubiquitinated on lysine residues in their intracellular tails in an activity-dependent
437 manner (Lin et al., 2011; Lussier et al., 2011; Schwarz et al., 2010; Widagdo et al., 2015).
438 Mutation of these lysine residues decreases localization of GluA1 and GluA2 AMPA receptor
439 subunits in the endolysosomal compartment in neurons (Widagdo et al., 2015). However, GluA1

440 and GluA2 subunits lack any obvious intracellular direct binding motif to the WW domain of
441 NEDD4 ubiquitin ligases, raising questions about the precise mechanism allowing regulation of
442 AMPA subunits trafficking and degradation by these enzymes. We showed that SUSD4 and
443 GluA2 AMPA receptor subunits interact in cells, and partially colocalize in neurons. SUSD4
444 could thus play a role in regulating targeting of NEDD4 ubiquitin ligases to AMPA receptors in
445 an activity-dependent manner in neurons. Alternatively, the interaction of SUSD4 with NEDD4
446 ubiquitin ligases might regulate the trafficking of the SUSD4/GluA2 complex to the degradation
447 pathway. Furthermore, among the potential partners of SUSD4 identified by our proteomics
448 analysis, several other candidates have functions that are relevant for the regulation of synaptic
449 plasticity, such as receptor anchoring, clathrin-mediated endocytosis and proteasome function
450 **(Figure 5E)**. Further work is needed to determine the precise mechanism of action of SUSD4 in
451 neurons in the context of synaptic plasticity.

452

453 **SUSD4 and neurodevelopmental disorders**

454 *Susd4* loss-of-function leads to motor impairments, a symptom that is also found in ASD patients
455 (Fournier et al., 2010). Deficits in LTD such as the one found in the *Susd4* KO mice are a
456 common feature of several mouse models of ASDs (Auerbach et al., 2011; Baudouin et al., 2012;
457 Piochon et al., 2014). Because of the broad expression of SUSD4 and of ubiquitin ligases of the
458 NEDD4 subfamily in the mammalian central nervous system, whether motor impairments in the
459 *Susd4* KO mice are directly the results of synaptic deficits in cerebellar Purkinje cells remain to
460 be demonstrated. Very recently, a reduction in exploratory behavior, in addition to impairments
461 of motor coordination, was reported after *Susd4* loss-of-function (Zhu et al., 2020). Thus,
462 mutations in the *Susd4* gene might contribute to the etiology of neurodevelopmental disorders by
463 impairing synaptic plasticity at many synapse types.

464 In humans, the 1q41-42 deletion syndrome is characterized by many symptoms including IDs
465 and seizures, and in a high majority of the cases the microdeletion encompasses the *SUSD4* gene
466 (Rosenfeld et al., 2011). A *SUSD4* copy number variation has been identified in a patient with
467 autism spectrum disorder (ASD; Cuscó et al., 2009). *SUSD4* was recently identified amongst the
468 124 genes with genome wide significance for *de novo* mutations in a cohort of more than 10,000
469 patients with ASD or IDs (Coe et al., 2019). The *GRIA2* gene (coding for the GluA2 subunit) has
470 been found as an ASD susceptibility gene (Salpietro et al., 2019; Satterstrom et al., 2018) and
471 mutations or misregulation of ubiquitin ligases have been found in many models of ASDs or
472 intellectual deficiencies (Cheon et al., 2018; Lee et al., 2018; Satterstrom et al., 2018). For
473 example, ubiquitination of GluA1 by NEDD4-2 is impaired in neurons from a model of Fragile
474 X syndrome (Lee et al., 2018). Understanding the molecular mechanism linking activity-
475 dependent degradation of GluA2 and the SUSD4/NEDD4 complex will thus be of particular
476 importance for our understanding of the etiology of these neurodevelopmental disorders.

477

478 **Materials and Methods**

479 **Animals**

480 *Susd4* knockout (KO) mice were generated using 129S5/SvEvBrd ES microinjected in C57BL/6J
481 blastocysts and maintained on the C57BL/6J background (generated by Lexicon Genetics
482 Incorporated, The Woodlands, USA)(Tang et al., 2010). Out of the 8 *Susd4* exons, coding exon 1

483 (NCBI accession NM_144796.2) and the 5'UTR (NCBI accession BM944003) were targeted by
484 homologous recombination. This resulted in the deletion of a 1.3kb sequence spanning the
485 transcription initiation site and exon 1 (**Figure 1E** and **Supplementary Figure 2A**). Subsequent
486 genotyping of mice was performed using PCR to detect the wild-type (WT) allele (forward
487 primer: 5' CTG TGG TTT CAA CTG GCG CTG TG 3'; reverse primer: 5' GCT GCC GGT
488 GGG TGT GCG AAC CTA 3') or the targeted allele (forward primer: 5' TTG GCG GTT TCG
489 CTA AAT AC 3'; reverse primer: 5' GGA GCT CGT TAT CGC TAT GAC 3'). Heterozygous
490 *Susd4*$^{+/-}$ mice were bred to obtain all the genotypes needed for the experiments (*Susd4*$^{+/+}$ (WT)
491 and *Susd4*$^{-/-}$ (KO) mice) as littermates.
492 The Htr5b-GFP mouse line was used for labeling of climbing fibers (CF; The Gene Expression
493 Nervous System Atlas (GENSAT) Project, NINDS Contracts N01NS02331 &
494 HHSN271200723701C to The Rockefeller University (New York, NY)). Genotyping was
495 performed using the following primers: 5' TTG GCG CGC CTC CAA CAG GAT GTT AAC
496 AAC 3' and 5' CGC CCT CGC CGG ACA CGC TGA AC 3' (**Figure Supplementary 2A**).
497 The L7Cre mouse line was obtained from Jackson laboratories (B6.129-Tg(Pcp2-cre)2Mpin/J ;
498 Stock Number: 004146) and genotyping was performed using the following primers: 5' GGT
499 GAC GGT CAG TAA ATT GGA C 3'; 5' CAC TTC TGA CTT GCA CTT TCC TTG G 3' and
500 5' TTC TTC AAG CTG CCC AGC AGA GAG C 3'.
501 All animal protocols were approved by the *Comité Regional d'Ethique en Experimentation*
502 *Animale* (no. 00057.01) and animals were housed in authorized facilities of the CIRB (# C75 05
503 12).
504
505 **Antibodies**
506 The following primary antibodies were used: mouse monoclonal anti-CABP (1:1000; Swant,
507 Switzerland, Cat#300), rabbit polyclonal anti-CABP (1:1000; Swant, Cat#CB38), mouse
508 monoclonal anti-GFP (1:1000; Abcam, Cambridge, United Kingdom, Cat#ab1218), rabbit
509 polyclonal anti-GFP (1:1000; Abcam, Cat#ab6556), mouse monoclonal anti-GluA2 (clone 6C4;
510 1:500; Millipore, Massachusetts, USA, Cat#MAB397 and BD, New Jersey, USA, Cat#556341),
511 rabbit monoclonal anti-GluA2 (1:1000; Abcam, Cat#ab206293), rabbit polyclonal anti-
512 GluRδ1/2 (1:1000; Millipore, Cat#AB2285), rat monoclonal anti-HA (1:1000; Roche Life
513 Science, Penzberg, Germany, Cat#11867423001), rabbit monoclonal anti-ITCH (1:1000; Cell
514 Signaling Technology, Massachusetts, USA, Cat#12117), rabbit polyclonal anti-NEDD4
515 (1:10000; Millipore, Cat#07-049), guinea pig polyclonal anti-VGLUT1 (1:5000; Millipore,
516 Cat#AB5905), guinea pig polyclonal anti-VGLUT2 (1:5000; Millipore, Cat#AB2251) and
517 rabbit polyclonal anti-WWP1 (1:2000; Proteintech, Chicago, USA, Cat#13587-1-AP).
518 The following secondary antibodies were used: donkey polyclonal anti-Goat Alexa Fluor 568
519 (1:1000; Invitrogen, California, USA, Cat#A11057), donkey anti-Mouse Alexa Fluor 488
520 (1:1000; Invitrogen, Cat#R37114), donkey polyclonal anti-Mouse Alexa Fluor 568 (1:1000;
521 Invitrogen, #A10037), donkey polyclonal anti-Rabbit Alexa Fluor 488 (1:1000; Invitrogen,
522 Cat#A21206), donkey polyclonal anti-Rat Alexa Fluor 594 (1:1000; Invitrogen, #A21209),
523 donkey polyclonal anti-Rat Alexa Fluor 568 (1:1000; Abcam, Cat#175475), goat polyclonal
524 anti-Guinea Pig Alexa Fluor 488 (1:1000; Invitrogen, Cat#A110-73), goat polyclonal anti-
525 Guinea Pig Alexa Fluor 647 (1:1000; Invitrogen, Cat#A21450), goat polyclonal anti-Mouse
526 HRP (1:10000; Jackson Immune Research Laboratories, Pennsylvania, USA, Cat#115-035-
527 174), goat polyclonal anti-rat HRP (1:10000; Jackson Immune Research Laboratories, #112-

528 035-175) and mouse polyclonal anti-rabbit HRP (1:10000; Jackson Immune Research
529 Laboratories, #211-032-171).
530 The following conjugated antibodies were used: sheep polyclonal anti-digoxigenin alkaline
531 phosphatase (1:2000 - 1:5000; Roche Life Science, Cat#11093274910), mouse monoclonal anti-
532 βACTIN (clone AC-15) HRP (1:25000; Abcam, Cat#ab49900).
533
534 **Plasmids**
535 Full-length *Susd4* mouse gene was cloned into the mammalian expression vector pEGFP-N1
536 (Addgene, Massachusetts, USA, Cat#6085-1) to express a SUSD4-GFP fusion construct under
537 the control of the CMV promoter (pSUSD4-GFP). An N-terminal HA tag was inserted just after
538 the signal peptide (pHA-SUSD4-GFP). pHA-SUSD4 was obtained by removal of the C-terminal
539 GFP of pHA-SUSD4-GFP. A truncated form of *Susd4*, expressing the HA-SUSD4-ΔC_T mutant,
540 was obtained by inserting a stop codon downstream of the sixth exon, 39bp after the
541 transmembrane domain using PCR on the pHA-SUSD4-GFP plasmid and the following primers:
542 forward primer 5' GCG CTA GCG ATG TAT CCT TAT GAT GTT CCT G 3'; reverse primer
543 5'TAG CGG CCG CTA TTA GGG GGG GAA GTG GGC CTT 3'. Other mutant constructs
544 were similarly obtained: the truncated form HA-SUSD4-ΔN_T corresponding to aminoacids 294-
545 490, and the extracellular form of SUSD4, HA-SUSD4-N_T, corresponding to aminoacids 2-299.
546 The HA-SUSD4-ΔPY contains a mutation in aminoacids 411 and 414 changing PPAY to APAA
547 while HA-SUSD4-ΔLY is mutated in aminoacids 376 and 379 changing LPTY to APTA.
548 Mutagenesis was performed using the QuikChange Lightning Multi site directed mutagenesis kit
549 (Agilent, Santa Clara, USA, Cat#210513) according to the manufacturer's instructions. The
550 plasmid pIRES2-eGFP (Addgene, Cat#6029-1) was used as transfection control. The plasmid
551 expressing SEPGluA2 (Addgene, Cat#24001) was used to follow GluA2. The control
552 transmembrane protein PVRL3α was cloned into the mammalian expression vector pCAG-
553 mGFP (Addgene, Cat#14757) to express the protein under the pCAG promoter (pCAG-
554 PVRL3α).
555
556 **Viral mediated *in vivo* expression of HA-SUSD4**
557 AAV2 particles were generated using a hSYN-DIO-HA-SUSD4-2A-eGFP-WPRE construct
558 (Vector biolabs, Malvern, USA) and injected stereotaxically in cerebella of adult mice
559 expressing the CRE recombinase in cerebellar Purkinje cells (PCs) using the L7Cre mice. In the
560 absence of Cre expression, the transgene is not produced. In the presence of Cre expression, the
561 transgene will be "FLip-EXchanged" leading to expression of the transgene specifically in PCs.
562
563 ***In situ* hybridization**
564 Fresh frozen 20µm thick-sections were prepared using a cryostat (Cryostar NX 70, Thermo
565 Fisher Scientific, Ref.: 957000H) from brains of *Susd4* WT and KO mice at P0, P7 or P21. The
566 probe sequence corresponded to the nucleotide residues 287-1064bp (encompassing exons 2-5)
567 for mouse *Susd4* (NM_144796.4) cDNA. The riboprobes were used at a final concentration of
568 0.05µg/µL, and hybridization was done overnight at a temperature of 72°C. The anti-
569 digoxigenin-AP antibody (for details see antibodies section above) was used at a dilution of
570 1:5000. Alkaline phosphatase detection was done using BCIP/NBT colorimetric revelation
571 (Roche Life Science, Cat#11681451001).
572
573 **Behavioral Study**

574 12-14 weeks old male mice were used in this study. They were housed in groups of 3-5 in
575 standard conditions: 12h light/dark cycle, with *ad libitum* food and water access. Seven days
576 before the beginning of behavioral test, mice were housed individually to limit inter-houses
577 variability resulting from social relationships. All behavioral tests took place in the light cycle.
578 S.H.I.R.P.A. protocol: Mice performed a series of tests to ensure their general good health and
579 motor performance and habituate them to being manipulated (Crawley, 2006). The test includes
580 observation of appearance, spontaneous behavior, neurological reflexes, anxiety, motor
581 coordination, balance rotarod and muscular strength tests and were performed within five days.
582 Individuals presenting deficits during the S.H.I.R.P.A. protocol were not used for other
583 behavioral tests.
584 Footprint analysis: The fore and hind paws of mice were dipped in magenta and cyan non-toxic
585 paint, respectively. Mice were allowed to walk through a rectangular plastic tunnel (9cm W x
586 57cm L x 16cm H), whose floor was covered with a sheet of white paper. Habituation was done
587 the day before the test. Five footsteps were considered for the analysis. Footprints were scanned
588 and length measurements were made using ImageJ.
589 Rotarod: Mice were first habituated to the rotarod apparatus, three days before the acceleration
590 test. The habituation protocol consists of 5min at 4 r.p.m. To evaluate the motor coordination,
591 mice were placed on immobile rotarod cylinders, which ramped up from 0 to 45 rotations per
592 minute in 10min. The timer was stopped when the mouse fell off the cylinder or did a whole turn
593 with it. For a given session, this procedure was repeated three times per day separated by 60min.
594 The session was repeated during five consecutive days.
595
596 **Whole-cell patch-clamp on acute cerebellar slices**
597 Responses to parallel fiber (PF) and CF stimulation were recorded in PCs of the lobule VI in
598 acute parasagittal and horizontal (long-term potentiation (LTP) experiments) cerebellar slices
599 from *Susd4* KO juvenile (from P25 to P35) or adult (~P60) mice. *Susd4* WT littermates were
600 used as controls. Mice were anesthetized using isoflurane 4% and sacrificed by decapitation. The
601 cerebellum was dissected in ice cold oxygenated (95% O_2 and 5% CO_2) Bicarbonate Buffered
602 Solution (BBS) containing (in mM): NaCl 120, KCl 3, $NaHCO_3$ 26, NaH_2PO_4 1.25, $CaCl_2$ 2,
603 $MgCl_2$ 1 and D(+)-glucose 35. 300µm-thick cerebellar slices were cut with a vibratome (Microm
604 HM650V: Thermo Scientific Microm, Massachusetts, USA or 7000smz-2 Campden Instruments
605 Ltd., UK) in slicing solution (in mM): N-Methyl-D-Glucamine 93, KCl 2.5, NaH_2PO_4 1.2,
606 $NaHCO_3$ 30, HEPES 20, D(+)-Glucose 25, $MgCl_2$ 10, sodium ascorbate 5, thiourea 2, sodium
607 pyruvate 3, N-acetyl-cystein 1, kynurenic acid 1 and $CaCl_2$ 0.5 (pH 7.3). Immediately after
608 cutting, slices were allowed to briefly recover at 37°C in the oxygenated sucrose-based buffer (in
609 mM): sucrose 230, KCl 2.5, $NaHCO_3$ 26, NaH_2PO_4 1.25, D(+)-glucose 25, $CaCl_2$ 0.8 and $MgCl_2$
610 8. D-APV and minocycline at a final concentration of 50µM and 50nM, respectively, were added
611 to the sucrose-based buffer. Slices were allowed to fully recover in bubbled BBS with 50mM
612 minocycline at 37°C for at least 40min before starting the experiment, then maintained at RT for
613 a maximum time of 8h (from slicing time). Patch clamp borosilicate glass pipettes with 3-6MΩ
614 resistance were filled with the following internal solutions:
615
616 1. Cesium metanesulfonate solution (CsMe solution, for EPSC elicited from CF and PF),
617 containing (in mM) $CsMeSO_3$ 135, NaCl 6, $MgCl_2$ 1, HEPES 10, MgATP 4, Na_2GTP 0.4, EGTA
618 1.5, QX314Cl 5, TEA 5 and biocytin 2.6 (pH 7.3).
619

620 2. CsMe S-solution (for delayed EPSC quanta events), containing (in mM): $CsMeSO_3$ 140,
621 $MgCl_2$ 0.5, HEPES 10, MgATP 4, Na_2GTP 0.5, BAPTA 10 and neurobiotin 1% (pH 7.35).
622
623 3. Potasium Gluconate solution (KGlu solution, for PF long-term plasticity), containing (in mM):
624 K Gluconate 136, KCl 10, HEPES 10, $MgCl_2$ 1, sucrose 16, MgATP 4 and Na_2GTP 0.4 (pH
625 7.35).
626
627 Stimulation electrodes with ~5 MΩ resistances were pulled from borosilicate glass pipettes and
628 filled with BBS. Recordings were performed at room temperature on slices continuously
629 perfused with oxygenated BBS. The experiment started at least 20min after the whole-cell
630 configuration was established. The Digitimer DS3 (Digitimer Ltd) stimulator was used to elicit
631 CF and PF and neuronal connectivity responses in PCs. Patch-clamp experiments were
632 conducted in voltage clamp mode (except for the LTP and long-term depression (LTD) induction
633 protocols that were made under current clamp mode) using a MultiClamp 700B amplifier
634 (Molecular Devices, California, USA) and acquired using the freeware WinWCP written by John
635 Dempster (https://pureportal.strath.ac.uk/en/datasets/strathclyde-electrophysiology-software-
636 winwcp-winedr). Series resistance was compensated by 60-100% and cells were discarded if
637 significant changes were detected. Currents were low-pass filtered at 2.2kHz and digitized at
638 20kHz.
639
640 CF and PF-EPSC experiments: To isolate the AMPARs current, the BBS was supplemented with
641 (in mM) picrotoxin 0.1, D-AP5 10, CGP52432 0.001, JNJ16259685 0.002, DPCPX 0.0005 and
642 AM251 0.001. CF and PF EPSCs were monitored at a holding potential of -10mV. During CF
643 recordings, the stimulation electrode was placed in the granule cell layer below the clamped cell;
644 CF-mediated responses were identified by the typical all-or-none response and strong depression
645 displayed by the second response elicited during paired pulse stimulations (20Hz). The number
646 of CFs innervating the recorded PC was estimated from the number of discrete CF-EPSC steps.
647 PF stimulation was achieved by placing the stimulation electrode in the molecular layer at the
648 minimum distance required to avoid direct stimulation of the dendritic tree of the recorded PC.
649 The input-output curve was obtained by incrementally increasing the stimulation strength. Peak
650 EPSC values for PF were obtained following averaging of three consecutive recordings, values
651 for CF-EPSC correspond to the first recording. Short-term plasticity experiments were analyzed
652 using a software written in Python by Antoine Valera (http://synaptiqs.wixsite.com/synaptiqs).
653
654 PF-Long-term plasticity experiments: PCs were clamped at -60mV. Each PF-induced response
655 was monitored by a test protocol of paired stimulation pulses (20Hz) applied every 20s. A
656 baseline was established during 10min of paired-pulse stimulation in the voltage clamp
657 configuration. After that, an induction protocol was applied in current-clamp mode with cells
658 held at -60mV. During LTD induction, the PFs were stimulated with two pulses at high
659 frequency (200Hz) and, after 100ms, the CF was stimulated with four pulses at high frequency
660 (200Hz) repeated every 2 seconds for a period of 10min. During LTP induction, recordings were
661 made using BBS not supplemented with picrotoxin and the PFs were stimulated with bursts of 15
662 pulses at high frequency (100 Hz) repeated every 3s for a period of 5min (Binda et al., 2016).
663 Then, PCs were switched to the voltage clamp mode and paired stimulation pulses applied again,
664 lasting 40min. All the data were normalized to the mean baseline. Long-term plasticity was
665 analyzed with the software Igor Pro 6.05 (WaveMetrics INC, Oregon, USA).

666
667 PF and CF delayed EPSC quanta events were detected and analyzed using the software Clampfit
668 10.7 (Molecular Devices). PF- and CF-delayed EPSC quanta superposed events were discarded
669 manually based on the waveform. A threshold of 10pA for minimal amplitude was used to select
670 the CF events. 100 (PF) and 300 (CF) events for each neuron were studied by analyzing
671 consecutive traces.
672
673 **High density microelectrode array (MEA) analysis of Purkinje cell spiking in acute**
674 **cerebellar slices**
675 Experiments were performed on acute cerebellar slices obtained from 3-6 months-old mice in
676 artificial cerebrospinal fluid (ACSF) containing (in mM): NaCl 125, KCl 2.5, D(+)Glucose 25,
677 $NaHCO_3$ 25 , NaH_2PO_4 1.25, $CaCl_2$ 2, and $MgCl_2$ 1 and oxygenated (95% O_2 and 5% CO_2).
678 Parasagittal slices (320µm) were cut at 30°C (Huang and Uusisaari, 2013) with a vibratome
679 (7000smz-2, Campden Instruments Ltd.) at an advance speed of 0.03mm/s and vertical vibration
680 set to 0.1 - 0.3µm. Slices were then transferred to a chamber filled with oxygenated ACSF at
681 37°C and allowed to recover for 1h before recordings.
682 For recording, the slices were placed over a high-density micro electrode array of 4096
683 electrodes (electrode size, 21 × 21µm; pitch, 42µm; 64 × 64 matrix; Biocam X, 3Brain,
684 Wädenswil, Switzerland), and constantly perfused with oxygenated ACSF at 37C°. Extracellular
685 activity was digitized at 17 kHz and data were analyzed with the Brainwave software (3Brain).
686 The signal was filtered with a butterworth high-pass filter at 200 Hz, spikes were detected with a
687 hard threshold set at -100µV, and unsupervised spike sorting was done by the software. We
688 selected units with a firing rate between 15 and 100 spikes per second and we excluded units
689 presenting more than 5% of refractory period violation (set to 3ms). Recordings were performed
690 on two slices per animal, each slice containing between 20 and 200 active neurons, and results
691 were then pooled for each animal.
692 To quantify the average variability in the firing rate, the coefficient of variation (CV) of the
693 interspike interval (ISI) in seconds) was calculated as the ratio of the standard deviation (SD) of
694 ISIs to the mean ISI of a given cell. To measure the firing pattern variability within a short
695 period of two ISIs, CV2 was calculated [$CV2 = 2|ISI_{n+1} - ISI_n|/(ISI_{n+1} + ISI_n)$] (Holt and
696 Douglas, 1996).
697
698 **Affinity-purification of SUSD4 interactors from synaptosome preparations**
699 HEK293H (Gibco, Massachusetts, USA, Cat#11631-017) were maintained at 37ºC in a
700 humidified incubator with 5% CO_2 in Dulbecco's Modified Eagle's Medium (DMEM;
701 containing high glucose and glutamax, Life Technologies, Cat#31966047) supplemented with
702 10% fetal bovine serum (FBS, Gibco, Cat#16141-079), and 1% penicillin/streptomycin (Gibco,
703 Cat#15140122). 10^6 cells were plated per well in a 6-well plate and transfected 24 hours (h) after
704 plating with the indicated plasmids (1µg plasmid DNA per well) using Lipofectamine 2000
705 (Invitrogen, Cat#11668-019) according to manufacturer's instructions.
706 48h after transfection, cells were lysed and proteins were solubilized for 1h at 4°C under gentle
707 rotation in lysis buffer (10mM Tris-HCl pH7.5, 10mM EDTA, 150mM NaCl, 1% Triton X100
708 (Tx; Sigma, Cat#x100), 0.1% SDS) supplemented with a protease inhibitor cocktail (1:100;
709 Sigma, Cat#P8340) and MG132 (100µM; Sigma, Cat#C2211). Lysates were sonicated for 10
710 seconds, further solubilized for 1h at 4°C and clarified by centrifugation at 6000 r.p.m. during 8
711 minutes (min). Supernatants were collected, incubated with 5µg of rat monoclonal anti-HA

712 antibody (for details see antibodies), together with 60µL of protein G-sepharose beads (Sigma;
713 Cat#10003D) for 3h at 4°C, to coat the beads with the HA-tagged SUSD4 proteins. When
714 SUSD4-GFP was expressed for affinity-pulldowns, GFP-Trap was done according to the
715 instructions of GFP-Trap®_A (Chromotek, New York, USA, Cat#ABIN509397). Coated beads
716 were washed 3 times with 1mL lysis buffer.
717 To prepare synaptosome fractions, cerebella from WT mice (P30) were homogenized at 4°C in
718 10 volumes (w/v) of 10mM Tris buffer (pH7.4) containing 0.32M sucrose and protease inhibitor
719 cocktail (1:100). The resulting homogenate was centrifuged at 800g for 5min at 4ºC to remove
720 nuclei and cellular debris. Synaptosomal fractions were purified by centrifugation for 20min at
721 20000 r.p.m. (SW41Ti rotor) at 4ºC using Percoll-sucrose density gradients (2-6-10-20%; v/v).
722 Each fraction from the 10 - 20% interface was collected and washed in 10mL of a 5mM HEPES
723 buffer pH 7.4 (NaOH) containing 140mM NaCl, 3mM KCl, 1.2mM $MgSO_4$, 1.2mM $CaCl_2$,
724 1mM NaH_2PO_4, 5mM $NaHCO_3$ and 10mM D(+)-Glucose by centrifugation. The suspension was
725 immediately centrifuged at 10000g at 4ºC for 10min. Synaptosomes in the pellet were
726 resuspended in 100µL of lysis buffer (10mM Tris-HCl pH7.5, 10mM EDTA, 150mM NaCl, 1%
727 Tx) supplemented with a protease inhibitor cocktail (1:100) and MG132 (100µM). Lysates were
728 sonicated for 10 seconds, and further incubated for 1h at 4°C. HA-SUSD4, GFP-SUSD4 or its
729 control GFP coated beads were then incubated with the synaptosomal lysates for 3h at 4°C.
730 Beads were washed three times with lysis buffer supplemented with 0.1% SDS. Bound proteins
731 were eluted for 10min at 75°C using Laemmli buffer (160mM Tris ph6.8, 4% SDS, 20%
732 glycérol, 0.008% BBP) with 5% β-mercaptoethanol before SDS-PAGE followed by western
733 blotting or mass spectrometry.
734
735 **Co-Immunoprecipitation experiments in HEK293 cells**
736 10^6 HEK293H cells were plated per well in 6-well plates and transfected 24h after plating with
737 the indicated plasmids (1.6µg plasmid SEPGluA2 per well, using a molar ratio of 2:1
738 SEPGluA2:other plasmid) using Lipofectamine 2000 according to manufacturer's instructions.
739 For anti-HA pull downs, proteins from HEK293 cell lysates were solubilized in lysis buffer (1M
740 Tris-HCl pH8, 10mM EDTA, 1,5M NaCl, 1% Tergitol TM. (sigma; Cat#NP40), 2% Na azide,
741 10% SDS and 10% Na deoxycholate) supplemented with a protease inhibitor cocktail (1:100)
742 and MG132 (1%). Then, lysates were sonicated for 15s, further clarified by a centrifugation at
743 14000 r.p.m. for 10min. Supernatants were collected and incubated with Dynabeads protein G
744 (life technologies, Cat#10004D) and 28.8µg of rat monoclonal anti-HA antibody (for details see
745 antibodies) under gentle rotation for 1h at 4°C. Precipitates were washed three times in lysis
746 buffer and then eluted by boiling (65°C) the beads 15min in sample buffer (made from sample
747 buffer 2X concentrate, Sigma, Cat#S3401) before SDS-PAGE. For SEPGluA2 pull downs, 48h
748 after transfection, cells were washed twice in 1X PBS, lysed with 200µL of lysis buffer (50mM
749 Tris-HCl pH8 and 1% Tx) supplemented with a protease inhibitor cocktail (1:100) and MG132
750 (50µM), scraped, sonicated 3 x 5 seconds, and proteins were further solubilized for 30min at 4°C
751 under rotation. Lysates were clarified by centrifugation at 14000 r.p.m. for 10min at 4°C.
752 Supernatants (inputs) were collected and incubated with G-protein Dynabeads (ThermoFisher
753 Scientific, Cat#10004D), previously linked to mouse anti-GFP antibody (for details see
754 antibodies section), under gentle rotation for 1h at 4°C, to coat the beads with the SEP-tagged
755 GluA2 proteins and interactors. Using a magnet, coated beads were washed five times in lysis
756 buffer and bound proteins were then eluted by boiling for 15min at 65°C in 1X sample buffer
757 before SDS-PAGE and western blot analysis for detection of HA-SUSD4, GluA2 and PVRL3α.

758
759 **Mass spectrometry analysis**
760 Proteins were separated by SDS-PAGE on 10% polyacrylamide gels (Mini-PROTEAN® TGX™
761 Precast Gels, Bio-Rad, Hercules USA) and stained with Protein Staining Solution (Euromedex,
762 Souffelweyersheim France). Gel lanes were cut into five pieces and destained with 50mM
763 triethylammonium bicarbonate (TEABC) and three washes in 100% acetonitrile. Proteins were
764 digested in-gel using trypsin (1.2µg/band, Gold, Promega, Madison USA), as previously
765 described (Thouvenot et al., 2008). Digest products were dehydrated in a vacuum centrifuge.
766
767 Nano-flow liquid chromatography coupled to tandem mass spectrometry (NanoLC-MS/MS):
768 Peptides, resuspended in 3µL formic acid (0.1%, buffer A), were loaded onto a 15cm reversed
769 phase column (75mm inner diameter, Acclaim Pepmap 100® C18, Thermo Fisher Scientific)
770 and separated with an Ultimate 3000 RSLC system (Thermo Fisher Scientific) coupled to a Q
771 Exactive Plus (Thermo Fisher Scientific) *via* a nano-electrospray source, using a 120min
772 gradient of 5 to 40% of buffer B (80% ACN, 0.1% formic acid) and a flow rate of 300nL/min.
773
774 MS/MS analyses were performed in a data-dependent mode. Full scans (375 - 1,500m/z) were
775 acquired in the Orbitrap mass analyzer with a 70000 resolution at 200m/z. For the full scans, 3 x
776 10^6 ions were accumulated within a maximum injection time of 60ms and detected in the
777 Orbitrap analyzer. The twelve most intense ions with charge states ≥ 2 were sequentially isolated
778 to a target value of 1 x 10^5 with a maximum injection time of 45ms and fragmented by HCD
779 (Higher-energy collisional dissociation) in the collision cell (normalized collision energy of
780 28%) and detected in the Orbitrap analyzer at 17500 resolution.
781
782 MS/MS data analysis: Raw spectra were processed using the MaxQuant environment ((Cox and
783 Mann, 2008), v.1.5.5.1) and Andromeda for database search (Cox et al., 2011). The MS/MS
784 spectra were matched against the UniProt Reference proteome (Proteome ID UP000000589) of
785 *Mus musculus* (release 2017_03; http://www.uniprot.org) and 250 frequently observed
786 contaminants (MaxQuant contaminants database) as well as reversed sequences of all entries.
787 The following settings were applied for database interrogation: mass tolerance of 7ppm (MS)
788 and 0.5 Th (MS/MS), trypsin/P enzyme specificity, up to two missed cleavages allowed, only
789 peptides with at least seven amino acids in length considered, and Oxidation (Met) and
790 acetylation (protein N-term) as variable modifications. The "match between runs" (MBR) feature
791 was allowed, with a matching time window of 0.7min. FDR was set at 0.01 for peptides and
792 proteins.
793
794 A representative protein ID in each protein group was automatically selected using an in-house
795 bioinformatics tool (leading v2.1). First, proteins with the most numerous identified peptides are
796 isolated in a "match group" (proteins from the "Protein IDs" column with the maximum number
797 of "peptides counts"). For the match groups where more than one protein ID is present after
798 filtering, the best annotated protein in UniProtKB (reviewed entries rather than automatic ones),
799 highest evidence for protein existence, most annotated protein according to the number of Gene
800 Ontology Annotations (GOA Mouse version 151) is defined as the "leading" protein. Only
801 proteins identified with a minimum of two unique peptides, without MS/MS in control
802 immunoprecipitation and exhibiting more than 4-fold enrichment (assessed by spectral count
803 ratio) in Sushi domain-containing protein 4 (SUSD4) immunoprecipitation, *vs* control

804 immunoprecipitation, in the two biological replicates, were considered as potential partners of
805 SUSD4 (**Table 1**).
806
807 Gene Ontology analysis: The statistically enriched gene ontology (GO) categories for the 28
808 candidate proteins were determined by Cytoscape (v3.6) plugin ClueGO v2.5.3 (Bindea et al.,
809 2009). The molecular function category was considered (release 18.12.2018,
810 https://www.ebi.ac.uk/GOA), except evidences inferred from electronic annotations. Terms are
811 selected by different filter criteria from the ontology source: 3-8 GO level intervals, minimum of
812 4 genes per GO term and 10% of associated genes/term. A two-sided hypergeometric test for
813 enrichment analysis (Benjamini-Hochberg standard correction used for multiple testing) was
814 applied against the whole identified protein as reference set. Other predefined settings were used.
815 Each node representing a specific GO term is color-coded based on enrichment significance (p-
816 value). Edge thickness represents the calculated score (kappa, κ) to determine the association
817 strength between the terms.
818
819 **Chemical LTD and GluA2 surface biotinylation assay in cerebellar acute slices**
820 300 µm-thick parasagittal cerebellar slices were obtained from P31-P69 WT and *Susd4* KO mice
821 following the same protocol described before (Patch-clamp section). Slices were incubated for
822 2h at 37°C in oxygenated BBS with or without proteasome (50µM MG132 in DMSO,) and
823 lysosomal (100µg/mL leupeptine in water, Sigma, Cat#11034626001) inhibitors. Chemical LTD
824 was induced by incubating the slices for 5min at 37°C in BBS containing 50mM K^+ and 10µM
825 glutamate (diluted in HCl), followed by a recovery period in BBS for 30min at 37°C all under
826 oxygenation; in presence or not of inhibitors. Control slices were incubated in parallel in BBS
827 solution containing HCl. Slices were then homogenized in lysis buffer, containing: 50mM Tris-
828 HCl, 150mM NaCl, 0.1% SDS, 0.02% Na Azide, 0.5% Na Deoxycholate, 1% NP-40 and
829 protease inhibitor cocktail (1:100). Homogenates were incubated 45min at 4°C, then sonicated
830 and centrifuged at 14000 r.p.m. for 10min at 4°C. Supernatants were then heated at 65°C in 2X
831 sample buffer (Sigma, Cat#S3401) prior to western blot analysis for detection of GluA2 and
832 GluD2.
833 For GluA2 surface biotinylation assay, cerebellar slices (obtained from mice aged between P27-
834 P61) were treated as above. After a recovery period of 30min at 37°C in BBS, slices were
835 incubated in a biotinylation solution (ThermoFisher Scientific, EZ-Link™ Sulfo-NHS-SS-Biotin,
836 Cat#A39258, 0,125mg/mL) for 30min on ice without oxygen. Slices were finally washed three
837 times for 10min in PBS pH7.4 at 4°C and then homogenized in lysis buffer, containing: 50mM
838 Tris-HCl pH8, 150mM NaCl, 0.1% SDS, 0.02% Na Azide, 0.5% Na Deoxycholate, 1% NP-40
839 and protease inhibitor cocktail (1:100). Homogenates were incubated 45min at 4°C, then
840 sonicated and centrifuged at 14000 r.p.m. for 10min at 4°C. Supernatants (inputs) were collected
841 and incubated with Dynabeads MyOne Streptavidin C1 (Thermo Fisher Scientific, Cat#65001)
842 under gentle rotation overnight at 4°C. Using a magnet, beads were washed five times in lysis
843 buffer and biotinylated proteins were then eluted by boiling for 15min at 65°C in 1X sample
844 buffer before SDS-PAGE and western blot analysis for detection of GluA2.
845
846 **Immunocytochemistry**
847 Labeling of primary hippocampal neurons: Hippocampi were dissected from E18 mice embryos
848 and dissociated. $1.2x10^5$ neurons were plated onto 18 mm diameter glass cover-slips precoated
849 with 80µg/mL poly-L-ornithine (Sigma, Cat#P3655) and maintained at 37ºC in a 5% CO_2

850 humidified incubator in neurobasal medium (Gibco, Cat#21103049) supplemented with 2% B-
851 27 supplement (Gibco, Cat#17504044) and 2mM Glutamax (Gibco, Cat#35050-038). Fresh
852 culture medium (neurobasal medium supplemented with 2% B-27, 2mM L-glutamine (Gibco,
853 Cat#A2916801) and 5% horse serum (Gibco, Cat#26050088) was added every week for
854 maintenance of the neuronal cultures.

855 Hippocampal neurons at days *in vitro* 13 (DIV13) were transfected using Lipofectamine 2000
856 and 0.5µg plasmid DNA per well. After transfection, neurons were maintained in the incubator
857 for 24h, then fixed with 100% methanol for 10min at -20ºC. After rinsing with PBS, non-
858 specific binding sites were blocked using PBS containing 4% donkey serum (DS, Abcam,
859 Cat#ab7475) and 0.2% Tx Primary and secondary antibodies were diluted in PBS 1% DS / 0.2%
860 Tx and incubated 1h at room temperature. Three washes in PBS 0.2% Tx were performed before
861 and after each antibody incubation. Nuclear counterstaining was performed with Hoechst 33342
862 (Sigma, Cat#14533) for 15min at room temperature.
863 Labeling of primary cerebellar mixed cultures: Cerebellar mixed cultures were prepared from P0
864 tg/0 "B6.129-Tg(Pcp2-cre)2Mpin/J" (Stock Number: 004146, outbred, C57Bl/6J background)
865 mouse cerebella and were dissected and dissociated according to previously published protocol
866 (Tabata et al., 2000). Neurons were seeded at a density of 5x106 cells/mL. Mixed cerebellar
867 cultures were transduced at DIV3 using a Cre-dependent AAV construct that express HA-tagged
868 SUSD4 and soluble GFP (2µL of AAV2-hSYN-DIO-HA-SUSD4-2A-eGFP-WPRE at
869 4,1.10^12 GC/mL or control AAV2-hSYN-DIO-eGFP-WPRE at 5.10^12 GC/mL). At DIV17,
870 neurons were fixed with 4% PFA in PBS1X for 30min at room temperature. After rinsing with
871 PBS, non-specific binding sites were blocked using PBS containing 4% DS and 0.2% Tx.
872 Primary and secondary antibodies were diluted in PBS 1% DS and 0.2% Tx and incubated one
873 hour at room temperature. Three PBS 0.2% Tx washes were performed before and after each
874 antibody incubation. Nuclear counterstaining was performed with Hoechst 33342 for 15min at
875 room temperature.

876 **Immunohistochemistry**
877 Labeling of brain sections: 30µm-thick parasagittal brain sections were obtained using a
878 freezing microtome (SM2010R, Leica) and brains obtained after intracardiac perfusion with 4%
879 PFA in PBS solution of mice sedated with 100mg/kg pentobarbital sodium. Sections were then
880 washed three times for 5min in PBS, then blocked with PBS 4% DS for 30min. The primary
881 antibodies were diluted in PBS, 1% DS, 1% Tx. The sections were incubated in the primary
882 antibody solution overnight at 4ºC and then washed three times for 5min in PBS 1% Tx.
883 Sections were incubated in the secondary antibody, diluted in PBS 1% DS 1% Tx solution, for
884 1h at room temperature. The sections were then incubated for 15min at room temperature with
885 the nuclear marker Hoechst 33342 in PBS 0.2% Tx. Finally, the sections were washed three
886 times for 5min in PBS 1% Tx, recovered in PBS and mounted with Prolong Gold (Thermo
887 Fisher Scientific, Cat#P36934) between microscope slides and coverslips (Menzel-gläser,
888 Brunswick, Germany, Cat#15165252).
889
890 **RT-PCR and quantitative RT-PCR**
891 For standard RT-PCR, total RNA was isolated from the cortex, cerebellum and brainstem of 2-
892 month-old *Susd4* KO mice and WT control littermates, using the RNeasy mini kit (Qiagen,
893 Venlo, Netherlands, Cat#74104). Equivalent amounts of total RNA (100 ng) were reverse-
894 transcribed according to the protocol of SuperScript® VILO™ cDNA Synthesis kit (Life

895 Technologies, California, USA, Cat#11754-250) as stated by manufacturer's instructions. The
896 primers used were forward 5' TGT TAC TGC TCG TCA TCC TGG 3' and reverse 5' GAG
897 AGT CCC CTC TGC ACT TGG 3'. PCR was performed with an annealing temperature of
898 61°C, for 39 cycles, using the manufacturer's instructions (*Taq* polymerase; New England
899 Biolabs, Massachusetts, USA, Cat#M0273S). Quantitative PCR was performed using the
900 TaqMan universal master mix II with UNG (applied biosystems, Cat# 4440038) and the
901 following TaqMan probes: *Rpl13a* (#4331182_Mm01612986_gH) and *Susd4*
902 (#4331182_Mm01312134_m1).
903
904 **Western Blot analysis**
905 After samples were mixed with sample buffer, proteins were resolved by electrophoresis on a 4-
906 12% NuPAGE Bis-Tris-Gel according to Invitrogen protocols, then electrotransferred using
907 TransBlot DS Semi-dry transfer Cell or TransBlot Turbo transfer system (Bio-Rad) to PVDF
908 membrane (Immobilon-P transfer membrane, Millipore, Cat#IPVH00010). Membranes were
909 blocked in PBS supplemented with Tween 0.2% (PBST) and non-fat milk 5% and incubated
910 with primary antibodies in PBST-milk 5%. After washing three times in PBST, membranes
911 were incubated with Horseradish Peroxidase-conjugated secondary antibodies in PBST-milk
912 5%. Membranes were finally washed three times and bound antibodies were revealed
913 using Immobilon Western (Millipore, Cat#WBKLS) or Western Femto Maximum Sensitivity
914 (Thermo Fisher Scientific, Cat#34095) or SuperSignal West Dura (Thermo Fisher Scientific,
915 Cat#34075) or ECL Western Blotting substrate (Thermo Fisher Scientific,
916 Cat#32209) chemiluminescent solutions and images acquired on a Fusion FX7 system
917 (Vilber Lourmat, Île-de-France, France). Quantitation of Western blots was performed using the
918 ImageJ software on raw images under non-saturating conditions. Band intensities of proteins of
919 interest were obtained after manually selecting a rectangular region around the band. The signal
920 intensity of the band of interest was then normalized to the signal intensity of the corresponding
921 βACTIN (used as a loading control). For quantifications of immunoprecipitation experiments,
922 input intensities were normalized to βACTIN, and then the intensities of immunoprecipitated
923 protein bands were normalized to the normalized inputs, unless otherwise stated.
924
925 **Image acquisition and quantification**
926 *In situ* hybridization images were acquired using an Axio Zoom. V16 (Zeiss, Oberkochen,
927 Germany) microscope equipped with a digital camera (AxioCam HRm) using a 10x objective
928 (pixel size 0.650µm).
929 Immunofluorescence image stacks were acquired using a confocal microscope (SP5, Leica),
930 using a 63x objective (1,4NA, oil immersion, pixel size: 57nm for cell culture imaging, pixel
931 size: 228nm for 63x; 76nm, 57nm, 45nm for higher magnifications for *in vivo* imaging). The
932 pinhole aperture was set to 1 Airy Unit and a z-step of 200 nm was used. Laser intensity and
933 photomultiplier tube (PMT) gain was set so as to occupy the full dynamic range of the detector.
934 Images were acquired in 16-bit range. Immunofluorescence images and image stacks from
935 figure 1C, 1D and 4F were acquired using a Zeiss LSM 980 Confocal with an Airyscan detector
936 (v2.0), using a 63x objective (1,4NA, oil immersion, pixel size: 43nm, z-step of 150nm).
937 Deconvolution was performed for the VGLUT1 images with Huygens 4.1 software (Scientific
938 Volume Imaging) using Maximum Likelihood Estimation algorithm from Matlab. 40 iterations
939 were applied in classical mode, background intensity was averaged from the voxels with lowest
940 intensity, and signal to noise ratio values were set to a value of 25.

941 VGLUT1 and VGLUT2 puncta were analyzed using the Matlab software and a homemade code
942 source (Dr. Andréa Dumoulin). The number, area and intensity of puncta were quantified using
943 the mask of each puncta generated by the Multidimensional Image analysis software (MIA)
944 from Metamorph® (Molecular Devices). For each animal, puncta parameters were measured
945 from four equidistant images within a 35-image stack at 160 nm interval, acquired from three
946 different lobules (n=12).
947 The software ImageJ was used to measure the total area of a cerebellar section from images of
948 staining obtained with the nuclear marker Hoechst. The extension of the molecular layer was
949 measured using images of the anti-CABP staining. Nine parasagittal sections were analyzed per
950 animal. The data presented correspond to the mean per animal.
951
952 **Statistical analysis**
953 Data from all experiments were imported in Prism (GraphPad Software, California, USA) for
954 statistical analysis, except for electrophysiology data that were imported to Igor Pro 6.05
955 (WaveMetrics INC) for statistical analysis.
956 In the case of two column analyses of means, the differences between the two groups were
957 assessed using two-tailed Student's t-test. Normality of populations were assessed using
958 D'Agostino & Pearson, Shapiro-Wilk and Kolmogorov-Smirnov normality tests. When groups
959 did not fit the normal distribution, the non-parametric Mann-Whitney test was used. For the
960 rotarod behavioral test (two variables, genotype and trial), two-way repeated measures ANOVA
961 followed by Bonferroni post hoc test was performed. The two-tailed Student's one sample t-test
962 (when normality criterion was met) or the two-tailed Wilcoxon Signed Rank Test was used to
963 compare ratios to a null hypothesis of 1 for biochemical experiments or 100 for long-term
964 plasticity (Fay, 2013). Differences in cumulative probability were assessed with the
965 Kolmogorov-Smirnov distribution test, and differences in distribution were tested using the Chi-
966 squared test.
967
968 **Acknowledgments:** We gratefully acknowledge the Collège de France imaging facility
969 (IMACHEM-IBiSA), in particular P. Mailly for help with the design of the macro for GluA2
970 quantification and Estelle Anceaume for help with image acquisition. We also thank the
971 personnel from the CIRB, INCI and chronobiotron CNRS UMS 3415, IBPS and IBENS animal
972 facilities. We would like to thank Philippe Marin for advice on proteomics analysis. Mass
973 spectrometry experiments were carried out using facilities of the Functional Proteomics Platform
974 of Montpellier.

975 **Supplementary Information:**
976 Table S1
977

978 **References**

979 Anggono V, Huganir RL. 2012. Regulation of AMPA receptor trafficking and synaptic
980 plasticity. *Curr Opin Neurobiol* **22**:461–469. doi:10.1016/j.conb.2011.12.006

981 Atluri PP, Regehr WG. 1996. Determinants of the Time Course of Facilitation at the Granule
982 Cell to Purkinje Cell Synapse. *J Neurosci* **16**:5661–5671.

983 Auerbach BD, Osterweil EK, Bear MF. 2011. Mutations causing syndromic autism define an
984 axis of synaptic pathophysiology. *Nature* **480**:63–68. doi:10.1038/nature10658

985 Badura A, Verpeut JL, Metzger JW, Pereira TD, Pisano TJ, Deverett B, Bakshinskaya DE, Wang
986 SS-H. 2018. Normal cognitive and social development require posterior cerebellar activity.
987 *Elife* **7**:1–36. doi:10.7554/eLife.36401

988 Bassani S, Cingolani LA, Valnegri P, Folci A, Zapata J, Gianfelice A, Sala C, Goda Y, Passafaro
989 M. 2012. The X-Linked Intellectual Disability Protein TSPAN7 Regulates Excitatory
990 Synapse Development and AMPAR Trafficking. *Neuron* **73**:1143–1158.
991 doi:10.1016/j.neuron.2012.01.021

992 Baudouin SJ, Gaudias J, Gerharz S, Hatstatt L, Zhou K, Punnakkal P, Tanaka KF, Spooren W,
993 Hen R, De Zeeuw CI, Vogt K, Scheiffele P. 2012. Shared synaptic pathophysiology in
994 syndromic and nonsyndromic rodent models of autism. *Science (80-).*
995 doi:10.1126/science.1224159

996 Binda F, Dorgans K, Reibel S, Sakimura K, Kano M, Poulain B, Isope P. 2016. Inhibition
997 promotes long-Term potentiation at cerebellar excitatory synapses. *Sci Rep* **6**:1–12.
998 doi:10.1038/srep33561

999 Bindea G, Mlecnik B, Hackl H, Charoentong P, Tosolini M, Kirilovsky A, Fridman W, Pagès F,
1000 Trajanoski Z, Galon J. 2009. ClueGO : a Cytoscape plug-in to decipher functionally
1001 grouped gene ontology and pathway annotation networks **25**:1091–1093.
1002 doi:10.1093/bioinformatics/btp101

1003 Boase NA, Kumar S. 2015. NEDD4: The founding member of a family of ubiquitin-protein
1004 ligases. *Gene* **557**:113–122. doi:10.1016/j.gene.2014.12.020

1005 Bolliger MF, Martinelli DC, Sudhof TC. 2011. The cell-adhesion G protein-coupled receptor
1006 BAI3 is a high-affinity receptor for C1q-like proteins. *Proc Natl Acad Sci* **108**:2534–2539.
1007 doi:10.1073/pnas.1019577108

1008 Buitrago MM, Schulz JB, Dichgans J, Luft AR. 2004. Short and long-term motor skill learning
1009 in an accelerated rotarod training paradigm. *Neurobiol Learn Mem* **81**:211–216.
1010 doi:10.1016/j.nlm.2004.01.001

1011 Chen Z, Jiang H, Xu W, Li X, Dempsey DR, Zhang X, Devreotes P, Wolberger C, Amzel LM,
1012 Gabelli SB, Cole PA. 2017. A Tunable Brake for HECT Ubiquitin Ligases. *Mol Cell*
1013 **66**:345-357.e6. doi:10.1016/j.molcel.2017.03.020

1014 Cheon S, Dean M, Chahrour M. 2018. The ubiquitin proteasome pathway in neuropsychiatric
1015 disorders. *Neurobiol Learn Mem* 106791. doi:10.1016/j.nlm.2018.01.012

1016 Chiu SL, Diering GH, Ye B, Takamiya K, Chen CM, Jiang Y, Niranjan T, Schwartz CE, Wang
1017 T, Huganir RL. 2017. GRASP1 Regulates Synaptic Plasticity and Learning through
1018 Endosomal Recycling of AMPA Receptors. *Neuron* **93**:1405-1419.e8.
1019 doi:10.1016/j.neuron.2017.02.031

1020 Choquet D, Triller A. 2013. The dynamic synapse. *Neuron* **80**:691–703.
1021 doi:10.1016/j.neuron.2013.10.013

1022 Chung HJ, Steinberg JP, Huganir RL, Linden DJ. 2003. Requirement of AMPA receptor GluR2
1023 phosphorylation for cerebellar long-term depression. *Science (80-)* **300**:1751–1755.
1024 doi:10.1126/science.1082915

1025 Coe BP, Stessman HAF, Sulovari A, Geisheker MR, Bakken TE, Lake AM, Dougherty JD, Lein

1026 ES, Hormozdiari F, Bernier RA, Eichler EE. 2019. Neurodevelopmental disease genes
1027 implicated by de novo mutation and copy number variation morbidity. *Nat Genet* **51**:106–
1028 116. doi:10.1038/s41588-018-0288-4

1029 Coesmans M, Weber JT, De Zeeuw CI, Hansel C. 2004. Bidirectional parallel fiber plasticity in
1030 the cerebellum under climbing fiber control. *Neuron* **44**:691–700.
1031 doi:10.1016/j.neuron.2004.10.031

1032 Collingridge GL, Peineau S, Howland JG, Wang YT. 2010. Long-term depression in the CNS.
1033 *Nat Rev Neurosci* **11**:459–473. doi:10.1038/nrn2867

1034 Cong Q, Soteros BM, Wollet M, Kim JH, Sia GM. 2020. The endogenous neuronal complement
1035 inhibitor SRPX2 protects against complement-mediated synapse elimination during
1036 development. *Nat Neurosci*. doi:10.1038/s41593-020-0672-0

1037 Cox J, Mann M. 2008. MaxQuant enables high peptide identification rates, individualized p.p.b.-
1038 range mass accuracies and proteome-wide protein quantification. *Nat Biotechnol* **26**:1367–
1039 72. doi:10.1038/nbt.1511

1040 Cox J, Neuhauser N, Michalski A, Scheltema RA, Olsen J V., Mann M. 2011. Andromeda: A
1041 peptide search engine integrated into the MaxQuant environment. *J Proteome Res* **10**:1794–
1042 1805. doi:10.1021/pr101065j

1043 Crawley JN. 2006. What's Wrong With My Mouse?: Behavioral Phenotyping of Transgenic and
1044 Knockout Mice: Second Edition, What's Wrong With My Mouse?: Behavioral Phenotyping
1045 of Transgenic and Knockout Mice: Second Edition. doi:10.1002/9780470119051

1046 Crepel F, Mariani J, Delhaye-Bouchaud N. 1976. Evidence for a multiple innervation of purkinje
1047 cells by climbing fibers in the immature rat cerebellum. *J Neurobiol* **7**:567–578.
1048 doi:10.1002/neu.480070609

1049 Cuscó I, Medrano A, Gener B, Vilardell M, Gallastegui F, Villa O, González E, Rodríguez-
1050 Santiago B, Vilella E, Del Campo M, Pérez-Jurado LA. 2009. Autism-specific copy number
1051 variants further implicate the phosphatidylinositol signaling pathway and the glutamatergic
1052 synapse in the etiology of the disorder. *Hum Mol Genet* **18**:1795–1804.
1053 doi:10.1093/hmg/ddp092

1054 Diering GH, Huganir RL. 2018. The AMPA Receptor Code of Synaptic Plasticity. *Neuron*
1055 **100**:314–329. doi:10.1016/j.neuron.2018.10.018

1056 Ehlers MD. 2000. Reinsertion or degradation of AMPA receptors determined by activity-
1057 dependent endocytic sorting. *Neuron* **28**:511–525. doi:10.1016/S0896-6273(00)00129-X

1058 Fay DS. 2013. A biologist's guide to statistical thinking and analysis. *WormBook*.
1059 doi:10.1895/wormbook.1.159.1

1060 Fernandez-Monreal M, Brown TC, Royo M, Esteban JA. 2012. The Balance between Receptor
1061 Recycling and Trafficking toward Lysosomes Determines Synaptic Strength during Long-
1062 Term Depression. *J Neurosci* **32**:13200–13205. doi:10.1523/JNEUROSCI.0061-12.2012

1063 Fiuza M, Rostosky C, Parkinson G, Bygrave A, Halemani N, Baptista M, Milosevic I, Hanley
1064 JG. 2017. PICK1 regulates AMP receptor endocytosis via direct interaction with AP2 a-
1065 appendage and dynamin. *Rockefeller Univ Press J Cell Biol* **216**:3323–3338.
1066 doi:10.1083/jcb.201701034

1067 Fournier KA, Hass CJ, Naik SK, Lodha N, Cauraugh JH. 2010. Motor coordination in autism
1068 spectrum disorders: A synthesis and meta-analysis. *J Autism Dev Disord* **40**:1227–1240.
1069 doi:10.1007/s10803-010-0981-3

1070 Gao Z, Van Beugen BJ, De Zeeuw CI. 2012. Distributed synergistic plasticity and cerebellar
1071 learning. *Nat Rev Neurosci*. doi:10.1038/nrn3312

1072 Gendrel M, Rapti G, Richmond JE, Bessereau J-L. 2009. A secreted complement-control-related
1073 protein ensures acetylcholine receptor clustering. *Nature* **461**:992–996.
1074 doi:10.1038/nature08430

1075 Gotow T, Sotelo C. 1987. Postnatal development of the inferior olivary complex in the rat: IV.
1076 Synaptogenesis of GABAergic afferents, analyzed by glutamic acid decarboxylase
1077 immunocytochemistry. *JComp Neurol* **263**:526–552. doi:10.1002/cne.902630406

1078 Gutierrez-Castellanos N, Da Silva-Matos CM, Zhou K, Canto CB, Renner MC, Koene LMC,
1079 Ozyildirim O, Sprengel R, Kessels HW, De Zeeuw CI. 2017. Motor Learning Requires
1080 Purkinje Cell Synaptic Potentiation through Activation of AMPA-Receptor Subunit GluA3.
1081 *Neuron* **93**:409–424. doi:10.1016/j.neuron.2016.11.046

1082 Hashimoto K, Kano M. 2003. Functional differentiation of multiple climbing fiber inputs during
1083 synapse elimination in the developing cerebellum. *Neuron* **38**:785–796. doi:10.1016/S0896-
1084 6273(03)00298-8

1085 Hirai H, Pang Z, Bao D, Miyazaki T, Li L, Miura E, Parris J, Rong Y, Watanabe M, Yuzaki M,
1086 Morgan JI. 2005. Cbln1 is essential for synaptic integrity and plasticity in the cerebellum.
1087 *Nat Neurosci* **8**:1534–1541. doi:10.1038/nn1576

1088 Hirano T. 2018. Regulation and Interaction of Multiple Types of Synaptic Plasticity in a Purkinje
1089 Neuron and Their Contribution to Motor Learning. *Cerebellum* **17**:756–765.

1090 Holmquist E, Okroj M, Nodin B, Jirström K, Blom AM. 2013. Sushi domain-containing protein
1091 4 (SUSD4) inhibits complement by disrupting the formation of the classical C3 convertase.
1092 *FASEB J* **27**:2355–2366. doi:10.1096/fj.12-222042

1093 Holt GR, Douglas J. 1996. Comparison of Discharge Variability Visual Cortex Neurons. *J*
1094 *Neurophysiol* **75**:1806–1814.

1095 Huang S, Uusisaari MY. 2013. Elevated temperature during slicing enhances acute slice
1096 preparation quality. *Front Cell Neurosci* **7**:1–8. doi:10.3389/fncel.2013.00048

1097 Ichise T, Kano M, Hashimoto K, Yanagihara D, Nakao K, Shigemoto R, Katsuki M, Aiba a.
1098 2000. mGluR1 in cerebellar Purkinje cells essential for long-term depression, synapse
1099 elimination, and motor coordination. *Science* **288**:1832–1835.
1100 doi:10.1126/science.288.5472.1832

1101 Ito M. 2006. Cerebellar circuitry as a neuronal machine. *Prog Neurobiol* **78**:272–303.
1102 doi:10.1016/j.pneurobio.2006.02.006

1103 Ito M. 2001. Cerebellar Long-Term Depression: Characterization, Signal Transduction, and
1104 Functional Roles. *Physiol Rev* **81**:1143–1195. doi:10.1152/physrev.2001.81.3.1143

1105 Ito M, Kano M. 1982. Long-lasting depression of parallel fiber-Purkinje cell transmission
1106 induced by conjunctive stimulation of parallel fibers and climbing fibers in the cerebellar

1107 cortex. *Neurosci Lett* **33**:253–258. doi:10.1016/0304-3940(82)90380-9

1108 Kakegawa W, Katoh A, Narumi S, Miura E, Motohashi J, Takahashi A, Kohda K, Fukazawa Y,
1109 Yuzaki M, Matsuda S. 2018. Optogenetic Control of Synaptic AMPA Receptor Endocytosis
1110 Reveals Roles of LTD in Motor Learning. *Neuron* **99**:985-998.e6.
1111 doi:10.1016/j.neuron.2018.07.034

1112 Kakegawa W, Mitakidis N, Miura E, Abe M, Matsuda K, Takeo YH, Kohda K, Motohashi J,
1113 Takahashi A, Nagao S, Muramatsu S ichi, Watanabe M, Sakimura K, Aricescu AR, Yuzaki
1114 M. 2015. Anterograde C1ql1 signaling is required in order to determine and maintain a
1115 single-winner climbing fiber in the mouse cerebellum. *Neuron* **85**:316–330.
1116 doi:10.1016/j.neuron.2014.12.020

1117 Kashiwabuchi N, Ikeda K, Araki K, Hirano T, Shibuki K, Takayama C, Inoue Y, Kutsuwada T,
1118 Yagi T, Kang Y, Aizawa S, Mishina M. 1995. Impairment of Motor Coordination, Purkinje
1119 Cell Synapse Formation, and Cerebellar Long-Term Depression in GluRd2 Mutant Mice.
1120 *Cell* **81**:245–252.

1121 Kawabe H, Neeb A, Dimova K, Young SM, Takeda M, Katsurabayashi S, Mitkovski M,
1122 Malakhova OA, Zhang DE, Umikawa M, Kariya K ichi, Goebbels S, Nave KA, Rosenmund
1123 C, Jahn O, Rhee JS, Brose N. 2010. Regulation of Rap2A by the Ubiquitin Ligase Nedd4-1
1124 Controls Neurite Development. *Neuron* **65**:358–372. doi:10.1016/j.neuron.2010.01.007

1125 Kayakabe M, Kakizaki T, Kaneko R, Sasaki A, Nakazato Y, Shibasaki K, Ishizaki Y, Saito H,
1126 Suzuki N, Furuya N, Yanagawa Y. 2014. Motor dysfunction in cerebellar Purkinje cell-
1127 specific vesicular GABA transporter knockout mice. *Front Cell Neurosci* **7**:1–11.
1128 doi:10.3389/fncel.2013.00286

1129 Kim T, Yamamoto Y, Tanaka-Yamamoto K. 2017. Timely regulated sorting from early to late
1130 endosomes is required to maintain cerebellar long-term depression. *Nat Commun* **8**.
1131 doi:10.1038/s41467-017-00518-3

1132 Konnerth A, Llanot I, Armstrongt CM. 1990. Synaptic currents in cerebellar Purkinje cells.
1133 *Neurobiology* **87**:2662–2665. doi:10.1073/pnas.87.7.2662

1134 Lalonde R, Strazielle C. 2001. Motor performance and regional brain metabolism of spontaneous
1135 murine mutations with cerebellar atrophy **125**:103–108.

1136 Lee KY, Jewett KA, Chung HJ, Tsai NP. 2018. Loss of fragile X protein FMRP impairs
1137 homeostatic synaptic downscaling through tumor suppressor p53 and ubiquitin E3 ligase
1138 Nedd4-2. *Hum Mol Genet* **27**:2805–2816. doi:10.1093/hmg/ddy189

1139 Lee SH, Liu L, Wang YT, Sheng M. 2002. Clathrin adaptor AP2 and NSF interact with
1140 overlapping sites of GluR2 and play distinct roles in AMPA receptor trafficking and
1141 hippocampal LTD. *Neuron* **36**:661–674. doi:10.1016/S0896-6273(02)01024-3

1142 Lee SH, Simonetta A, Sheng M. 2004. Subunit rules governing the sorting of internalized AMPA
1143 receptors in hippocampal neurons. *Neuron* **43**:221–236. doi:10.1016/j.neuron.2004.06.015

1144 Lefort JM, Vincent J, Tallot L, Jarlier F, De Zeeuw CI, Rondi-Reig L, Rochefort C. 2019.
1145 Impaired cerebellar Purkinje cell potentiation generates unstable spatial map orientation and
1146 inaccurate navigation. *Nat Commun* **10**:1–13. doi:10.1038/s41467-019-09958-5

1147 Leto K, Arancillo M, Becker EBE, Buffo A, Chiang C, Ding B, Dobyns WB, Dusart I, Haldipur

1148 P, Hatten ME, Hoshino M, Joyner AL, Kano M, Kilpatrick DL, Koibuchi N, Marino S,
1149 Martinez S, Millen KJ, Millner TO, Miyata T, Parmigiani E, Schilling K, Sekerková G,
1150 Sillitoe R V., Sotelo C, Uesaka N, Wefers A, Wingate RJT, Hawkes R. 2016. Consensus
1151 Paper: Cerebellar Development. *The Cerebellum* **15**:789–828. doi:10.1007/s12311-015-
1152 0724-2

1153 Lin A, Hou Q, Jarzylo L, Amato S, Gilbert J, Shang F, Man HY. 2011. Nedd4-mediated AMPA
1154 receptor ubiquitination regulates receptor turnover and trafficking. *J Neurochem* **119**:27–39.
1155 doi:10.1111/j.1471-4159.2011.07221.x

1156 Lussier MP, Nasu-Nishimura Y, Roche KW. 2011. Activity-dependent ubiquitination of the
1157 AMPA receptor subunit GluA2. *J Neurosci* **31**:3077–3081. doi:10.1523/JNEUROSCI.5944-
1158 10.2011

1159 Masugi-Tokita M, Tarusawa E, Watanabe M, Molnár E, Fujimoto K, Shigemoto R. 2007.
1160 Number and density of AMPA receptors in individual synapses in the rat cerebellum as
1161 revealed by SDS-digested freeze-fracture replica labeling. *J Neurosci* **27**:2135–2144.
1162 doi:10.1523/JNEUROSCI.2861-06.2007

1163 Mathy A, Ho SSN, Davie JT, Duguid IC, Clark BA, Häusser M. 2009. Encoding of Oscillations
1164 by Axonal Bursts in Inferior Olive Neurons. *Neuron* **62**:388–399.
1165 doi:10.1016/j.neuron.2009.03.023

1166 Matsuda K, Miura E, Miyazaki T, Kakegawa W, Emi K, Narumi S, Fukazawa Y, Ito-Ishida A,
1167 Kondo T, Shigemoto R, Watanabe M, Yuzaki M. 2010. Cbln1 is a ligand for an orphan
1168 glutamate receptor delta2, a bidirectional synapse organizer. *Science* **328**:363–368.

1169 Matsuda S, Kakegawa W, Budisantoso T, Nomura T, Kohda K, Yuzaki M. 2013. Stargazin
1170 regulates AMPA receptor trafficking through adaptor protein complexes during long-term
1171 depression. *Nat Commun* **4**:1–15. doi:10.1038/ncomms3759

1172 Nakayama M, Suzuki E, Tsunoda S -i., Hama C. 2016. The Matrix Proteins Hasp and Hig
1173 Exhibit Segregated Distribution within Synaptic Clefts and Play Distinct Roles in
1174 Synaptogenesis. *J Neurosci* **36**:590–606. doi:10.1523/JNEUROSCI.2300-15.2016

1175 Nicoll RA. 2017. A Brief History of Long-Term Potentiation. *Neuron* **93**:281–290.
1176 doi:10.1016/j.neuron.2016.12.015

1177 Park M, Penick E, Edwards J, Kauer J, Ehlers MD. 2004. Recycling Endosomes Supply AMPA
1178 Receptors for Long-term Potentiation. *Science (80-)* **305**:1972–1975.

1179 Penn AC, Zhang CL, Georges F, Royer L, Breillat C, Hosy E, Petersen JD, Humeau Y, Choquet
1180 D. 2017. Hippocampal LTP and contextual learning require surface diffusion of AMPA
1181 receptors. *Nature* **549**:384–388. doi:10.1038/nature23658

1182 Piochon C, Kloth AD, Grasselli G, Titley HK, Nakayama H, Hashimoto K, Wan V, Simmons
1183 DH, Eissa T, Nakatani J, Cherskov A, Miyazaki T, Watanabe M, Takumi T, Kano M, Wang
1184 SSH, Hansel C. 2014. Cerebellar plasticity and motor learning deficits in a copy-number
1185 variation mouse model of autism. *Nat Commun* **5**:1–12. doi:10.1038/ncomms6586

1186 Rochefort C, Arabo A, Andre M, Poucet B, Save E, Rondi-Reig L. 2011. Cerebellum Shapes
1187 Hippocampal Spatial Code. *Science (80-)* **334**:385–389.

1188 Rondi-Reig L, Delhaye-Bouchaud N, Mariani J, Caston J. 1997. Role of the inferior olivary

1189 complex in motor skills and motor learning in the adult rat. *Neuroscience* **77**:955–963.
1190 doi:10.1016/S0306-4522(96)00518-0

1191 Rosenfeld JA, Lacassie Y, El-Khechen D, Escobar LF, Reggin J, Heuer C, Chen E, Jenkins LS,
1192 Collins AT, Zinner S, Babcock M, Morrow B, Schultz RA, Torchia BS, Ballif BC,
1193 Tsuchiya KD, Shaffer LG. 2011. New cases and refinement of the critical region in the
1194 1q41q42 microdeletion syndrome. *Eur J Med Genet* **54**:42–49.
1195 doi:10.1016/j.ejmg.2010.10.002

1196 Salpietro V, Dixon CL, Guo H, Bello OD, Vandrovcova J, Efthymiou S, Maroofian R, Heimer
1197 G, Burglen L, Valence S, Torti E, Hacke M, Rankin J, Tariq H, Colin E, Procaccio V,
1198 Striano P, Mankad K, Lieb A, Chen S, Pisani L, Bettencourt C, Männikkö R, Manole A,
1199 Brusco A, Grosso E, Ferrero GB, Armstrong-Moron J, Gueden S, Bar-Yosef O, Tzadok M,
1200 Monaghan KG, Santiago-Sim T, Person RE, Cho MT, Willaert R, Yoo Y, Chae JH, Quan
1201 Y, Wu H, Wang T, Bernier RA, Xia K, Blesson A, Jain M, Motazacker MM, Jaeger B,
1202 Schneider AL, Boysen K, Muir AM, Myers CT, Gavrilova RH, Gunderson L, Schultz-
1203 Rogers L, Klee EW, Dyment D, Osmond M, Parellada M, Llorente C, Gonzalez-Peñas J,
1204 Carracedo A, Van Haeringen A, Ruivenkamp C, Nava C, Heron D, Nardello R, Iacomino
1205 M, Minetti C, Skabar A, Fabretto A, Hanna MG, Bugiardini E, Hostettler I, O'Callaghan B,
1206 Khan A, Cortese A, O'Connor E, Yau WY, Bourinaris T, Kaiyrzhanov R, Chelban V,
1207 Madej M, Diana MC, Vari MS, Pedemonte M, Bruno C, Balagura G, Scala M, Fiorillo C,
1208 Nobili L, Malintan NT, Zanetti MN, Krishnakumar SS, Lignani G, Jepson JEC, Broda P,
1209 Baldassari S, Rossi P, Fruscione F, Madia F, Traverso M, De-Marco P, Pérez-Dueñas B,
1210 Munell F, Kriouile Y, El-Khorassani M, Karashova B, Avdjieva D, Kathom H, Tincheva R,
1211 Van-Maldergem L, Nachbauer W, Boesch S, Gagliano A, Amadori E, Goraya JS, Sultan T,
1212 Kirmani S, Ibrahim S, Jan F, Mine J, Banu S, Veggiotti P, Zuccotti G V., Ferrari MD, Van
1213 Den Maagdenberg AMJ, Verrotti A, Marseglia GL, Savasta S, Soler MA, Scuderi C,
1214 Borgione E, Chimenz R, Gitto E, Dipasquale V, Sallemi A, Fusco M, Cuppari C, Cutrupi
1215 MC, Ruggieri M, Cama A, Capra V, Mencacci NE, Boles R, Gupta N, Kabra M, Papacostas
1216 S, Zamba-Papanicolaou E, Dardiotis E, Maqbool S, Rana N, Atawneh O, Lim SY, Shaikh
1217 F, Koutsis G, Breza M, Coviello DA, Dauvilliers YA, AlKhawaja I, AlKhawaja M, Al-
1218 Mutairi F, Stojkovic T, Ferrucci V, Zollo M, Alkuraya FS, Kinali M, Sherifa H, Benrhouma
1219 H, Turki IBY, Tazir M, Obeid M, Bakhtadze S, Saadi NW, Zaki MS, Triki CC, Benfenati F,
1220 Gustincich S, Kara M, Belcastro V, Specchio N, Capovilla G, Karimiani EG, Salih AM,
1221 Okubadejo NU, Ojo OO, Oshinaike OO, Oguntunde O, Wahab K, Bello AH, Abubakar S,
1222 Obiabo Y, Nwazor E, Ekenze O, Williams U, Iyagba A, Taiwo L, Komolafe M, Senkevich
1223 K, Shashkin C, Zharkynbekova N, Koneyev K, Manizha G, Isrofilov M, Guliyeva U,
1224 Salayev K, Khachatryan S, Rossi S, Silvestri G, Haridy N, Ramenghi LA, Xiromerisiou G,
1225 David E, Aguennouz M, Fidani L, Spanaki C, Tucci A, Raspall-Chaure M, Chez M, Tsai A,
1226 Fassi E, Shinawi M, Constantino JN, De Zorzi R, Fortuna S, Kok F, Keren B, Bonneau D,
1227 Choi M, Benzeev B, Zara F, Mefford HC, Scheffer IE, Clayton-Smith J, Macaya A,
1228 Rothman JE, Eichler EE, Kullmann DM, Houlden H. 2019. AMPA receptor GluA2 subunit
1229 defects are a cause of neurodevelopmental disorders. *Nat Commun* **10**. doi:10.1038/s41467-
1230 019-10910-w

1231 Satterstrom FK, Kosmicki JA, Wang J, Breen MS. 2018. Large-scale exome sequencing study
1232 implicates both developmental and functional changes in the neurobiology of autism 1–43.

1233 Savas JN, De Wit J, Comoletti D, Zemla R, Ghosh A, Yates JR. 2014. Ecto-Fc MS identifies

1234 ligand-receptor interactions through extracellular domain Fc fusion protein baits and
1235 shotgun proteomic analysis. *Nat Protoc* **9**:2061–74. doi:10.1038/nprot.2014.140

1236 Schwarz LA, Hall BJ, Patrick GN. 2010. Activity-dependent ubiquitination of GluA1 mediates a
1237 distinct AMPA receptor endocytosis and sorting pathway. *J Neurosci* **30**:16718–16729.
1238 doi:10.1523/JNEUROSCI.3686-10.2010

1239 Sia GM, Clem RL, Huganir RL. 2013. The human language-associated gene SRPX2 regulates
1240 synapse formation and vocalization in mice. *Science (80-)* **342**:987–991.
1241 doi:10.1126/science.1245079

1242 Sigoillot SM, Iyer K, Binda F, González-Calvo I, Talleur M, Vodjdani G, Isope P, Selimi F.
1243 2015. The Secreted Protein C1QL1 and Its Receptor BAI3 Control the Synaptic
1244 Connectivity of Excitatory Inputs Converging on Cerebellar Purkinje Cells. *Cell Rep* 820–
1245 832. doi:10.1016/j.celrep.2015.01.034

1246 Sotelo C. 2004. Cellular and genetic regulation of the development of the cerebellar system.
1247 *Prog Neurobiol* **72**:295–339. doi:10.1016/j.pneurobio.2004.03.004

1248 Stevens B, Allen NJ, Vazquez LE, Howell GR, Christopherson KS, Nouri N, Micheva KD,
1249 Mehalow AK, Huberman AD, Stafford B, Sher A, Litke AM, Lambris JD, Smith SJ, John
1250 SWM, Barres BA. 2007. The Classical Complement Cascade Mediates CNS Synapse
1251 Elimination. *Cell* **131**:1164–1178. doi:10.1016/j.cell.2007.10.036

1252 Stoodley CJ. 2016. The Cerebellum and Neurodevelopmental Disorders. *The Cerebellum* **15**:34–
1253 37. doi:10.1007/s12311-015-0715-3

1254 Stoodley CJ, D'Mello AM, Ellegood J, Jakkamsetti V, Liu P, Nebel MB, Gibson JM, Kelly E,
1255 Meng F, Cano CA, Pascual JM, Mostofsky SH, Lerch JP, Tsai PT. 2018. Author
1256 Correction: Altered cerebellar connectivity in autism and cerebellar-mediated rescue of
1257 autism-related behaviors in mice (Nature Neuroscience DOI: 10.1038/s41593-017-0004-1).
1258 *Nat Neurosci* **21**:1016. doi:10.1038/s41593-018-0096-2

1259 Suvrathan A, Payne HL, Raymond JL. 2016. Timing Rules for Synaptic Plasticity Matched to
1260 Behavioral Function. *Neuron* **92**:959–967. doi:10.1016/j.neuron.2017.12.019

1261 Tabata T, Sawada S, Araki K, Bono Y, Furuya S, Kano M. 2000. A reliable method for culture
1262 of dissociated mouse cerebellar cells enriched for Purkinje neurons. *J Neurosci Methods*
1263 **104**:45–53. doi:https://doi.org/10.1016/S0165-0270(00)00323-X

1264 Tai H, Schuman EM. 2008. Ubiquitin , the proteasome and protein degradation in neuronal
1265 function and dysfunction. *Nat Rev Neurosci* **9**. doi:10.1038/nrn2499

1266 Tang T, Li L, Tang J, Li Y, Lin WY, Martin F, Grant D, Solloway M, Parker L, Ye W, Forrest
1267 W, Ghilardi N, Oravecz T, Platt KA, Rice DS, Hansen GM, Abuin A, Eberhart DE,
1268 Godowski P, Holt KH, Peterson A, Zambrowicz BP, De Sauvage FJ. 2010. A mouse
1269 knockout library for secreted and transmembrane proteins. *Nat Biotechnol* **28**:749–755.
1270 doi:10.1038/nbt.1644

1271 Thouvenot E, Urbach S, Dantec C, Poncet J, Séveno M, Demettre E, Jouin P, Touchon J,
1272 Bockaert J, Marin P. 2008. Enhanced detection of CNS cell secretome in plasma protein-
1273 depleted cerebrospinal fluid. *J Proteome Res* **7**:4409–4421. doi:10.1021/pr8003858

1274 Titley HK, Kislin M, Simmons DH, Wang SSH, Hansel C. 2019. Complex spike clusters and

false-positive rejection in a cerebellar supervised learning rule. *J Physiol* **597**:4387–4406. doi:10.1113/JP278502

Tsai PT, Hull C, Chu Y, Greene-Colozzi E, Sadowski AR, Leech JM, Steinberg J, Crawley JN, Regehr WG, Sahin M. 2012. Autistic-like behaviour and cerebellar dysfunction in Purkinje cell Tsc1 mutant mice. *Nature* **488**:647–51. doi:10.1038/nature11310

Uemura T, Lee S-J, Yasumura M, Takeuchi T, Yoshida T, Ra M, Taguchi R, Sakimura K, Mishina M. 2010. Trans-Synaptic Interaction of GluRδ2 and Neurexin through Cbln1 Mediates Synapse Formation in the Cerebellum. *Cell* **141**:1068–1079. doi:10.1016/j.cell.2010.04.035

Valera AM, Doussau F, Poulain B, Barbour B, Isope P. 2012. Adaptation of Granule Cell to Purkinje Cell Synapses to High-Frequency Transmission. *J Neurosci* **32**:3267–3280. doi:10.1523/JNEUROSCI.3175-11.2012

Wang SSH, Kloth AD, Badura A. 2014. The Cerebellum, Sensitive Periods, and Autism. *Neuron* **83**:518–532. doi:10.1016/j.neuron.2014.07.016

Weber J, Polo S, Maspero E. 2019. HECT E3 ligases: A tale with multiple facets. *Front Physiol* **10**:1–8. doi:10.3389/fphys.2019.00370

Widagdo J, Chai YJ, Ridder MC, Chau YQ, Johnson RC, Sah P, Huganir RL, Anggono V. 2015. Activity-Dependent ubiquitination of GluA1 and GluA2 regulates AMPA receptor intracellular sorting and degradation. *Cell Rep* **10**:783–795. doi:10.1016/j.celrep.2015.01.015

Widagdo J, Guntupalli S, Jang SE, Anggono V. 2017. Regulation of AMPA Receptor Trafficking by Protein Ubiquitination. *Front Mol Neurosci* **10**:1–10. doi:10.3389/fnmol.2017.00347

Xia J, Chung HJ, Wihler C, Huganir RL, Linden DJ. 2000. Cerebellar long-term depression requires PKC-regulated interactions between GluR2/3 and PDZ domain-containing proteins. *Neuron* **28**:499–510. doi:10.1016/S0896-6273(00)00128-8

Zhao HM, Wenthold RJ, Petralia RS. 1998. Glutamate receptor targeting to synaptic populations on Purkinje cells is developmentally regulated. *J Neurosci* **18**:5517–5528. doi:10.1046/j.1471-4159.1997.68031041.x

Zhu H, Meissner LE, Byrnes C, Tuymetova G, Tifft CJ, Proia RL. 2020. The Complement Regulator Susd4 Influences Nervous-System Function and Neuronal Morphology in Mice. *iScience* **23**:100957. doi:10.1016/j.isci.2020.100957

1308 **Figure legends**

1309 **Figure 1. SUSD4 is necessary for motor coordination adaptation and learning**.

1310 **(A)** Diagram of the protein SUSD4 showing its domain organization with four extracellular
1311 Complement Control Protein (CCP) domains, one transmembrane (TM) domain and a
1312 cytoplasmic domain (C_T).

1313 **(B)** Quantitative RT-PCR shows an increase in *Susd4* mRNA expression (relative to the
1314 housekeeping gene *Rpl13a*) during postnatal development in the cerebellum and in the
1315 brainstem. Extracts were prepared from tissue samples of mice aged from 0 to 21 days (P0-
1316 21) and three months (3mo). Mean ± s.e.m. (n=3 independent experiments).

1317 **(C)** HA-tagged SUSD4 is found in dendrites (left panel, single plane) and in some of the distal
1318 dendritic spines (right panel, arrowheads, projection of a 1,95µm z-stack) in adult cerebellar
1319 Purkinje cells. Anti-HA and anti-GFP immunolabeling was performed on parasagittal
1320 cerebellar sections obtained from adult L7-Cre mice after stereotaxic injection of AAV
1321 particles driving the expression of HA-SUSD4 and soluble GFP. Scale bars: 10 µm (left
1322 panel) and 2µm (right panel).

1323 **(D)** Purkinje cells from primary mixed cerebellar culture of L7-Cre mice were transduced at 3
1324 days in vitro (DIV3) with a HA-tagged SUSD4 expressing virus (AAV2-hSYN-DIO-HA-
1325 SUSD4-2A-eGFP) or with a control virus expressing GFP (AAV2-hSYN-DIO-eGFP), and
1326 immunostained in non-permeabilizing conditions at DIV17 for HA to localize surface
1327 SUSD4 (anti-HA, red), and in permeabilizing conditions to detect the green fluorescent
1328 protein (anti-GFP, green) and the endogenous GluD2 subunit (anti-GRID2, blue). Scale bar:
1329 5 µm.

1330 **(E)** Genomic structure of the *Susd4* gene. White boxes represent exons. Exon 1 is deleted in the
1331 *Susd4* loss-of-function mouse model. See also **Figure 1-figure supplement 2**.

1332 **(F)** Motor coordination and learning is deficient in adult male *Susd4* $^{-/-}$ (KO) mice compared to
1333 age-matched *Susd4*$^{+/+}$ (WT) littermates. Each mouse was tested three times per day during
1334 five consecutive days on an accelerating rotarod (4 to 40 r.p.m. in 10 minutes) and the time
1335 spent on the rotarod was measured. Mean ± s.e.m. (WT n=11 and KO n=7 mice, two-way
1336 ANOVA with repeated measures, Interaction (time and genotype): ** P=0.0079, F(14, 224)
1337 = 2.22; Time: **** P<0.0001, F(14, 224) = 3.469; Genotype: P=0.0553, F(1, 16) = 4.272).

1338 **(G)** *In situ* hybridization experiments were performed on brain sections from one month-old WT
1339 and *Susd4* KO mice to detect *Susd4* mRNA using a probe encompassing exons 2 to 5 (See
1340 also **Figure 1-figure supplement 2**). *Susd4* expression was found in many regions of the
1341 brain in *Susd4*$^{+/+}$ (WT) mice (see also **Figure 1-figure supplement 1**) including the cerebral
1342 cortex (CTX), the cerebellum (CB), and the brainstem (BS). No labeling was found in the
1343 brain of *Susd4* $^{-/-}$ (KO) mice. Scale bars: 500 µm.
1344
1345

1346 **Figure 1-figure supplement 1. *Susd4* mRNA expression in the developing mouse brain.**
1347 **(A)** *Susd4* mRNA expression was visualized in the brain of wild-type (WT) mice by *in situ*
1348 hybridization. Coronal (left) and sagittal (right) sections are presented at postnatal day 0
1349 (P0),
1350 **(B)** postnatal day 7 (P7) and
1351 **(C)** postnatal day 30 (P30). *Susd4* expression was found in many regions including the cerebral
1352 cortex (CTX), the dentate gyrus (DG) and CA3 regions in the hippocampus (coronal section,
1353 left), the cerebellum (CB), in particular Purkinje cells (PCs), and the inferior olive (IO;
1354 sagittal section, right). Scale bars: 250µm and 500µm (inset **C**).
1355
1356 **Figure 1-figure supplement 2. Characterization of *Susd4* knockout (KO) mice.**
1357 **(A)** Structure of the *Susd4* gene and strategy for the generation of the knockout mouse. The gene
1358 coding for the *Susd4* mRNA contains 8 exons. The wild-type WT allele is presented
1359 indicating the localization of the primers used for genotyping and of the probes used for
1360 TaqMan RT-qPCR. In the knockout allele, the 5'UTR and first exon are entirely deleted and
1361 replaced by the selection cassette.
1362 **(B)** *Susd4* expression was assessed by RT-PCR using primers encompassing exons 6 to 8 in
1363 extracts from cortex (CTX), cerebellum (CB) and brainstem (BS) in control and *Susd4* KO
1364 mice.
1365
1366 **Figure 1-figure supplement 3. Footprint analysis in *Susd4* KO mice.**
1367 Footprint patterns of P30 WT and *Susd4* KO mice were quantitatively analyzed by measuring
1368 stride length for the fore paws (magenta) and hind paws (cyan), stance length for the
1369 forelimbs and hindlimbs, and print separation. Mean ± s.e.m. (WT n=9 and KO n=10 mice;
1370 unpaired Student's t-test; Forelimb stance: P=0.3059; Forelimb stride: P=0.5882; Hindlimb
1371 stance: P=0.4533; Hindlimb stride: P=0.3580; Print separation: * P=0.0148).
1372
1373 **Figure 1-figure supplement 4. Normal cerebellar cytoarchitecture in *Susd4* KO mice.**
1374 **(A)** Parasagittal sections of P30 WT and *Susd4* KO cerebella were stained with Hoechst and
1375 used for quantitative analysis of the mean area of the cerebellum. Mean ± s.e.m. (n=3 WT
1376 mice and n=3 KO mice). Scale bar: 500µm.
1377 **(B)** Calbindin protein (CABP) immunostaining was used for quantitative analysis of the mean
1378 height of the molecular layer. Mean ± s.e.m. (WT n=5 and KO n=6 mice). Scale bar: 30µm.
1379
1380 **Figure 1-figure supplement 5. High density microelectrode array (MEA) analysis of**
1381 **Purkinje cell spiking in acute cerebellar slices from *Susd4* KO compared to WT.**
1382 **(A)** Image of a cerebellar acute slice from a WT mouse overlapped with the image of the color
1383 map of the MEA recording. Each pixel represents one channel, where the active units are in
1384 red. The black square highlights one of the channels.
1385 **(B)** Representative traces of electrical activity recorded in one channel from control and *Susd4*
1386 KO mice. Each tick points out one action potential that has been detected and sorted by the
1387 Brainwave software.
1388 **(C)** Histograms of the mean firing rate, coefficient of variation (CV) of Inter Spike Intervals and
1389 CV2. Mean ± s.e.m. (WT n=5 and KO n=4 mice; Mann Whitney test; Mean Firing Rate:
1390 P=0.2857; CV: P=0.4127; CV2: P=0.5373).
1391

1392 **Figure 1-source data :** Numerical data to support graphs in Figure 1
1393
1394 **Figure 2. *Susd4* loss-of-function leads to deficient long-term depression and facilitated long-**
1395 **term potentiation of parallel fiber/Purkinje cell synapses.**
1396 **(A)** Quantitative analysis of the morphology of parallel fiber presynaptic boutons
1397 immunolabeled by an anti-VGLUT1 antibody (red) in Purkinje cells (anti-CABP, blue).
1398 Quantifications of the density and the area of the VGLUT1 clusters did not reveal any
1399 difference between *Susd4* KO and *Susd4* WT mice. Mean ± s.e.m. (WT n=5 and KO n=7
1400 mice; VGLUT1 clusters density: Mann-Whitney test, P>0.9999; area VGLUT1 clusters:
1401 Unpaired Student t-test, P=0.3089). Scale bars: 30 µm (left) and 10 µm (right).
1402 **(B)** Diagram of the setup for patch-clamp recordings (REC) of Purkinje cells in 300 µm-thick
1403 parasagittal cerebellar slices. Parallel fiber and climbing fiber responses were elicited by
1404 electrical stimulation (STIM). ML: molecular layer; PCL: Purkinje cell layer; GCL: granule
1405 cell layer.
1406 **(C)** Input-output curve of the parallel fiber/Purkinje cell transmission. The amplitude of the
1407 elicited EPSCs increases with the intensity of the stimulus and is not significantly different
1408 between *Susd4* KO and WT littermates. The fitted curves for each genotype are presented in
1409 the inset. Representative sample traces are presented. Mean ± s.e.m. (WT n=18 cells from 8
1410 mice and KO n=16 cells from 6 mice; Kolmogorov-Smirnov test, P=0.8793). Short-term
1411 plasticity of parallel fiber/Purkinje cell synapses is not affected by *Susd4* loss-of-function.
1412 Parallel fibers were stimulated twice at 50 ms interval and the paired-pulse ratio (PPR) was
1413 calculated by dividing the amplitude of the second peak by the amplitude of the first peak.
1414 Mean ± s.e.m. (WT n=21 cells from 8 mice and KO n=16 cells from 6 mice; Mann-Whitney
1415 test, P=0.9052).
1416 **(D)** Climbing fiber-dependent parallel fiber/Purkinje cell synapse long-term depression (LTD) is
1417 impaired in the absence of *Susd4* expression. LTD was induced by pairing stimulations of
1418 parallel fibers and climbing fibers at 100 milliseconds interval during 10 minutes at 0.5 Hz
1419 (see also **Figure 2-figure supplement 1**). The amplitude of the PF EPSC was measured
1420 using two consecutive PF stimulation at 50 milliseconds interval. Representative sample
1421 traces are presented. Right: EPSC amplitudes from the last 10 minutes (purple) of recordings
1422 were used to calculate the LTD ratio relative to baseline. Mean ± s.e.m. (WT n=16 cells
1423 from 11 mice and KO n=14 cells from 10 mice; Two-tailed Wilcoxon Signed Rank Test
1424 with null hypothesis of 100: WT **p=0.0063; KO p=0.2676; Mann-Whitney test, WT *vs*
1425 KO *p=0.0476).
1426 **(E)** Loss-of-function of *Susd4* facilitates parallel fiber/Purkinje cell synapse long-term
1427 potentiation (LTP). Tetanic stimulation of only parallel fibers at 0.3 Hz for 100 times (see
1428 also **Figure 2-figure supplement 1**) induced LTP in *Susd4* KO Purkinje cells while
1429 inducing only a transient increase in parallel fiber transmission in WT Purkinje cells.
1430 Representative sample traces are presented. Right: EPSC amplitudes from the last 7 minutes
1431 (purple) were used to calculate the LTP ratio relative to baseline. Mean ± s.e.m. (WT n=13
1432 cells from 9 mice and KO n=8 cells from 6 mice; Two-tailed Wilcoxon Signed Rank Test
1433 with null hypothesis of 100: WT p=0.5879; KO *p=0.0234; Mann-Whitney test, WT *vs* KO:
1434 *p=0.0199).
1435
1436
1437

1438 **Figure 2-figure supplement 1. Parallel fiber (PF) /Purkinje cell (PC) synapse EPSCs**
1439 **kinetics, long-term plasticity induction protocols, paired-pulse facilitation ratio and**
1440 **delayed EPSC quanta.**
1441 **(A)** Schematic representation of the recording location (internal lobule VIa of the vermis).
1442 **(B)** No change in the rise time and decay of Parallel fiber/Purkinje cell EPSCs was induced by
1443 *Susd4* deletion. Mean ± s.e.m. (WT n=21 cells from 8 mice and KO n=16 cells from 6 mice;
1444 Rise time: unpaired Student's t-test, P=0.4570; Decay time: Mann Whitney test, P=0.7276).
1445 **(C)** Parallel fiber long-term depression (LTD) induction protocol.
1446 **(D)** Paired-pulse ratio (A2/A1) during LTD measured at 20 Hz. Mean ± s.e.m. (WT n=16 cells
1447 from 11 mice and KO n=14 cells from 10 mice; two-way ANOVA with repeated measures,
1448 Interaction (time and genotype): P=0.9935, F(39, 1092)=0.5222).
1449 **(E)** Parallel fiber long-term potentiation (LTP) induction protocol.
1450 **(F)** Paired-pulse ratio (A2/A1) during LTP measured at 20Hz. Mean ± s.e.m. (WT n=13 cells
1451 from 9 mice and KO n=8 cells from 6 mice, two-way ANOVA with repeated measures,
1452 Interaction (time and genotype): P=0.9366, F(39, 741)=0.6745).
1453 **(G)** Delayed PF-EPSC quanta were evoked by PF stimulation in the presence of strontium
1454 (Sr^{++}) instead of calcium (Ca^{++}) to induce desynchronization of fusion events.
1455 Representative sample traces are presented. The cumulative probability for the amplitude
1456 shows no difference with *Susd4* loss-of-function. The individual frequency values for each
1457 cell (measured as interevent interval) present no differences between the genotypes. No
1458 change in the time to peak and in the rise time of PF/PC synapse delayed EPSC quanta was
1459 induced by *Susd4* deletion. Mean ± s.e.m. (WT n=8 cells from 6 mice and KO n=8 cells
1460 from 5 mice; Amplitude: Kolmogorov-Smirnov distribution test, P=0.1667; Frequency:
1461 Mann Whitney test, P=0.1913; Time to peak: Mann Whitney test, P=0.6454; Rise time 10%
1462 to 90%: unpaired Student's t-test, P=0.6486).
1463
1464 **Figure 2-source data:** Numerical data to support graphs in Figure 2
1465
1466

1467 **Figure 3. Transmission at the Climbing fiber/Purkinje cell synapses is increased in *Susd4***
1468 **knockout mice**.
1469 **(A)** Climbing fiber presynaptic boutons were immunostained with an anti-VGLUT2 antibody in
1470 cerebellar sections from P30 WT and *Susd4* KO mice. The extension of the climbing fiber
1471 territory was calculated by measuring the extent of the VGLUT2 (red) labeling relative to
1472 the height of the Purkinje cell dendritic tree (immunostained using an anti-CABP antibody,
1473 blue). Quantification of the mean density of VGLUT2 puncta and their mean area showed
1474 no differences between *Susd4* KO mice and their control littermates. Mean ± s.e.m. (WT
1475 n=5 and KO n=7 mice; VGLUT2 extension: Mann-Whitney test, P=0.6389; VGLUT2 area:
1476 Unpaired Student t-test, p=0.4311; VGLUT2 density: Unpaired Student t-test, p=0.8925).
1477 Scale bars: 30 µm (left) and 10 µm (right).
1478 **(B)** Short-term synaptic plasticity of climbing fiber/Purkinje cell synapses was elicited by two
1479 consecutive stimulations at various intervals. The amplitude of the climbing fiber elicited
1480 EPSC was increased in *Susd4* KO mice compared to WT littermates. (WT n=26 cells, 9
1481 mice and KO n=26 cells, 7 mice, Mann-Whitney test, ** P=0.0066). No difference in the
1482 paired pulse ratios (PPR) was detected at any interval between *Susd4* KO mice and WT
1483 mice. Representative sample traces are presented. See also **Figure 3-figure supplement 1**.
1484 Mean ± s.e.m. (WT n=12 cells from 3 mice and KO n=17 cells from 5 mice; Kolmogorov-
1485 Smirnov test, P=0.4740).
1486 **(C)** Delayed CF-EPSC quanta were evoked by CF stimulation in the presence of Sr^{++} instead of
1487 Ca^{++} to induce desynchronization of fusion events. Representative sample traces are
1488 presented. The cumulative probability for the amplitude of the events together with the
1489 individual amplitude values for each event show an increased amplitude associated with
1490 *Susd4* loss-of-function. The individual frequency values for each cell (measured as
1491 interevent interval, IEI) present no differences between the genotypes. See also **Figure 3-**
1492 **figure supplement 1**. Mean ± s.e.m. (WT n=10 cells from 6 mice and KO n=8 cells from 3
1493 mice; Amplitude: Kolmogorov-Smirnov distribution test, *** P<0.0001; Frequency: Mann
1494 Whitney test, P=0.6334).
1495
1496 **Figure 3-figure supplement 1. Characteristics of the climbing fiber/Purkinje cell synapse.**
1497 **(A)** Climbing fibers were visualized in *Susd4* WT and KO mice crossed with Htr5b-eGFP
1498 reporter mice expressing the green fluorescent protein specifically in inferior olivary
1499 neurons. Anti-GFP and anti-CABP (to visualize Purkinje cells) immunofluorescence was
1500 performed on parasagittal sections of P30 mice, and showed no qualitative differences in the
1501 absence of *Susd4* expression. Scale bar: 10 µm.
1502 **(B)** Patch-clamp recordings of Purkinje cells showed a similar percentage of mono- (1 climbing
1503 fiber) and multi-innervation (>1 climbing fibers) of Purkinje cells in P30 *Susd4* KO and WT
1504 mice, as measured by the number of steps elicited by electrical stimulation of the climbing
1505 fibers. (WT n=26 cells from 9 mice and KO n=26 cells from 7 mice; Chi-square test,
1506 P=0.5520).
1507 **(C)** No change in the rise and decay times of climbing fiber/Purkinje cell EPSCs was induced
1508 by *Susd4* deletion. Mean ± s.e.m. (WT n=26 cells from 9 mice and KO n=26 cells from 7
1509 mice; Rise time: unpaired Student's t-test, P=0.3750; Decay time: Mann Whitney test,
1510 P=0.7133).

1511 **(D)** No change in the time to peak and in the rise time of CF/PC synapse delayed EPSC quanta
1512 was induced by *Susd4* loss-of-function. Mean ± s.e.m. (WT n=10 cells from 6 mice and KO
1513 n=8 cells from 3 mice; Time to peak: unpaired Student's t-test, P=0.1692; Rise time 10% to
1514 90%: Mann Whitney test, P=0.0639).
1515 **(E)** Climbing fiber/Purkinje cell transmission was monitored during LTD induction in current-
1516 clamp mode. Representative traces of the CF-EPSP are shown. The quantification of the
1517 number of spikelets (spikes induced by repeated CF stimulation (Mathy et al., 2009; Titley
1518 et al., 2019)) did not reveal any difference between WT and KO Purkinje cells (unpaired
1519 Student's t-test, P=0.5791). Bottom: Measurements of the CF-EPSP area and
1520 hyperpolarization area during the LTD induction protocol. Mean ± s.e.m. (WT n=16 cells
1521 from 11 mice and KO n=14 cells from 10 mice).
1522
1523 **Figure 3-source data:** Numerical data to support graphs in Figure 3
1524
1525

1526 **Figure 4. Loss of SUSD4 leads to misregulation of the AMPA receptor subunit GluA2.**
1527 **(A)** The number of GluA2 clusters (anti-GluA2 immunolabeling, green) per climbing fiber
1528 presynaptic bouton (anti-VGLUT2 immunolabeling, red) and their intensity were quantified
1529 in cerebellar sections of juvenile *Susd4*$^{-/-}$ KO mice and *Susd4*$^{+/+}$ WT littermates. Cumulative
1530 plot for the mean GluA2 intensity per VGLUT2 bouton shows no significant change
1531 between WT and KO. The distribution of the VGLUT2 boutons according to the number of
1532 associated GluA2 clusters is significantly different between WT and KO. Mean ± s.e.m.
1533 (WT n= 5 and KO n= 5 mice; Intensity: Kolmogorov-Smirnov test, P=0.5009; Distribution:
1534 Chi-square contingency test, **** P<0.0001). Scale bars: 30 µm (top) and 15 µm (bottom).
1535 **(B)** Activity-dependent changes in surface localization of GluA2 was studied in cerebellar acute
1536 slices from *Susd4* KO mice and control *Susd4* WT littermates using a chemical LTD
1537 protocol (cLTD; K-Glu: K^+ 50mM and glutamate 10µM for 5 minutes followed by 30
1538 minutes of recovery). Surface biotinylation of GluA2 subunits was performed followed by
1539 affinity-purification of biotinylated GluA2 subunits and anti-GluA2 immunoblot analysis.
1540 The fraction of biotinylated GluA2 was obtained by measuring the levels of biotinylated
1541 GluA2 in affinity-purified samples and total GluA2 normalized to beta-actin in input
1542 samples for each condition. The ratios between the fraction of biotinylated GluA2 after
1543 cLTD and control conditions are represented. Mean ± s.e.m. (n=8 independent experiments;
1544 Two-tailed Student's one sample t-test was performed on the ratios with a null hypothesis of
1545 1, P_{WT} = 0.0212 and P_{KO} = 0.0538).
1546 **(C)** Activity-dependent degradation of GluA2 was assessed in cerebellar acute slices from *Susd4*
1547 KO and control mice after induction of chemical LTD (cLTD; K-Glu: K^+ 50mM and
1548 glutamate 10µM for 5 minutes followed by 30 minutes of recovery). This degradation was
1549 absent when slices were incubated with 100µg/mL leupeptin and with 50µM MG132 (to
1550 inhibit lysosomal and proteasome degradation, respectively), or when slices were obtained
1551 from *Susd4* KO mice. Band intensities of GluA2 were normalized to β-ACTIN. The ratios
1552 between levels with cLTD induction (K-Glu) and without cLTD induction (CTL) are
1553 represented. See also **Figure Figure 4-figure supplement 1**. Mean ± s.e.m. (n=8
1554 independent experiments; Two-tailed Student's one sample t-test was performed on the
1555 ratios with a null hypothesis of 1, P_{WT} = 0.0107, $P_{WT+Leu/MG132}$ = 0.3755, P_{KO} = 0.3176 and
1556 $P_{KO+Leu/MG132}$ = 0.2338).
1557 **(D)** Purkinje cells from primary cerebellar cultures of L7-Cre mice were transduced at 3 days in
1558 vitro (DIV3) with a virus driving expression of HA-tagged SUSD4 (AAV2-hSYN-DIO-HA-
1559 SUSD4-2A-eGFP) and immunolabeled at DIV17 in non-permeabilizing conditions to
1560 localize surface SUSD4 (anti-HA, red) and surface GluA2 subunits (anti-GluA2, blue).
1561 Direct green fluorescent protein is shown (GFP, green). Right panels are binarized images of
1562 the anti-HA and anti-GluA2 immunolabelings and of the colocalization of these signals
1563 (maximum projection of a 1.8 µm z-stack). Scale bar: 5 µm.
1564
1565 **Figure 4-figure supplement 1. Basal surface GluA2 levels and total GluA2 and GluD2 levels**
1566 **after modulation of SUSD4 expression.**
1567 **(A)** Surface GluA2 levels (relative to normalized GluA2 input) in basal conditions were not
1568 different on average in acute cerebellar slices from *Susd4* KO when compared to slices from
1569 WT mice.
1570 **(B)** and **(C)** Total protein levels (normalized to βACTIN) of GluA2 **(B)** and GluD2 **(C)** were
1571 not changed in acute cerebellar slices from WT or *Susd4* KO mice in basal conditions.

1572 Mean ± s.e.m. (n=8 independent experiments; unpaired Student's t-test; GluA2: P=0.5424;
1573 GluD2: P=0.6821).
1574 **(D)** Cerebellar acute slices from control WT and *Susd4* KO mice were incubated to induce
1575 chemical LTD (cLTD; K-Glu: K^+ 50mM and glutamate 10µM for 5min followed by 30min
1576 of recovery). Slices were incubated with 100µg/mL leupeptin and with 50µM MG132 (to
1577 inhibit lysosomal and proteasome degradation, respectively). Band intensities of GluD2
1578 were normalized to βACTIN. The ratios between levels with cLTD induction (K-Glu) and
1579 without cLTD induction (CTL) are represented. Mean ± s.e.m. (n=8 independent
1580 experiments; two-tailed Student's one sample t-test was performed on the ratios with a null
1581 hypothesis of 1, P_{WT} = 0.4973, $P_{WT+Leu/MG132}$ = 0.1433, P_{KO} = 0.3143, $P_{KO+Leu/MG132}$ = 0.9538,
1582 n.s.= not significant).
1583
1584 **Figure 4-figure supplement 2. HA-SUSD4 and the AMPA receptor subunit GluA2.**
1585 **(A)** SUSD4 interaction with GluA2 was assessed by co-immunoprecipitation using HEK293
1586 cells transfected with SEP-GluA2 together with PVRL3α as a control or HA-SUSD4.
1587 Affinity-purification was performed with an anti-GFP antibody and extracts were probed for
1588 co-immunoprecipitation of GluA2 (with an anti-GluA2 antibody) and of HA-SUSD4 (anti-
1589 HA antibody) or PVRL3α (anti- PVRL3α antibody). βACTIN was used as a loading control.
1590 Representative of N=3 independent experiments.
1591 **(B)** Mouse hippocampal neurons were transfected at 13 days *in vitro* (DIV13) with a GFP-
1592 tagged SUSD4 construct and immunostained at DIV17 for green fluorescent protein (GFP,
1593 green) to localize SUSD4 and for the endogenous GluA2 subunit (anti-GluA2, red). The
1594 arrowheads indicate the spines containing SUSD4 and GluA2. Scale bar: 10 µm.
1595
1596 **Figure 4-source data:** Numerical data to support graphs in Figure 4
1597
1598

1599 **Figure 5. SUSD4 binds NEDD4 ubiquitin ligases, known regulators of AMPA receptor**
1600 **turnover and degradation.**
1601 **(A)** Mass spectrometry identification of SUSD4 interactors. Left: Affinity-purification from
1602 cerebellar synaptosomes was performed using either GFP-SUSD4 as a bait or GFP as a
1603 control. Proteins were then resolved using SDS-PAGE followed by immunoblot for anti-
1604 GFP and coomassie staining of proteins. Right: Gene Ontology (GO) enrichment analysis
1605 network (Molecular Function category) of the 28 candidate proteins (Cytoscape plugin
1606 ClueGO) identified after affinity-purification of cerebellar synaptosomes using GFP-SUSD4
1607 as a bait followed by LC MS/MS. The Ubiquitin ligase activity term is significantly enriched
1608 in particular due to the identification of several members of the NEDD4 family of HECT-
1609 ubiquitin ligase. See also **Table 1**. (n=3 independent experiments).
1610 **(B)** Immunoblot confirmation of SUSD4 interaction with NEDD4 ubiquitin ligases. Affinity-
1611 purification from cerebellar synaptosomes was performed using either full length HA-
1612 SUSD4, HA-SUSD4ΔC_T or GFP as a bait. Proteins were then resolved using SDS-PAGE
1613 followed by immunoblot for NEDD4, ITCH, WWP1 or HA-SUSD4 (anti-HA). Full-length
1614 SUSD4 (HA-tagged, HA-SUSD4) interacts with all three members of the NEDD4 family.
1615 This interaction is lost when the C-terminal tail of SUSD4 is deleted (HA-SUSD4ΔC_T) or
1616 when GFP is used instead of SUSD4 as a control.
1617 **(C)** Schematic representation of HA-tagged SUSD4 and different mutant constructs: SUSD4ΔC_T
1618 (lacking the cytoplasmic tail), SUSD4ΔN_T (lacking the extracellular domain), SUSD4N_T
1619 (lacking the transmembrane and intracellular domains), SUSD4ΔPY (point mutation of the
1620 PPxY site), SUSD4ΔLY (point mutation of the LPxY) and SUSD4ΔPY/LY (double mutant
1621 at both PPxY and LPxY).
1622 **(D)** SUSD4 interaction with GluA2 and NEDD4 was assessed by co-immunoprecipitation using
1623 HEK293 cells transfected with SEP-GluA2 together with PVRL3α as a control or one of the
1624 HA-SUSD4 constructs represented in (C). Affinity-purification was performed with an anti-
1625 HA antibody and extracts were probed for co-immunoprecipitation of GluA2 (with an anti-
1626 GluA2 antibody) and of the HECT ubiquitin ligase NEDD4 (anti-NEDD4 antibody). Co-
1627 immunoprecipitated GluA2 levels are normalized to input GluA2 and then represented as
1628 relative to the immunoprecipitated levels for each SUSD4 construct. N=3 independent
1629 experiments.
1630 **(E)** Potential interactors of SUSD4 control several parameters of AMPA receptor turnover.
1631 Three different pools of AMPA receptors are found in dendrites and spines: synaptic,
1632 extrasynaptic and intracellular. AMPA receptors are synthetized and delivered close to the
1633 synaptic spine to reach the synaptic surface. At the surface, AMPA receptors can move
1634 laterally (lateral diffusion) or vertically by endocytosis and exocytosis. Endocytosis can be
1635 mediated by clathrin (CM-endocytosis) or be clathrin-independent (CI-endocytosis). CM-
1636 endocytosis is often related to activity-dependent processes. After endocytosis, AMPA
1637 receptors can choose between two different pathways from the early endosomes, one for
1638 recycling and the other for degradation. Potential molecular partners of SUSD4 identified by
1639 our proteomics analysis could regulate AMPA receptor turnover at several levels of this
1640 cycle (in red).
1641
1642 **Figure 5-figure supplement 1. Expression of HECT ubiquitin ligases in adult mouse brain**.

1643 **(A)** Schematic representation of four SUSD4 interactors: NEDD4, NEDD4L, ITCH and
1644 WWP1. Legends: N_T, N-terminus; HECT, Homologous to the E6-AP C-terminus domain;
1645 C_T, C-terminus.
1646 **(B)** Pattern of expression of *Nedd4* (RP_050712_03_C08),
1647 **(C)** *Nedd4l* (RP_040625_01_G10),
1648 **(D)** *Itch* (RP_050222_01_H06) and
1649 **(E)** *Wwp1* (RP_050510_02_E12) mRNA in the adult mouse brain. From Allen Brain Atlas
1650 (www.brain-map.org).
1651
1652 **Figure 5-figure supplement 2. Total protein levels in HEK293 cells transfected with SEP-**
1653 **GluA2 and different SUSD4 mutant constructs (related to Figures 5C and 5D)**
1654 HEK293 cells were transfected with SEP-GluA2 together with PVRL3α as a control or one of
1655 the HA-SUSD4 constructs for coimmunoprecipitation experiments. Input extracts were probed
1656 for GluA2 (with an anti-GluA2 antibody), the HECT ubiquitin ligase NEDD4 (anti-NEDD4
1657 antibody), and the HA-tagged SUSD4 constructs (anti-HA antibody). βACTIN was used as a
1658 loading control. Representative image of N=3 independent experiments. Quantifications
1659 represent the GluA2 or HA band intensity normalized to the intensity of the βACTIN band.
1660
1661 **Figure 5-source data:** Numerical data to support graphs in Figure 5

1662 **Table 1. List of SUSD4 interactors.** Proteomic identification of SUSD4 interacting partners affinity-purified from synaptosomes
1663 extracts using GFP-SUSD4 as a bait (≥2 unique peptides; enrichment factor ≥4).

UniProtKB accession num.	Protein Name	Gene Name	Mol. weight [kDa]	Unique peptides	MS/MS Count	Enrichment factor
Q8CFI0	E3 ubiquitin-protein ligase NEDD4-like	*Nedd4l*	115,42	28	319	159.5
Q8BH32	Sushi domain-containing protein 4	*Susd4*	53,796	4	97	48.5
Q8BZZ3	NEDD4-like E3 ubiquitin-protein ligase WWP1	*Wwp1*	104,69	13	90	45
Q8C863	E3 ubiquitin-protein ligase Itchy	*Itch*	98,992	24	83	41.5
Q3TXU5	Deoxyhypusine synthase	*Dhps*	40,642	9	81	40.5
Q9DBG3	AP-2 complex subunit beta	*Ap2b1*	104,58	9	47	23.5
P50171	Estradiol 17-beta-dehydrogenase 8	*Hsd17b8*	26,588	2	32	16
Q9DBH0	NEDD4-like E3 ubiquitin-protein ligase WWP2	*Wwp2*	98,76	14	31	15.5
Q922R8	Protein disulfide-isomerase A6	*Pdia6*	48,1	8	26	13
P27773	Protein disulfide-isomerase A3	*Pdia3*	56,678	12	24	12
P17427	AP-2 complex subunit alpha-2	*Ap2a2*	104,02	7	23	11.5
Q8BWG8	Beta-arrestin-1	*Arrb1*	46,972	4	23	11.5
Q91WC3	Long-chain-fatty-acid--CoA ligase 6	*Acsl6*	78,016	11	22	11
P27546	Microtubule-associated protein 4	*Map4*	117,43	9	18	9
Q505F5	Leucine-rich repeat-containing protein 47	*Lrrc47*	63,589	9	17	8.5
Q9Z2H5	Band 4.1-like protein 1	*Epb41l1*	98,314	8	17	8.5
P46935	E3 ubiquitin-protein ligase NEDD4	*Nedd4*	102,71	7	17	8.5
Q8BMK4	Cytoskeleton-associated protein 4	*Ckap4*	63,691	11	16	8
P47708	Rabphilin-3A	*Rph3a*	75,488	7	15	7.5
P42128	Forkhead box protein K1	*Foxk1*	74,919	6	15	7.5
P62812	Gamma-aminobutyric acid receptor subunit alpha-1	*Gabra1*	51,753	7	14	7
Q60737	Casein kinase II subunit alpha	*Csnk2a1*	45,133	7	13	6.5
Q99KV1	DnaJ homolog subfamily B member 11	*Dnajb11*	40,555	5	10	5
P63037	DnaJ homolog subfamily A member 1	*Dnaja1*	44,868	4	10	5
Q9QY76	Septin-11	*Sept11*	49,694	5	9	4.5
O70318	Band 4.1-like protein 2	*Epb41l2*	109,94	6	8	4
P62196	26S protease regulatory subunit 8	*Psmc5*	45,626	5	8	4
Q9Z2Q6	Septin-5	*Sept5*	42,747	4	8	4

1664
1665
1666

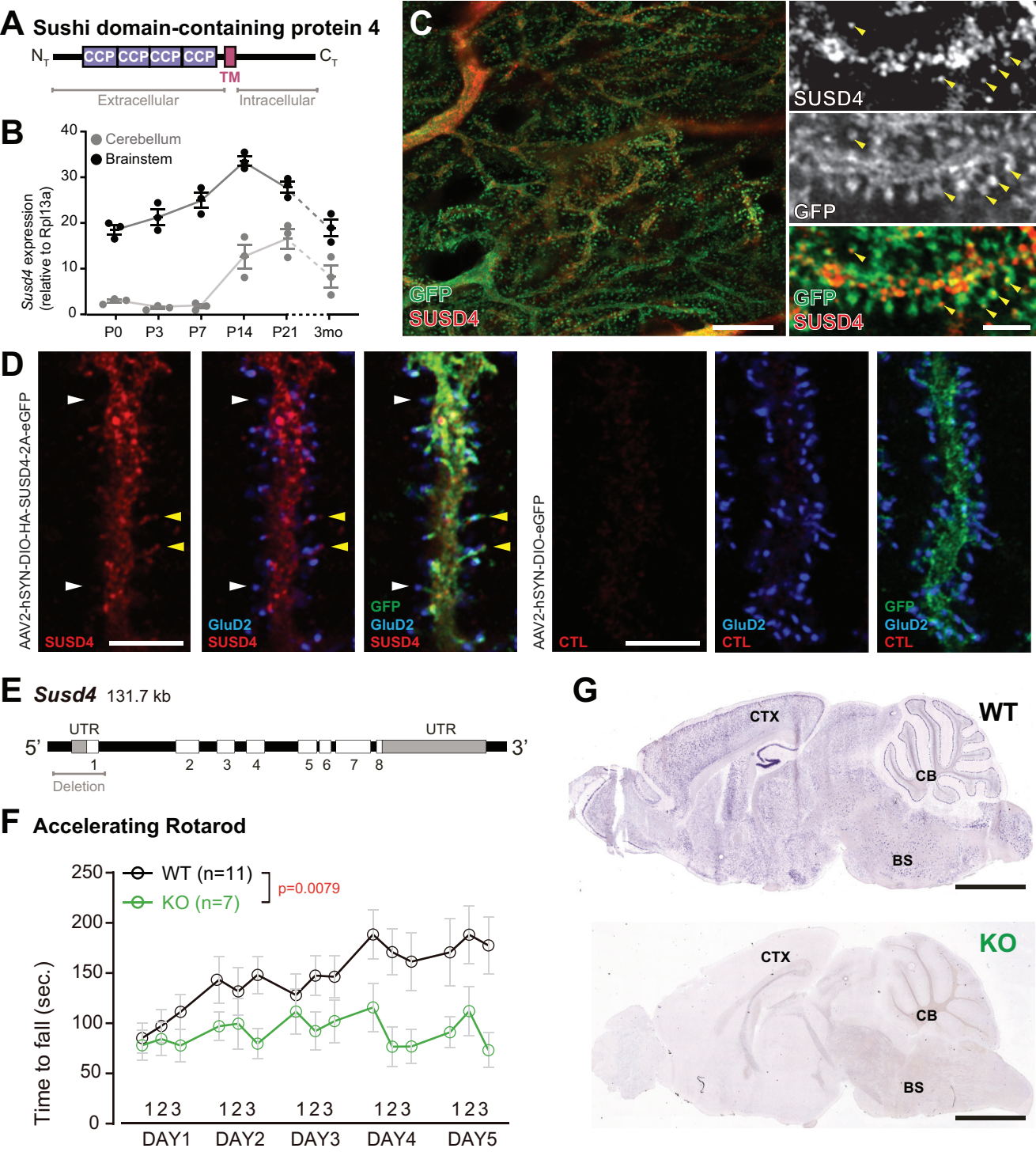
A
Sushi domain-containing protein 4
N_T
CCP
CCP
CCP
CCP
TM
C_T
Extracellular
Intracellular
B
Cerebellum
Brainstem
Susd4 expression (relative to Rpl13a)
40
30
20
10
0
P0
P3
P7
P14
P21
3mo
C
GFP
SUSD4
SUSD4
GFP
GFP
SUSD4
D
AAV2-hSYN-DIO-HA-SUSD4-2A-eGFP
SUSD4
GluD2
SUSD4
GFP
GluD2
SUSD4
AAV2-hSYN-DIO-eGFP
CTL
GluD2
CTL
GFP
GluD2
CTL
E
Susd4 131.7 kb
5'
UTR
UTR
3'
1
2
3
4
5
6
7
8
Deletion
F
Accelerating Rotarod
WT (n=11)
KO (n=7)
p=0.0079
Time to fall (sec.)
250
200
150
100
50
0
1 2 3
1 2 3
1 2 3
1 2 3
1 2 3
DAY1
DAY2
DAY3
DAY4
DAY5
G
WT
CTX
CB
BS
KO
CTX
CB
BS

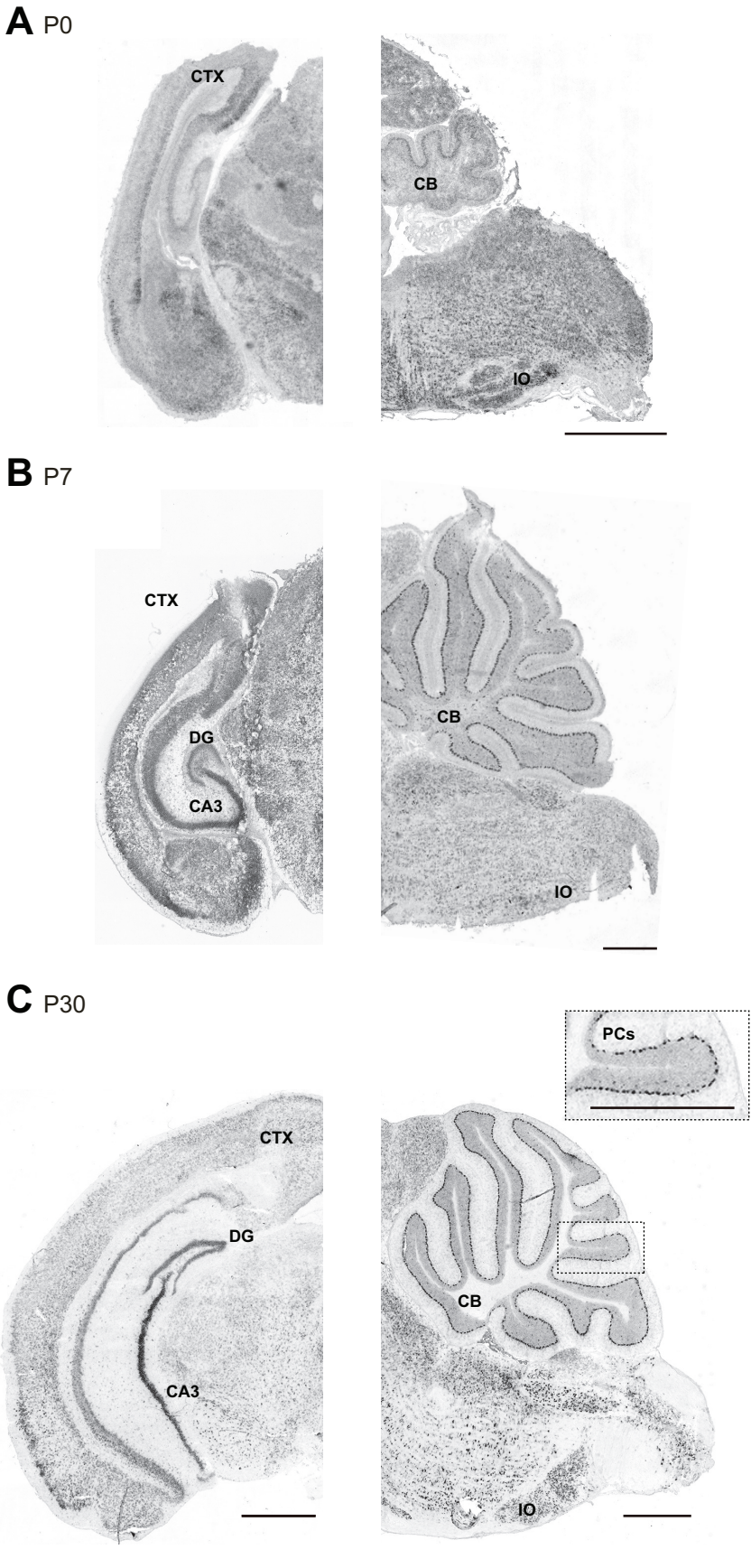
A P0
CTX
CB
IO
B P7
CTX
DG
CA3
CB
IO
C P30
PCs
CTX
DG
CA3
CB
IO

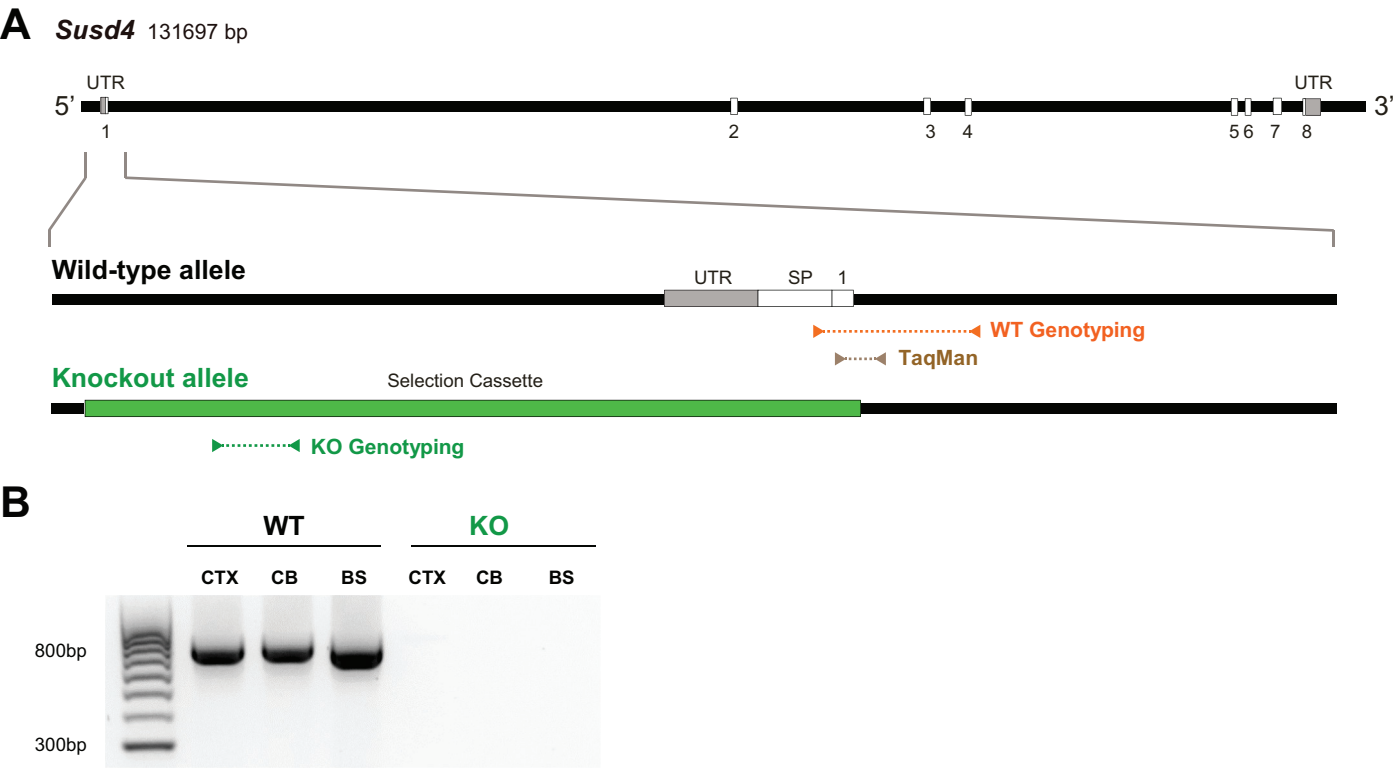
A
Susd4 131697 bp
UTR
UTR
5'
3'
1
2
3
4
5
6
7
8
Wild-type allele
UTR
SP
1
WT Genotyping
TaqMan
Knockout allele
Selection Cassette
KO Genotyping
B
WT
KO
CTX
CB
BS
CTX
CB
BS
800bp
300bp

Footprint Test

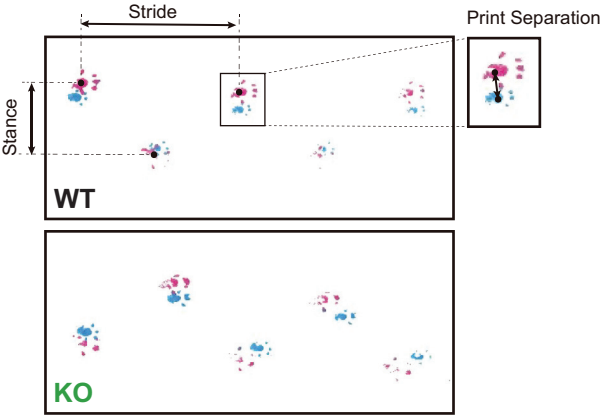

FORELIMB

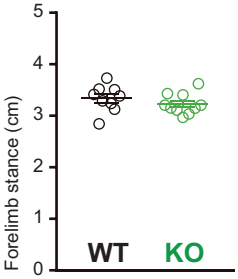

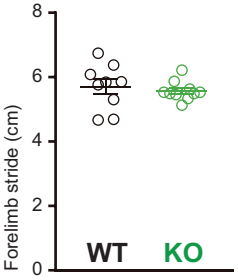

HINDLIMB

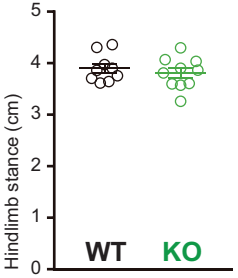

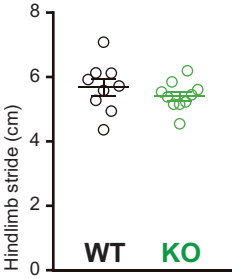

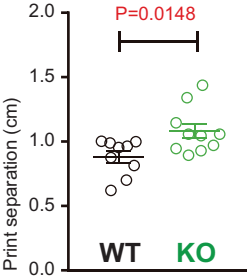

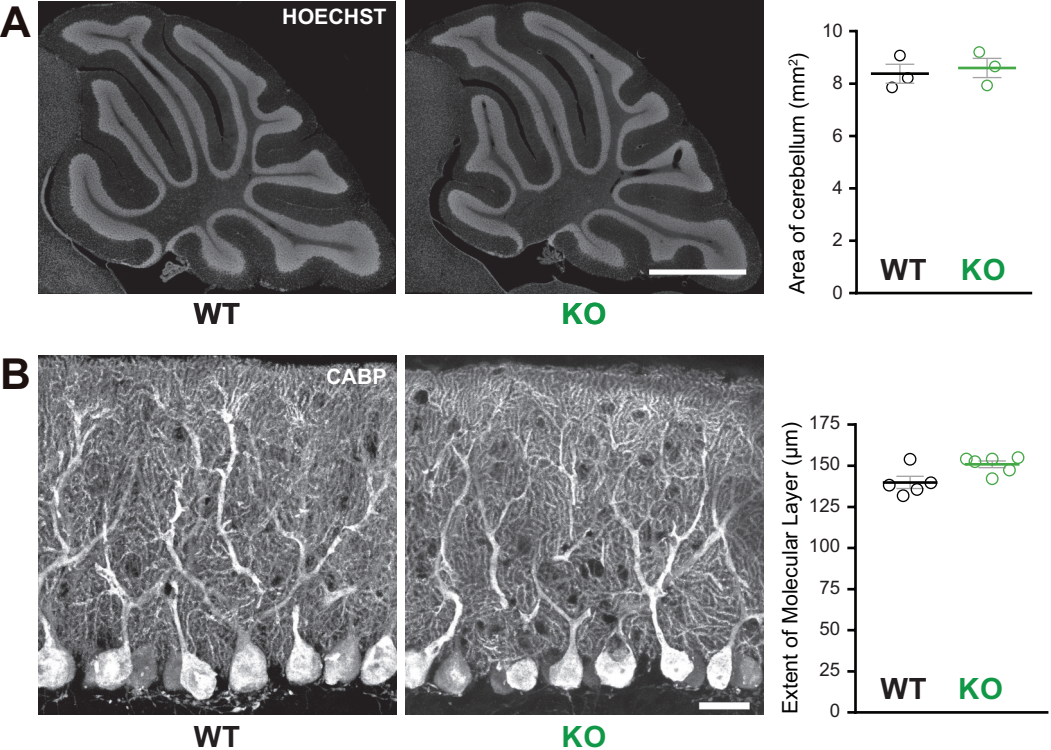
A
HOECHST
WT
KO
Area of cerebellum (mm²)
10
8
6
4
2
0
WT
KO
B
CABP
WT
KO
Extent of Molecular Layer (µm)
175
150
125
100
75
50
25
0
WT
KO

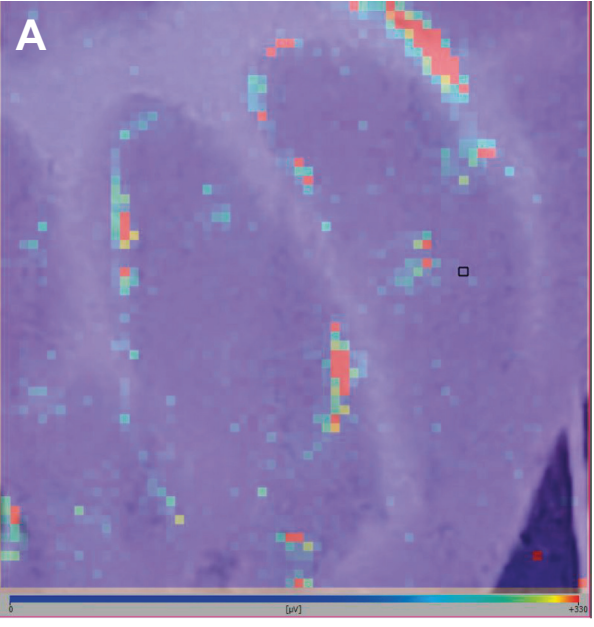
A
0
[µV]
+330

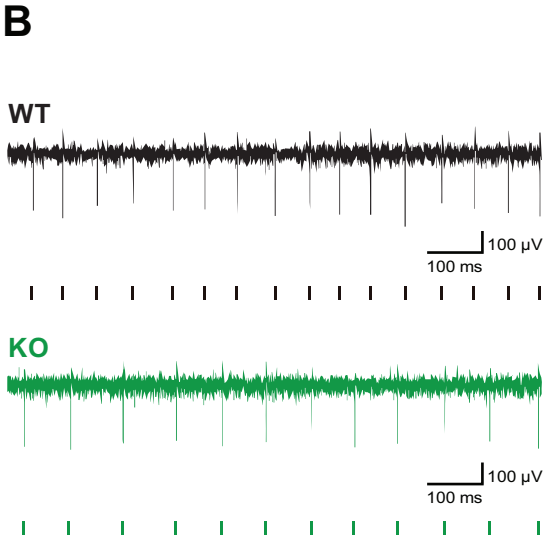
B
WT
100 µV
100 ms
KO
100 µV
100 ms

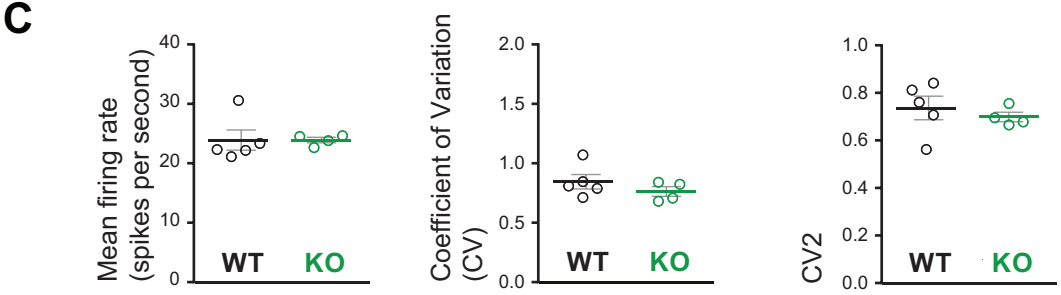
C
Mean firing rate (spikes per second)
40
30
20
10
0
WT
KO
Coefficient of Variation (CV)
2.0
1.5
1.0
0.5
0.0
WT
KO
CV2
1.0
0.8
0.6
0.4
0.2
0.0
WT
KO

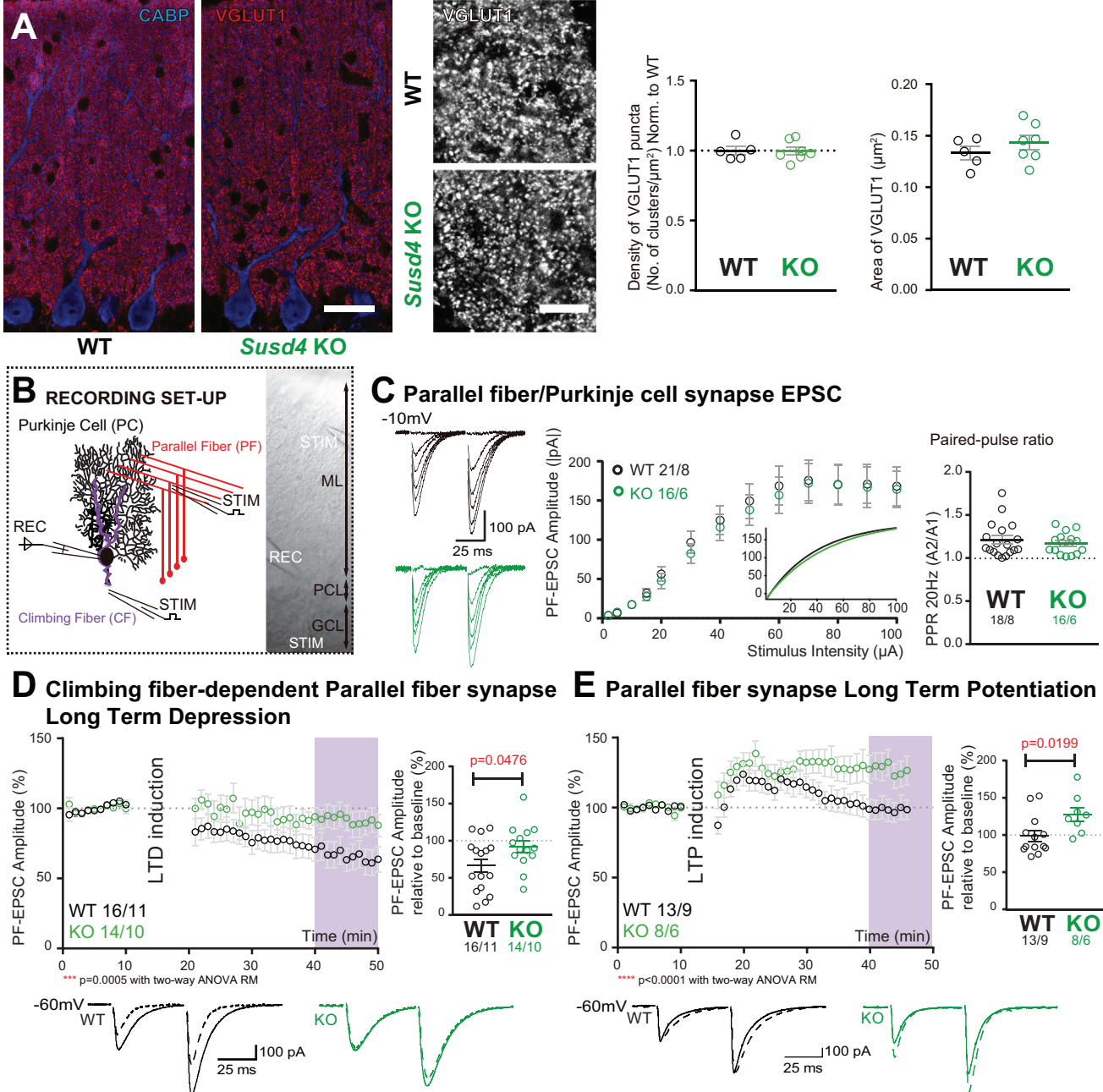
A
CABP
VGLUT1
WT
Susd4 KO
VGLUT1
WT
Susd4 KO
Density of VGLUT1 puncta (No. of clusters/μm²) Norm. to WT
WT
KO
Area of VGLUT1 (μm²)
WT
KO
B RECORDING SET-UP
Purkinje Cell (PC)
Parallel Fiber (PF)
STIM
REC
STIM
Climbing Fiber (CF)
STIM
ML
REC
PCL
GCL
STIM
C Parallel fiber/Purkinje cell synapse EPSC
-10mV
100 pA
25 ms
WT 21/8
KO 16/6
PF-EPSC Amplitude (|pA|)
Stimulus Intensity (μA)
Paired-pulse ratio
PPR 20Hz (A2/A1)
WT
18/8
KO
16/6
D Climbing fiber-dependent Parallel fiber synapse Long Term Depression
PF-EPSC Amplitude (%)
LTD induction
WT 16/11
KO 14/10
Time (min)
*** p=0.0005 with two-way ANOVA RM
PF-EPSC Amplitude relative to baseline (%)
p=0.0476
WT
16/11
KO
14/10
-60mV
WT
KO
100 pA
25 ms
E Parallel fiber synapse Long Term Potentiation
PF-EPSC Amplitude (%)
LTP induction
WT 13/9
KO 8/6
Time (min)
**** p<0.0001 with two-way ANOVA RM
PF-EPSC Amplitude relative to baseline (%)
p=0.0199
WT
13/9
KO
8/6
-60mV
WT
KO
100 pA
25 ms

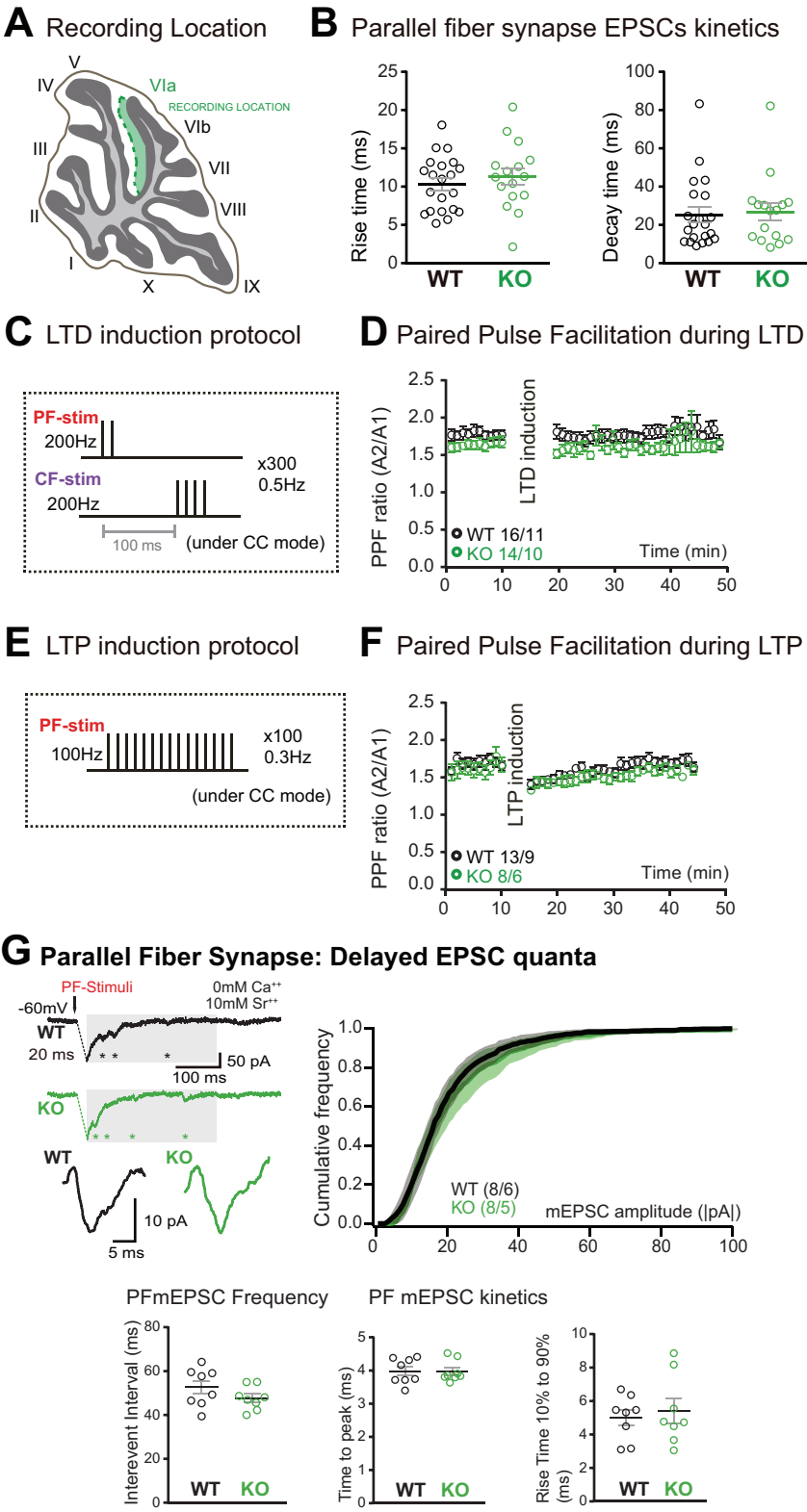
A Recording Location
V
IV
VIa
RECORDING LOCATION
VIb
III
VII
VIII
II
I
X
IX
B Parallel fiber synapse EPSCs kinetics
Rise time (ms)
Decay time (ms)
WT
KO
C LTD induction protocol
PF-stim
200Hz
x300
0.5Hz
CF-stim
200Hz
100 ms
(under CC mode)
D Paired Pulse Facilitation during LTD
PPF ratio (A2/A1)
LTD induction
WT 16/11
KO 14/10
Time (min)
E LTP induction protocol
PF-stim
100Hz
x100
0.3Hz
(under CC mode)
F Paired Pulse Facilitation during LTP
PPF ratio (A2/A1)
LTP induction
WT 13/9
KO 8/6
Time (min)
G Parallel Fiber Synapse: Delayed EPSC quanta
PF-Stimuli
0mM Ca++
10mM Sr++
-60mV
WT
20 ms
50 pA
100 ms
KO
WT
KO
10 pA
5 ms
Cumulative frequency
WT (8/6)
KO (8/5)
mEPSC amplitude (|pA|)
PFmEPSC Frequency
Interevent Interval (ms)
PF mEPSC kinetics
Time to peak (ms)
Rise Time 10% to 90% (ms)
WT
KO

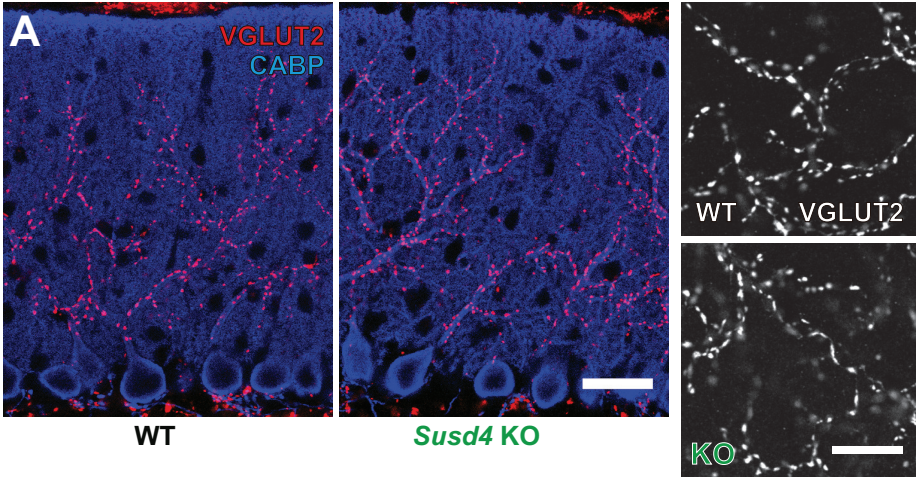

B Climbing fiber/Purkinje cell synapse EPSC

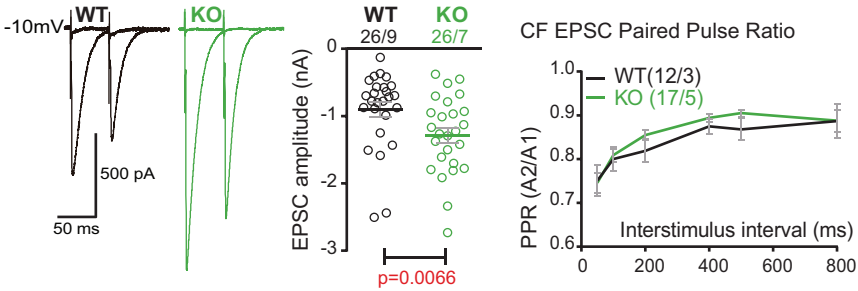

C Climbing Fiber Synapse: Delayed EPSC quanta

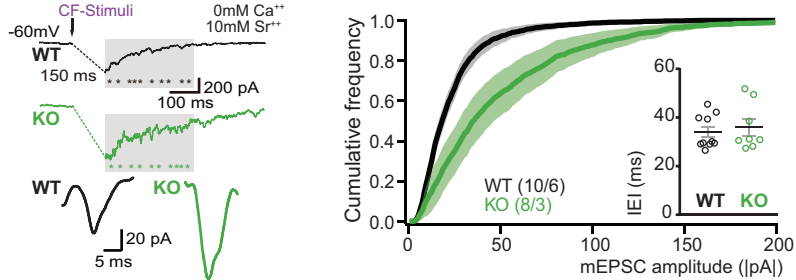

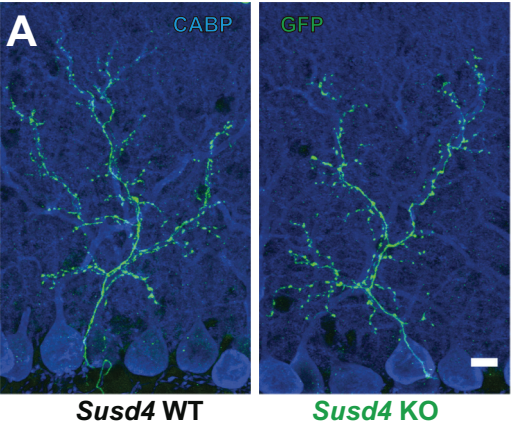
A
CABP
GFP
Susd4 WT
Susd4 KO

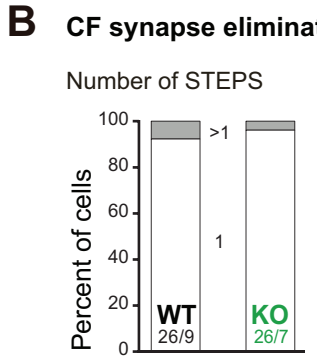
B
CF synapse elimination
Number of STEPS
Percent of cells
100
80
60
40
20
0
>1
1
WT
26/9
KO
26/7

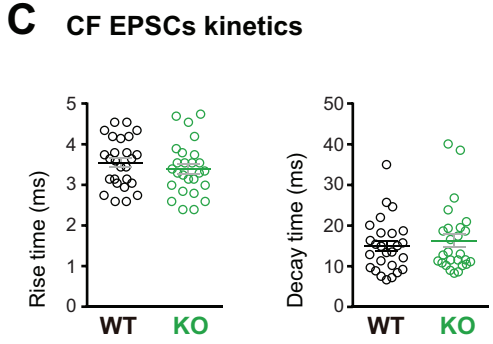
C
CF EPSCs kinetics
Rise time (ms)
Decay time (ms)
WT
KO

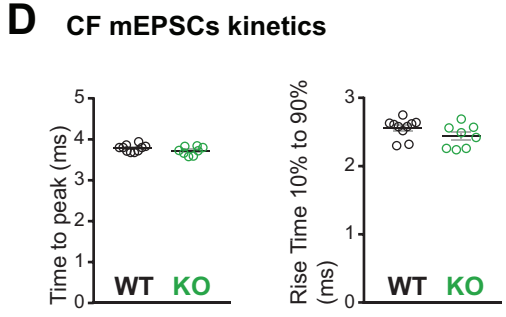
D
CF mEPSCs kinetics
Time to peak (ms)
Rise Time 10% to 90% (ms)
WT
KO

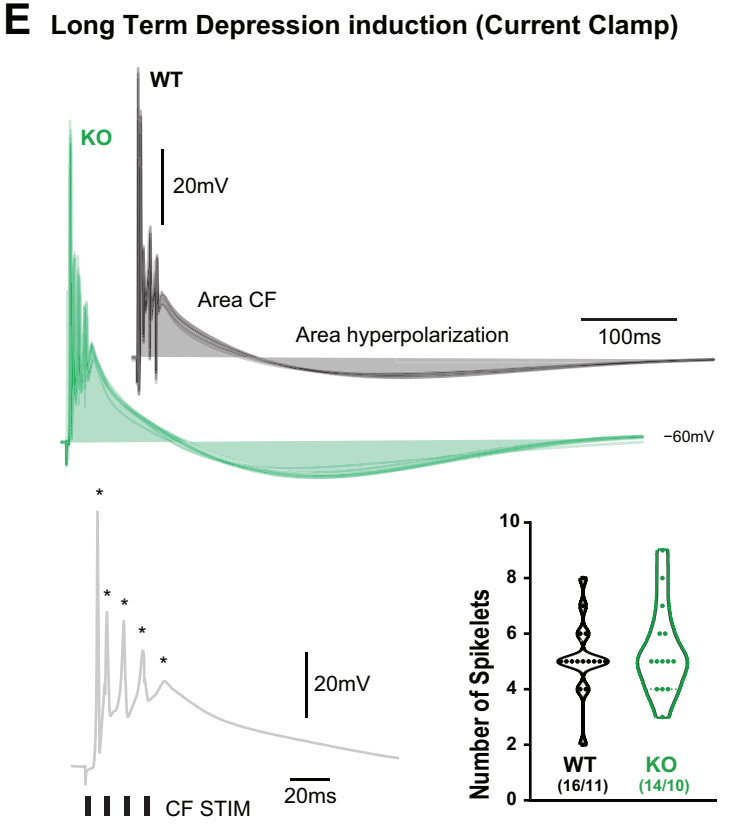
E
Long Term Depression induction (Current Clamp)
WT
KO
20mV
Area CF
Area hyperpolarization
100ms
−60mV
20mV
20ms
CF STIM
Number of Spikelets
WT
(16/11)
KO
(14/10)

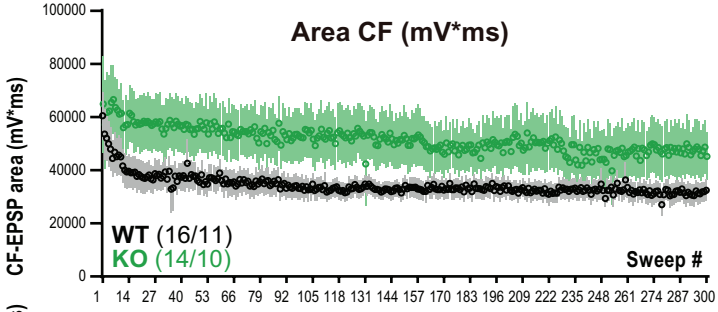
Area CF (mV*ms)
CF-EPSP area (mV*ms)
WT (16/11)
KO (14/10)
Sweep #

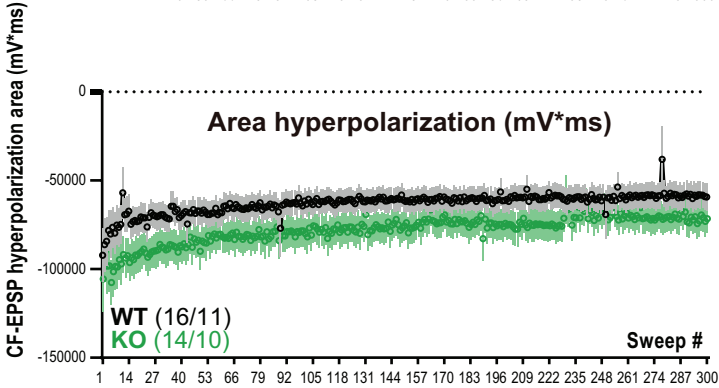
Area hyperpolarization (mV*ms)
CF-EPSP hyperpolarization area (mV*ms)
WT (16/11)
KO (14/10)
Sweep #

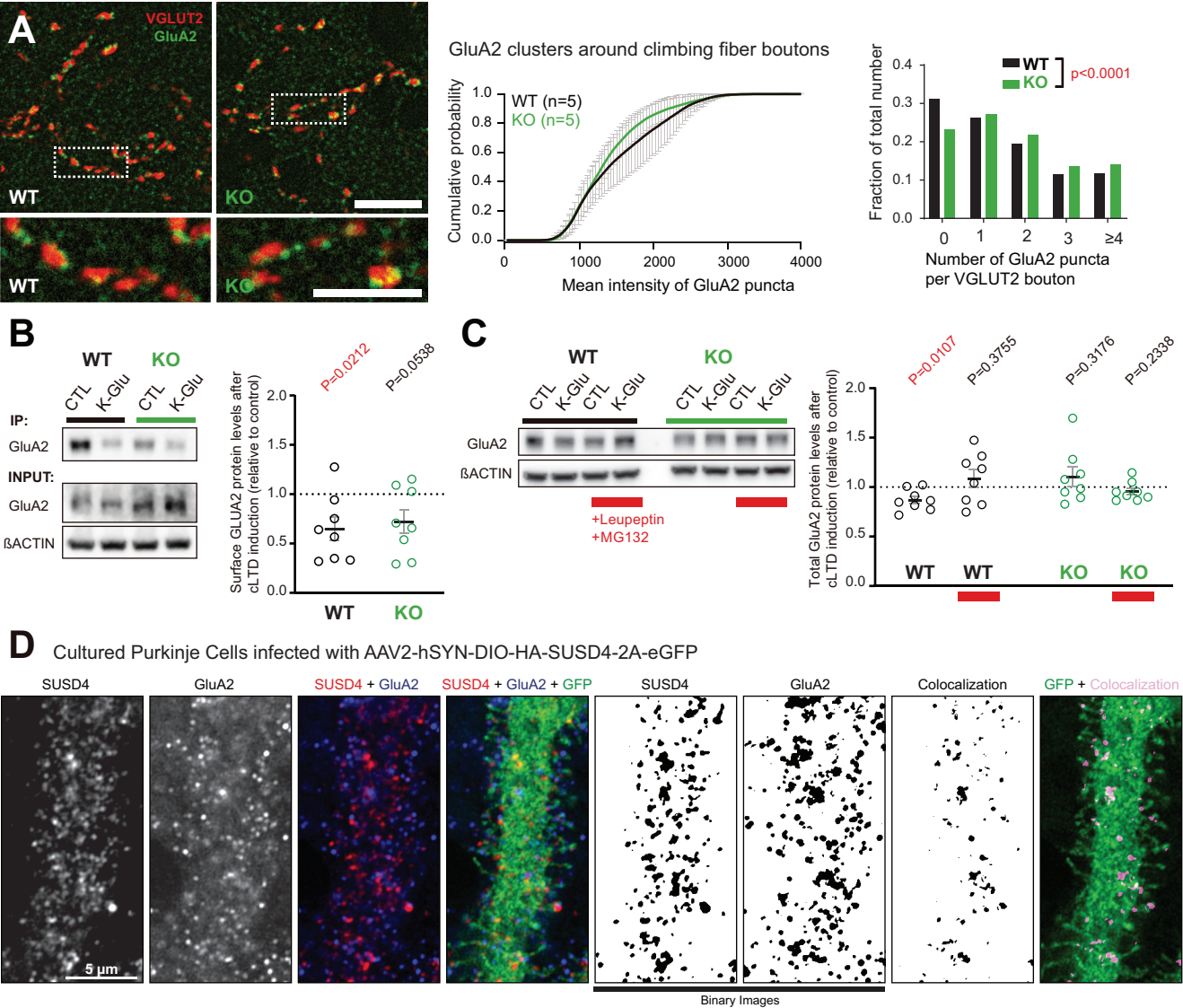
A
VGLUT2
GluA2
WT
KO
WT
KO
GluA2 clusters around climbing fiber boutons
Cumulative probability
WT (n=5)
KO (n=5)
Mean intensity of GluA2 puncta
Fraction of total number
WT
KO
p<0.0001
Number of GluA2 puncta per VGLUT2 bouton
B
WT
KO
CTL
K-Glu
IP:
GluA2
INPUT:
GluA2
ßACTIN
Surface GLUA2 protein levels after cLTD induction (relative to control)
P=0.0212
P=0.0538
C
GluA2
ßACTIN
+Leupeptin
+MG132
Total GluA2 protein levels after cLTD induction (relative to control)
P=0.0107
P=0.3755
P=0.3176
P=0.2338
D
Cultured Purkinje Cells infected with AAV2-hSYN-DIO-HA-SUSD4-2A-eGFP
SUSD4
GluA2
SUSD4 + GluA2
SUSD4 + GluA2 + GFP
SUSD4
GluA2
Colocalization
GFP + Colocalization
5 µm
Binary Images

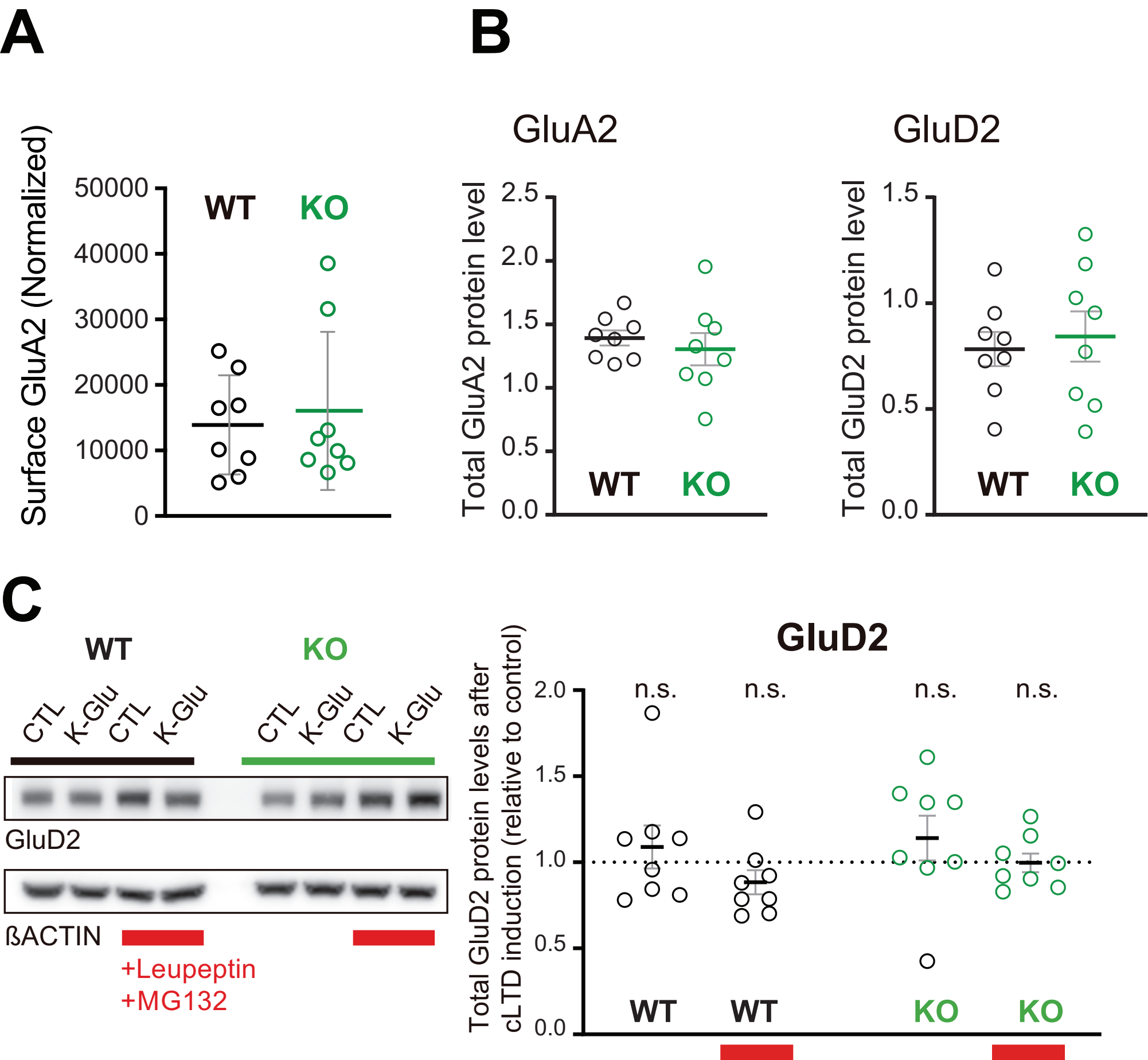
A
Surface GluA2 (Normalized)
50000
40000
30000
20000
10000
0
WT
KO
B
GluA2
Total GluA2 protein level
2.5
2.0
1.5
1.0
0.5
0.0
WT
KO
GluD2
Total GluD2 protein level
1.5
1.0
0.5
0.0
WT
KO
C
WT
KO
CTL
K-Glu
CTL
K-Glu
CTL
K-Glu
CTL
K-Glu
GluD2
ßACTIN
+Leupeptin
+MG132
GluD2
Total GluD2 protein levels after cLTD induction (relative to control)
2.0
1.5
1.0
0.5
0.0
n.s.
n.s.
n.s.
n.s.
WT
WT
KO
KO

A

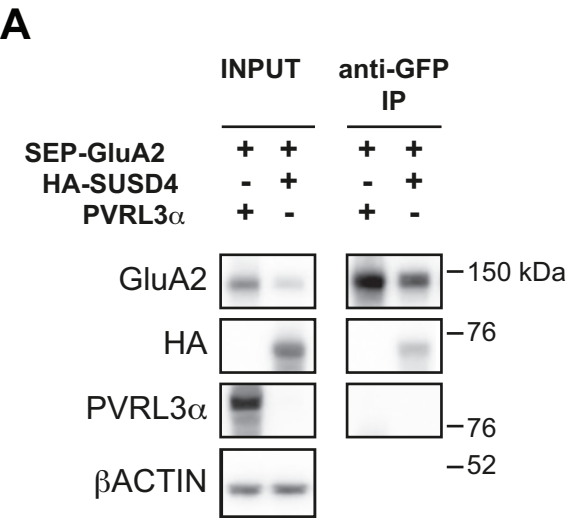
INPUT
anti-GFP IP
SEP-GluA2 + + + +
HA-SUSD4 - + - +
PVRL3α + - + -
GluA2
HA
PVRL3α
βACTIN
150 kDa
76
76
52

B

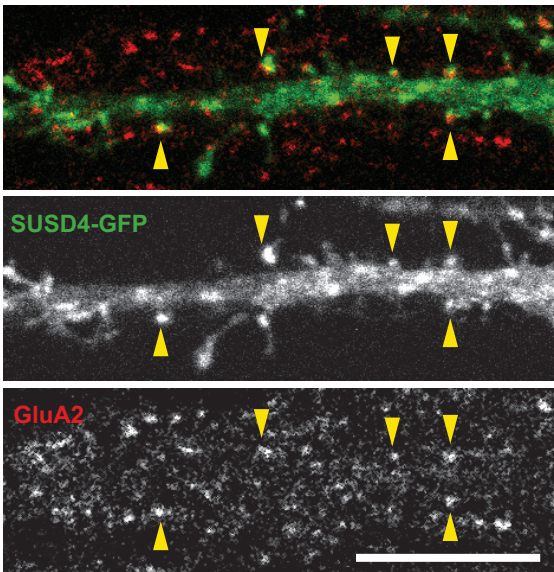
SUSD4-GFP
GluA2

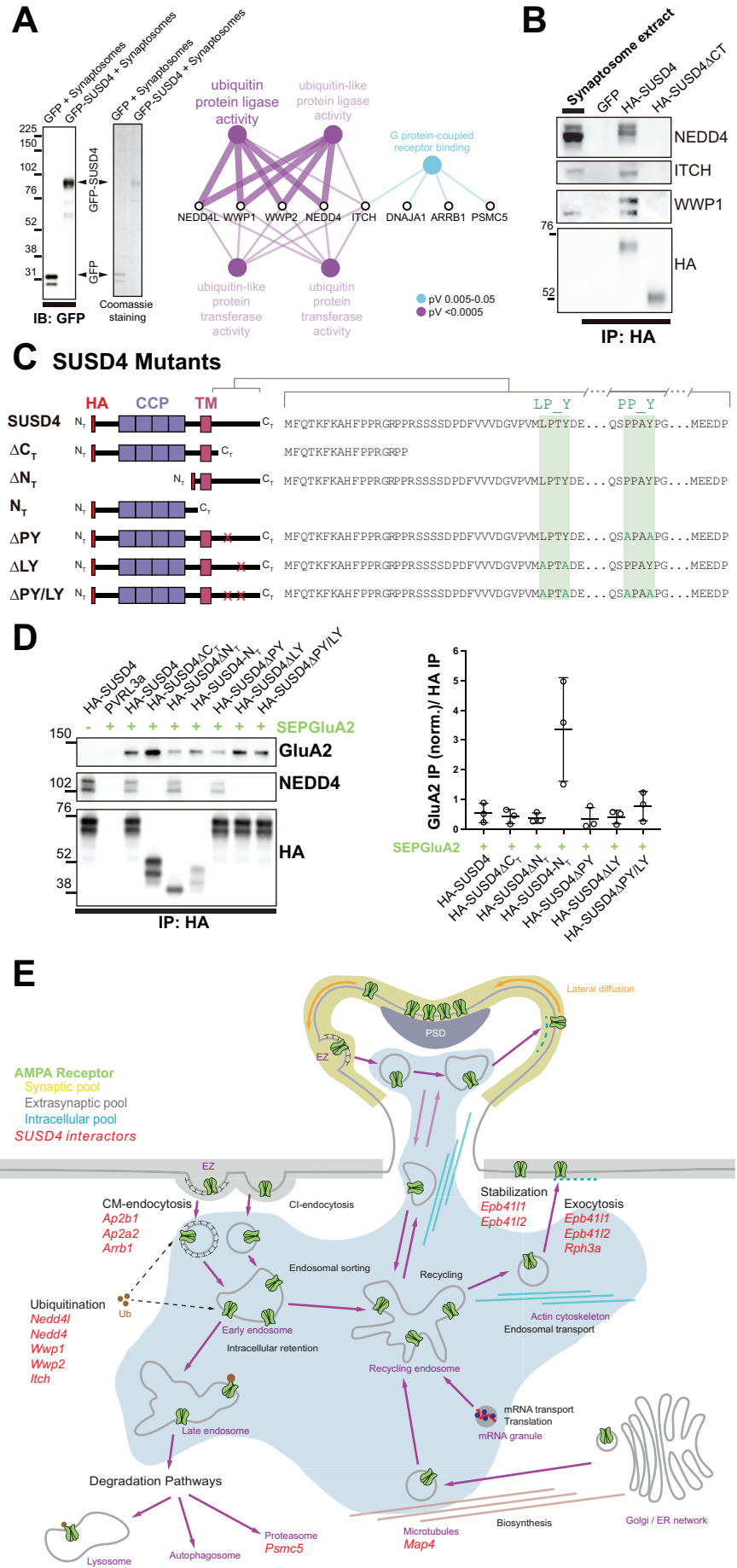
A
GFP + Synaptosomes
GFP-SUSD4 + Synaptosomes
225
150
102
76
52
38
31
GFP-SUSD4
GFP
IB: GFP
Coomassie staining
ubiquitin protein ligase activity
ubiquitin-like protein ligase activity
G protein-coupled receptor binding
NEDD4L WWP1 WWP2 NEDD4 ITCH DNAJA1 ARRB1 PSMC5
ubiquitin-like protein transferase activity
ubiquitin protein transferase activity
pV 0.005-0.05
pV <0.0005
B
Synaptosome extract
GFP
HA-SUSD4
HA-SUSD4ΔCT
NEDD4
ITCH
WWP1
HA
76
52
IP: HA
C SUSD4 Mutants
HA
CCP
TM
LP_Y
PP_Y
SUSD4
ΔC_T
ΔN_T
N_T
ΔPY
ΔLY
ΔPY/LY
MFQTKFKAHFPPRGRPPRSSSSDPDFVVVDGVPVMLPTYDE...QSPPAYPG...MEEDP
MFQTKFKAHFPPRGRPP
MFQTKFKAHFPPRGRPPRSSSSDPDFVVVDGVPVMLPTYDE...QSPPAYPG...MEEDP
MFQTKFKAHFPPRGRPPRSSSSDPDFVVVDGVPVMLPTYDE...QSAPAAPG...MEEDP
MFQTKFKAHFPPRGRPPRSSSSDPDFVVVDGVPVMAPTADE...QSPPAYPG...MEEDP
MFQTKFKAHFPPRGRPPRSSSSDPDFVVVDGVPVMAPTADE...QSAPAAPG...MEEDP
D
HA-SUSD4
PVRL3a
HA-SUSD4
HA-SUSD4ΔC_T
HA-SUSD4ΔN_T
HA-SUSD4-N_T
HA-SUSD4ΔPY
HA-SUSD4ΔLY
HA-SUSD4ΔPY/LY
SEPGluA2
150
102
76
52
38
GluA2
NEDD4
HA
IP: HA
GluA2 IP (norm.)/ HA IP
0
1
2
3
4
5
6
SEPGluA2
E
Lateral diffusion
PSD
EZ
AMPA Receptor
Synaptic pool
Extrasynaptic pool
Intracellular pool
SUSD4 interactors
CM-endocytosis
Ap2b1
Ap2a2
Arrb1
CI-endocytosis
Stabilization
Epb41l1
Epb41l2
Exocytosis
Epb41l1
Epb41l2
Rph3a
Endosomal sorting
Recycling
Ubiquitination
Ub
Nedd4l
Nedd4
Wwp1
Wwp2
Itch
Early endosome
Intracellular retention
Actin cytoskeleton
Endosomal transport
Recycling endosome
mRNA transport
Translation
mRNA granule
Late endosome
Degradation Pathways
Lysosome
Autophagosome
Proteasome
Psmc5
Microtubules
Map4
Biosynthesis
Golgi / ER network

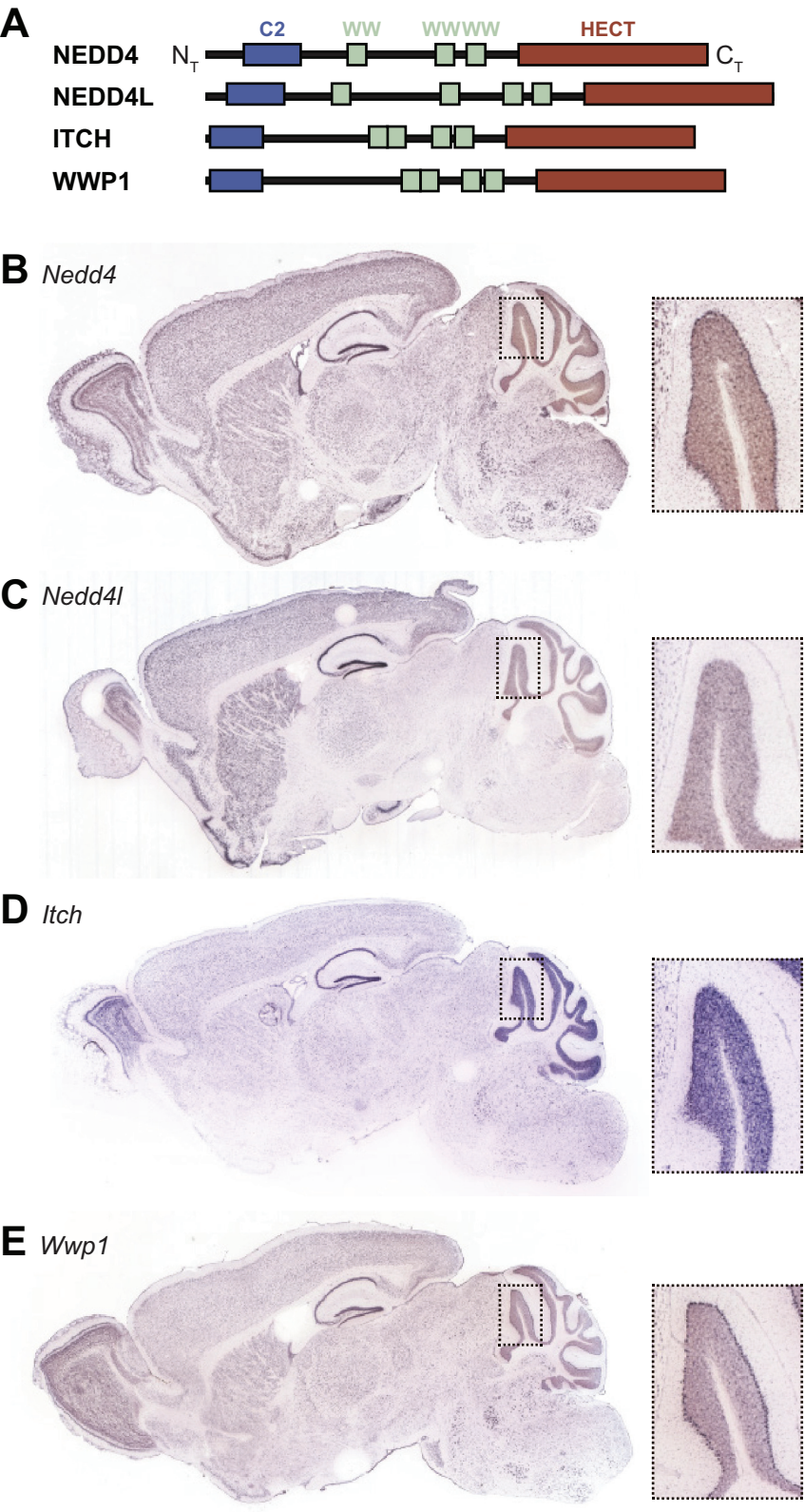
A
C2
WW
WWWW
HECT
NEDD4
N_T
C_T
NEDD4L
ITCH
WWP1
B
Nedd4
C
Nedd4l
D
Itch
E
Wwp1

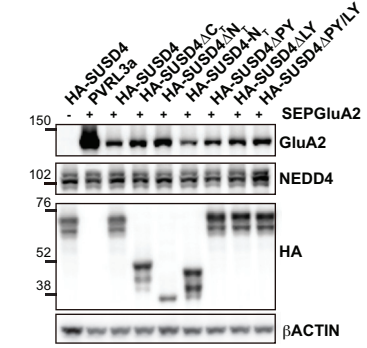
HA-SUSD4
PVRL3a
HA-SUSD4
HA-SUSD4ΔC
HA-SUSD4ΔN
HA-SUSD4-N
HA-SUSD4ΔPY
HA-SUSD4ΔLY
HA-SUSD4ΔPY/LY
SEPGluA2
- + + + + + + + +
150
GluA2
102
NEDD4
76
52
38
HA
βACTIN

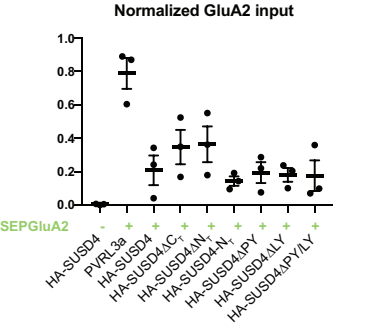
Normalized GluA2 input
1.0
0.8
0.6
0.4
0.2
0.0
SEPGluA2
- + + + + + + + +
HA-SUSD4
PVRL3a
HA-SUSD4
HA-SUSD4ΔC
HA-SUSD4ΔN
HA-SUSD4-N
HA-SUSD4ΔPY
HA-SUSD4ΔLY
HA-SUSD4ΔPY/LY

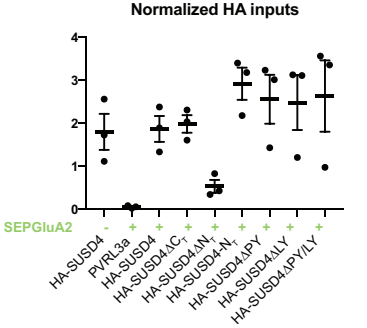
Normalized HA inputs
4
3
2
1
0
SEPGluA2
- + + + + + + + +
HA-SUSD4
PVRL3a
HA-SUSD4
HA-SUSD4ΔC
HA-SUSD4ΔN
HA-SUSD4-N
HA-SUSD4ΔPY
HA-SUSD4ΔLY
HA-SUSD4ΔPY/LY

Key Resources Table				
Reagent type (species) or resource	**Designation**	**Source or reference**	**Identifiers**	**Additional information**
gene (*Mus musculus*)	*Susd4*	NCBI	Gene ID: 96935	chr1:182,764,895-182,896,591
Strain (*Mus musculus*)	*Susd4* knockout mice	Lexicon Genetics Incorporated, Tang et al, 2010	B6:129S5-Susd4^{tm1Lex}	
Strain (*Mus musculus*)	Htr5b-GFP mouse line	Gene Expression Nervous System Atlas (GENSAT) Project	STOCK Tg(Htr5b-EGFP)BZ265Gsat/Mmmh	
Strain (*Mus musculus*)	L7Cre mouse line	Jackson Laboratories	B6.129-Tg(Pcp2-cre)2Mpin/J	Stock Number: 004146
Cell line (*Homo sapiens*)	HEK293H	Gibco	Cat. #: 11631-017	
Cell line (*Homo sapiens*)	HeLA	Sigma	Cat. #: 93021013	
antibody	mouse monoclonal anti-CABP	Swant	Cat. #: 300	(1:1000)
antibody	rabbit polyclonal anti-CABP	Swant	Cat. #: CB38	(1:1000)

antibody	mouse monoclonal anti-GFP	Abcam	Cat. #: ab1218	(1:1000)
antibody	rabbit polyclonal anti-GFP	Abcam	Cat. #: ab6556	(1:1000)
antibody	mouse monoclonal anti-GLUA2, clone 6C4	Millipore and BD	Cat. #: MAB397 and Cat. #: 556341	(1:500)
antibody	rabbit monoclonal anti-GLUA2	Abcam	Cat. #: ab206293	(1:1000)
antibody	rabbit polyclonal anti-GLURδ1/2	Millipore	Cat. #: AB2285	(1:1000)
antibody	rat monoclonal anti-HA	Roche Life	Cat. #: 11867423001	(1:1000)
antibody	rabbit monoclonal anti-ITCH	Cell Signaling Technology	Cat. #: 12117	(1:1000)
antibody	rabbit polyclonal anti-NEDD4	Millipore	Cat. #: 07-049	(1:100000)
antibody	guinea pig polyclonal anti-VGLUT1	Millipore	Cat. #: AB5905	(1:5000)
antibody	guinea pig polyclonal anti-VGLUT2	Millipore	Cat. #: AB2251	(1:5000)

antibody	rabbit polyclonal anti-WWP1	Proteintech	Cat. #: 13587-1-AP	(1:2000)
antibody	donkey polyclonal anti-Goat Alexa Fluor 568	Invitrogen	Cat. #: A11057	(1:1000)
antibody	donkey anti-Mouse Alexa Fluor 488	Invitrogen	Cat. #: R37114	(1:1000)
antibody	donkey polyclonal anti-Mouse Alexa Fluor 568	Invitrogen	#A10037	(1:1000)
antibody	donkey polyclonal anti-Rabbit Alexa Fluor 488	Invitrogen	Cat. #: A21206	(1:1000)
antibody	donkey polyclonal anti-Rat Alexa Fluor 594	Invitrogen	#A21209	(1:1000)
antibody	donkey polyclonal anti-Rat Alexa Fluor 568	Abcam	Cat. #: 175475	(1:1000)
antibody	goat polyclonal anti-Guinea Pig Alexa Fluor 488	Invitrogen	Cat. #: A110-73	(1:1000)
antibody	goat polyclonal anti-Guinea Pig Alexa Fluor 647	Invitrogen	Cat. #: A21450	(1:1000)
antibody	goat polyclonal anti-Mouse HRP	Jackson Immune Research Laboratories	Cat. #: 115-035-174	(1:10000)
antibody	goat polyclonal anti-rat HRP	Jackson Immune Research Laboratories	#112-035-175	(1:10000)

antibody	sheep polyclonal anti-digoxigenin alkaline phosphatase	Roche Life Science	Cat. #: 11093274910	(1:2000 - 1:5000)
antibody	mouse monoclonal anti-βACTIN HRP, clone AC-15	Abcam	Cat. #: ab49900	(1:25000)
recombinant DNA reagent	pHA-SUSD4-GFP	This paper		From pEGFP-N1 (Addgene, Cat. #: 6085-1)
recombinant DNA reagent	pHA-SUSD4	This paper		
recombinant DNA reagent	pHA-SUSD4-ΔN_T	This paper		
recombinant DNA reagent	pHA-SUSD4-N_T	This paper		
recombinant DNA reagent	HA-SUSD4-ΔPY	This paper		
recombinant DNA reagent	HA-SUSD4-ΔLY	This paper		
recombinant DNA reagent	HA-SUSD4-ΔPY/LY	This paper		
recombinant DNA reagent	pIRES2-eGFP	Addgene	Cat. #: 6029-1	
recombinant DNA reagent	pCAG-PVRL3α	This paper		From pCAG-mGFP (Addgene, Cat. #: 14757
sequenced-based reagent	Susd4_WT_F	This paper	PCR primers	CTG TGG TTT CAA CTG GCG CTG TG

sequenced-based reagent	Susd4_WT_R	This paper	PCR primers	GCT GCC GGT GGG TGT GCG AAC CTA
sequenced-based reagent	Susd4_KO_F	This paper	PCR primers	TTG GCG GTT TCG CTA AAT AC
sequenced-based reagent	Susd4_KO_R	This paper	PCR primers	GGA GCT CGT TAT CGC TAT GAC
sequenced-based reagent	Htr5b-GFP_F		PCR primers	TTG GCG CGC CTC CAA CAG GAT GTT AAC AAC
sequenced-based reagent	Htr5b-GFP_R		PCR primers	CGC CCT CGC CGG ACA CGC TGA AC
sequenced-based reagent	L7cre_1		PCR primers	GGT GAC GGT CAG TAA ATT GGA C
sequenced-based reagent	L7cre_2		PCR primers	CAC TTC TGA CTT GCA CTT TCC TTG G
sequenced-based reagent	L7cre_3		PCR primers	TTC TTC AAG CTG CCC AGC AGA GAG C
chemical compound, drug	picrotoxin	Sigma-aldrich	Cat. #: P1675	
chemical compound, drug	D-AP5	Tocris	Cat. #: 0106	
chemical compound, drug	CGP52432	Tocris	Cat. #: 1246	
chemical compound, drug	JNJ16259685	Tocris	Cat. #: 2333	

chemical compound, drug	DPCPX	Tocris	Cat. #: 0439	
chemical compound, drug	AM251	Tocris	Cat. #: 1117	
software, algorithm	Sinaptiqs	Antoine Valera	software written in Python	http://synaptiqs.wixsite.com/synaptiqs
other	Hoechst 33342	Sigma	Cat. #: 14533	
Recombinant viral particles	hSYN-DIO-HA-SUSD4-2A-eGFP-WPRE	Vector biolabs	AAV2 particles	

1